

ASD-TDR-63-754  
Part III

AD 664069

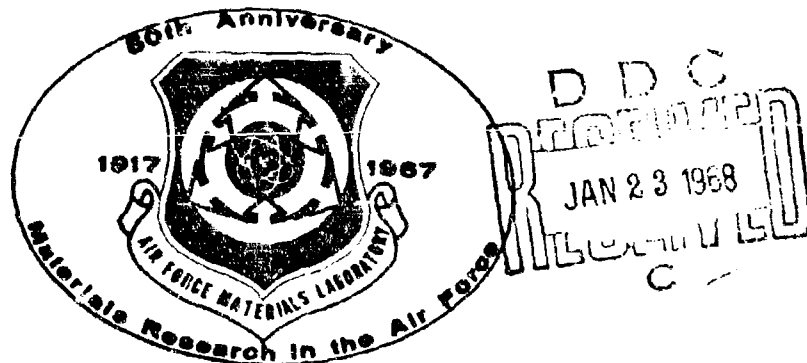
MOLECULAR FLOW AND THE EFFUSION PROCESS IN THE  
MEASUREMENT OF VAPOR PRESSURES

Robert D. Freeman  
Oklahoma State University

TECHNICAL DOCUMENTARY REPORT ASD-TDR-63-754, Pt. III  
November, 1967

This document has been approved for public release  
and sale; its distribution is unlimited.

Air Force Materials Laboratory  
Research and Technology Division  
Air Force Systems Command  
Wright-Patterson Air Force Base, Ohio



Reproduced by the  
CLEARINGHOUSE  
for Federal Scientific & Technical  
Information, Springfield, Va. 22151

92

**BEST**

**AVAILABLE**

**COPY**

NOTICES

When Government drawings, specifications, or other data are used for any purpose other than in connection with a definitely related Government procurement operation, the United States Government thereby incurs no responsibility nor any obligation whatsoever; and the fact that the Government may have formulated, furnished, or in any way supplied the said drawings, specifications, or other data, is not to be regarded by implication or otherwise as in any manner licensing the holder or any other person or corporation, or conveying any rights or permission to manufacture, use, or sell any patented invention that may in any way be related thereto.

Copies of this report should not be returned to the Aeronautical Systems Division unless return is required by security considerations, contractual obligations, or notice on a specific document.

ACCESSION FOR	
CPSTI	WHITE SECTION <input checked="" type="checkbox"/>
DDC	BLUE SECTION <input type="checkbox"/>
UNANNOUNCED	<input type="checkbox"/>
JUSTIFICATION	
BY	
DISTRIB/SECTION/AVAILABILITY CODES	
DIST.	AVAIL. OR SPECIAL

MOLECULAR FLOW AND THE EFFUSION PROCESS IN THE  
MEASUREMENT OF VAPOR PRESSURES

Robert D. Freeman

This document has been approved for public release  
and sale; its distribution is unlimited.

## FOREWORD

This report was prepared by the Research Foundation and the Department of Chemistry, Oklahoma State University, Stillwater, Oklahoma, under USAF Contract AF 33(657)-8767. This contract was initiated under Project No. 7360, "The Chemistry and Physics of Materials", Task No. 736004, "Special Problems in Materials Physics". The work was administered under the direction of the Air Force Materials Laboratory, Research and Technology Division, with Mr. Paul W. Dimiduk, MAYT, as project engineer. This report was submitted in August 1967 for publication.

This report is an account of the research accomplished between 1 September 1964 and 31 May 1967.

The author wishes to acknowledge the many contributions of the graduate students and research associates who have been associated with this research program, and who should be credited with co-authorship of the various sections. They are E. A. Elphingstone (section V), R. E. Gebelt (sections IV and V), J. G. Edwards (section II), and Ruth C. Erbar (section III). The excellent craftsmanship of the machinists and instrument makers in our departmental Machine and Instrument Shop has been invaluable and is gratefully acknowledged.

This technical documentary report has been reviewed and is approved.



HYMAN MARCUS, Actg. Chief  
Thermo and Chemical Physics Branch  
Materials Physics Division  
Air Force Materials Laboratory

#### ABSTRACT

Our extensions to conical orifices of Clausius's analysis of angular distribution of molecules effusing from cylindrical orifices has resulted in numerical values for transmission probabilities and recoil-force correction factors which are tabulated. With these results, it is demonstrated that the optimum orifice geometry for (1) recoil force measurements is a diverging conical orifice with semi-apex angle of  $30^\circ$ , (2) delivery of maximum fraction of effusing molecules onto (or into) a target (aperture) is a long cylindrical orifice.

Modifications to the angular distribution apparatus are described and experimental results given for four orifices and two gases over the pressure range 5 to 900 dyn/cm<sup>2</sup>. The most interesting aspect of the results, one apparently not previously noticed in angular distribution results, is the presence of maxima and minima in plots of  $\Delta$  vs.  $\theta$ , where  $\Delta$  is the (experimental value - theoretical value) of  $\underline{P}_\theta$ , the fraction of effusing molecules which flow per steradian at angle  $\theta$  from the orifice axis. These maxima and minima have been correlated with the relative contribution from the orifice wall to the total flux at angle  $\theta$ .

Additional results for experimental transmission probabilities of orifices determined by the Multicell technique are generally in agreement with theoretical values within 2 to 5%.

The Miker technique for simultaneous determination of vapor pressure by rate of effusion and by recoil force measurements has been refined to the point that recoil force data are as reproducible as rate of effusion measurements. Several sources of spurious recoil force have been identified and eliminated. A new furnace and a modified automatic control system for the microbalance are described.

TABLE OF CONTENTS

Section

- I. INTRODUCTION . . . . . 1
- II. THEORETICAL ANALYSIS OF MOLECULAR FLOW THROUGH  
CONICAL ORIFICES . . . . . 1
- III. MEASUREMENT OF ANGULAR DISTRIBUTION OF MOLECULAR  
FLOW THROUGH CONICAL ORIFICES . . . . . 19
  - A. Experimental Apparatus . . . . . 19
  - B. Experimental Results . . . . . 24
  - C. Discussion . . . . . 33
- IV. THE MULTICELL TECHNIQUE FOR EXPERIMENTAL DETERMINATION  
OF TRANSMISSION PROBABILITIES FOR MOLECULAR FLOW  
THROUGH CONICAL ORIFICES . . . . . 57
- V. THE MIKER TECHNIQUE . . . . . 67
  - A. Modifications to Apparatus . . . . . 67
  - B. Experimental Results . . . . . 71
- VI. CALORIMETRIC STUDIES OF VAPORIZATION PROCESSES . . . . . 73
- REFERENCES . . . . . 76

LIST OF ILLUSTRATIONS

Figure	Page
1. Conical Orifices and Parameters: <u>A</u> , Diverging Configuration, <u>T</u> positive; <u>B</u> , Converging Configuration, <u>T</u> negative . . . . .	3
2. The Transmission Probability <u>W</u> as a function of $\log (L/r_0)$ at various values of <u>T</u> . . . . .	7
3. The Recoil Force Correction <u>f</u> as a function of $\log (L/r_0)$ at various values of <u>T</u> . . . . .	8
4. Collimating effect of various orifice geometries on effusing molecules . . . . .	14
5. Collimating effect of various orifice geometries on effusing molecules . . . . .	15
6. Optimization of orifice geometry for recoil force . . . . .	17
7. Diagram of the Experimental Apparatus . . . . .	21
8. Experimental angular distribution data (Normalized beam intensity) for Nitrogen through orifice 1 ( $T = 25.65^\circ$ and $(L/r_m) = 4.010$ ) . . . . .	25
9. Experimental $[I(\theta)]$ and Normalized Theoretical $[Q_n \cos\theta]$ Angular Distribution Data for $T = 0.0^\circ$ , $L/r_m = 2.44$ . . . . .	27
10. Experimental $[I(\theta)]$ and Normalized Theoretical $[Q_n \cos\theta]$ Angular Distribution Data for $T = 30^\circ$ , $L/r_m = 2.0$ , with Nitrogen . . . . .	28
11. Normalized Experimental $[I(\theta)]$ and Theoretical $[Q_n \cos\theta]$ Angular Distribution Data for Nitrous Oxide through Orifice 2 ( $T = 8.500^\circ$ , $L/r_m = 10.08$ ) . . . . .	29
12. Normalized Experimental $[I(\theta)]$ and Theoretical $[Q_n \cos\theta]$ Angular Distribution Data for Nitrogen through Orifice 3 ( $T = -58.93^\circ$ , $L/r_m = 11.01$ ) . . . . .	30

Figure	Page
13. Normalized Experimental $[I(\theta)]$ and Theoretical $[Q_n \cos\theta]$ Angular Distribution Data for Nitrous Oxide through Orifice 3 ( $T = -58.95^\circ$ , $L/r_m = 11.01$ ) . . . . .	31
14. Normalized Experimental $[I(\theta)]$ and Theoretical $[Q_n \cos\theta]$ Angular Distribution Data for Nitrogen through Orifice 1 ( $T = 25.65^\circ$ , $L/r_m = 4.010$ ) . . . . .	32
15. $f(\Delta)$ plots for 120 series . . . . .	38
16. $\Delta$ plots for 120 series . . . . .	39
17. $f(\Delta)$ plots for 230 series . . . . .	40
18. $f(\Delta)$ plots for 320 series . . . . .	41
19. $f(\Delta)$ plots for 330 series . . . . .	42
20. $f(\Delta)$ plots for 420 series . . . . .	43
21. $\delta_2$ plot (cf. equation 26) for Run 125. Compare with Run 125 in Figure 15 . . . . .	44
22. The Critical Angles and the Angular Ranges for a Conical Orifice . . . . .	45
23. $\Delta$ plot for K. C. Wang's angular distribution data <sup>27</sup> for orifice with $T = 0.0^\circ$ and $L/r_0 = 0.934$ . . . . .	48
24. $\Delta$ plot for K. C. Wang's angular distribution data <sup>27</sup> for orifice with $T = 0.0^\circ$ and $L/r_0 = 2.59$ . . . . .	49
25. Normalized projected area of inside wall of Orifice 1 . . . . .	52
26. Normalized projected area of inside wall of Orifice 4 . . . . .	53
27. Normalized projected area of inside wall of Orifice 2 . . . . .	54
28. Normalized projected area of inside wall of Orifice 3 . . . . .	55
29. Weight loss through orifices with various $(L/D)$ ratios vs. theoretical transmission probability . . . . .	62

LIST OF TABLES

Table	Page
1. Transmission probabilities and Recoil Force Corrections for Conical Orifices . . . . .	4
2. Orifices, Gases, and Pressures Used in Angular Distribution Studies . . . . .	26
3. Comparison of Experimental and Theoretical Transmission Probabilities: Run 7 . . . . .	61
4. Experimental Transmission Probabilities for Eight Cylindrical Orifices (Set I) . . . . .	63
5. Experimental Transmission Probabilities for Eight Cylindrical Orifices (Set II) . . . . .	64
6. Experimental Transmission Probabilities for Eight Conical Orifices (Set III) . . . . .	65
7. Miker Data for Vaporization of Tin . . . . .	72
8. Identification of Major Commercial Components of Apparatus . . . . .	76

LIST OF SYMBOLS

<u>Symbol</u>	<u>Defined on Page</u>	<u>Definition or Explanation</u>
$A_L$	51	projection at angle $\theta$ of area of orifice exit.
$A_O$	51	projection at angle $\theta$ of area of orifice entrance.
$A_W$	51	projection at angle $\theta$ of orifice wall area visible from molecular beam detector.
$A_E$	51	projection at angle $\theta$ of the area $A$ ( $D_O$ ; $D_L$ ); see p. 51.
$A(D_O; D_L)$	51	area of overlap of circles $\pi r_o^2$ , and $\pi r_l^2$ projected at angle $\theta$ onto the plane of $\pi r_o^2$ .
$a_i$	58	cross sectional area of <u>ith</u> orifice.
$a_n$	16	integration limit.
$a_o$	11	cross sectional area of orifice entrance, $\pi r_o^2$ .
$b$	60	constant in equation for straight line.
$b_n$	16	integration limit.
$D$	58	diameter of orifice.
$dx$		differential of $x$ ; other differentials are listed under the function differentiated.
exp		designates experimental value.
$F_Y$	18	force exerted by molecules impinging on target subtending angle $Y$ .
$F_o$	18	force exerted by all molecules impinging on target, from an ideal orifice.
$F(L/D, T)$	59	function of $L/D$ and $T$ .
$f$	2	recoil force correction factor.
$f^*$	4	recoil force correction factor for converging conical orifice.
$f_Y$	18	angular recoil force correction factor.
$df_\theta$	16	incremental recoil force correction factor.
$f(\Delta)$	36	the fractional difference $(P_\theta^x - P_\theta^t) / P_\theta^t$ .
$g_i$	58	total mass effusing from cell in time $\tau$ .
$dg_i$	58	incremental effusing mass.
$\Delta H_{298}^o$	66	standard enthalpy change.
$I$	58	represents value of an integral.
$I_\theta^+$	33	measured ion current at angle $\theta$ .
$I_\theta$	33	relative molecular beam intensity, $I_\theta^+ / I_o^+$ .
$i$		index.

$J_i$	58	mass effusing per unit area of orifice in time $\tau$ .
$J_i^c$	59	mass effusing per unit area of orifice in time $\tau$ , calculated from least-squares line through experimental points.
$J_o$	59	mass effusing per unit area of ideal orifice in time $\tau$ .
$K_i$	58	experimental transmission probability.
$K_o$	59	experimental transmission probability for ideal orifice.
$K_i^p$	60	experimental transmission probability, from experimental points.
$K_i^c$	60	experimental transmission probability, from least-squares line through experimental points.
$\bar{K}_i$	60	experimental transmission probability, average.
$L$	2	length of orifice along its axis.
$M$	58	molecular weight.
$m$	58	the number of cells in a multicell experiment.
$n$	60	constant in equation for straight line.
$N_\gamma$	12	number of molecules which effuse per second into a cone with semi-apex angle $\gamma$ .
$N_o$	12	number of molecules which enter the orifice through $\underline{a}_o$ per second.
$N_L$	12	number of molecules which effuse from the orifice exit per second.
$dN_\omega$	19	number of molecules per second which pass through the incremental solid angle $d\omega$ .
$dN_\omega(L)$	33	number of molecules which effuse per second into the solid angle $d\omega$ .
$dN_\Omega(L)$	33	number of molecules which effuse per second into the solid angle $2\pi \sin\theta d\theta$ .
$N_\Omega(L)_\theta$	34	number of molecules which effuse per second into the finite, but small, solid angle $\Omega$ .
$P$	58	pressure in effusion cell.
$P_E$	72	pressure in effusion cell determined by effusion measurement.
$P_R$	72	pressure in effusion cell determined by recoil force measurement.
$P_\theta$	35	probability density function for effusing molecules.
$P_\theta^x$	35	$P_\theta$ , experimental.

$P_{\theta}^t$	35	$P_{\theta}$ , theoretical.
$P_{\theta}^x$	35	$P_{\theta}$ , experimental, at $\theta=0^{\circ}$ .
$Q_{\nu}$	33	angular distribution function; $Q_{\nu}=1$ for ideal orifice.
$Q_n$	12	$\pi Q_{\nu}$ .
$Q_1$	12	$Q_n$ with $n=1$ .
$R$	58	gas constant.
$r_o$	2	radius of entrance to orifice.
$r_L$	3	radius of exit from orifice.
$r_m$	4	radius of smaller end of orifice.
$T$	2	angle between orifice axis and orifice wall, measured in a plane which contains the orifice axis.
$T(\theta)$	10	Clausing's angular distribution function.
$th$		designates theoretical value.
$dt$	58	differential of time.
$W$	2	transmission probability (theoretical).
$W_{\nu}$	12	angular transmission probability.
$dW_{\theta}$	12	incremental transmission probability.
$\gamma$	12	angle.
$\Delta$	36	the difference ( $P_{\theta}^x - P_{\theta}^t$ ).
$\Delta H_{298}^{\circ}$	66	standard enthalpy change.
$\delta_1, \delta_2$	36	functions of $P_{\theta}^x$ and $I_{\theta}$ .
$\theta$	3	angle, especially the angle between a molecular trajectory and the orifice axis.
$\theta$	58	temperature, absolute (section IV only).
$\theta^*$	37	$\theta^* = \arctan (r_o + r_L) / L$ ; see Figure 1.
$\mu_o$	33	molecular flux incident on orifice entrance.
$\nu$	33	index.
$\pi$		3.14159
$\tau$	58	interval of time.
$\phi_i$	16	total recoil force for effusion from ideal orifice.
$d\phi$	16	incremental recoil force.
$\psi(x)$	10	normalized molecular flux on orifice walls.
$\Omega_d$	34	solid angle subtended at orifice by molecular beam detector aperture.
$w$		subscript; refers to a solid angle.
$dx$	12	incremental solid angle.

## SECTION I

### INTRODUCTION

The Knudsen effusion technique<sup>1,2</sup> is widely used, in varied guises, to obtain vapor and/or dissociation pressure data, especially at high temperatures. In actual laboratory operation the conditions under which effusion occurs are rarely, if ever, the ideal conditions assumed in the derivation of the simple Knudsen equation. This report summarizes work on several approaches designed to clarify the understanding of the effusion process under non-ideal conditions. More detailed introductory paragraphs are included in each of the following sections.

## SECTION II

### THEORETICAL ANALYSIS OF MOLECULAR FLOW THROUGH CONICAL ORIFICES

Vapor pressures and the composition of vapors at high temperatures are often determined by effusion techniques<sup>3</sup>, e.g., Knudsen effusion, torsion-Knudsen-effusion-recoil, and target-collection methods; furthermore, mass spectrometry of high temperature vapors is often facilitated by the use of an effusion cell as the vapor source<sup>3</sup>. Derivation of thermodynamically significant data from the results of effusion experiments requires knowledge of the relation between the measured quantities and the equilibrium pressure in the cell; this relation must take into account, among other factors, the non-ideality<sup>4</sup> of the geometry of physically-realizable effusion orifices.

The effect of orifice geometry upon the rate of molecular effusion through the orifice has been analyzed by several investigators<sup>5-9</sup>, whose results have usually been given as numerical values for the transmission probability, i.e., the probability that a molecule which enters the orifice through one end will exit from the opposite end. The effect of orifice geometry upon the angular distribution of molecules effusing from an orifice has received less attention but an analysis<sup>10</sup> for cylindrical orifices has been made and the results have been used<sup>11</sup> to obtain the "recoil-force correction factors" applicable to torsion-Knudsen-effusion-recoil measurements<sup>3</sup>.

In Part I<sup>12</sup> of this report and in a contribution to "Condensation and Evaporation of Solids"<sup>13</sup> (subsequently cited as CES) we have presented an analysis of the flow of rarefied gases through and from conical orifices. Equations were derived for calculation of the incident molecular flux density along the orifice walls, the transmission probability of the orifice, the angular distribution of molecules leaving the orifice, and various other functions. In Part I, but not in CES, the results of extensive computations of the various functions were reported; for convenience, one table and two Figures from Part I are repeated herein, and the results discussed briefly. Subsequently, these results are compared with other theoretical results; comparison with experimental results is deferred to Section III C and IV of this report.

In the last portion of this Section we shall exploit the angular distribution functions for conical orifices, which have not previously been available, to consider the determination of an optimum orifice geometry (within the class of right circular cones) for particular experimental configurations.

#### A. RESULTS OF THE NUMERICAL CALCULATIONS

In Figure 1 the various critical orifice parameters are defined by illustration. Values of the transmission probability  $\underline{W}$ , and the recoil-force correction factor  $\underline{f}$  are given in Table 1, and in Figures 2 and 3, respectively, for conical orifices with  $0 \leq (L/r_0) \leq 10$  and with  $-90^\circ \leq \underline{T} \leq 90^\circ$ , i.e., for both converging ( $\underline{T}$  negative) and diverging ( $\underline{T}$  positive) conical orifices. Transmission probabilities are given only for the diverging

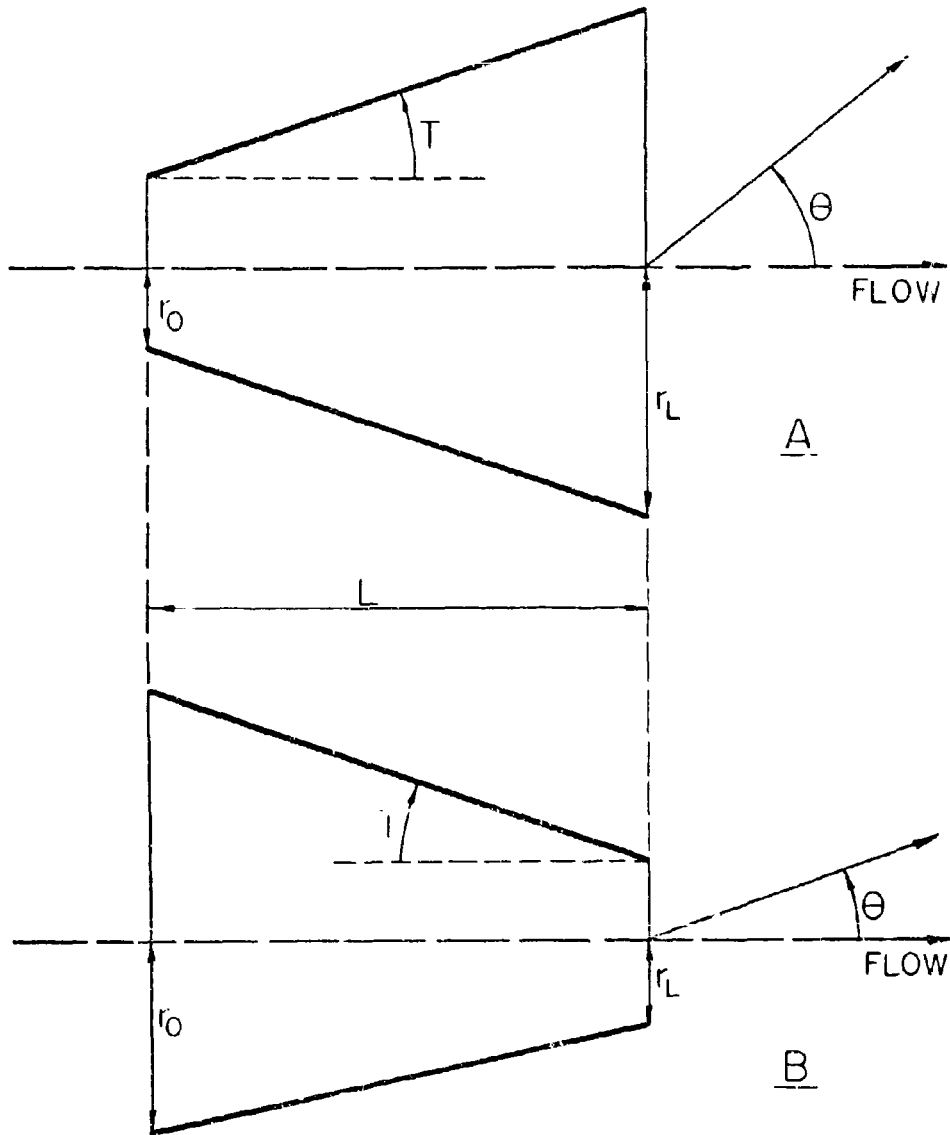


Figure 1. Conical Orifices and Parameters: A, Diverging Configuration,  $T$  positive; B, Converging Configuration,  $T$  negative.

TABLE I

TRANSMISSION PROBABILITIES AND RECOIL FORCE CORRECTIONS  
FOR CONICAL ORIFICES

T	$(L/r_m)^a$	W	f	$(f^*/r_m^2)^a$
0°	0.1	0.952399	0.968322	
	0.2	0.909215	0.937308	
	0.4	0.82408	0.87847	
	0.6	0.77115	0.82471	
	0.8	0.71778	0.77620	
	1.0	0.67198	0.73269	
	2.0	0.5142	0.5725	
	4.0	0.3566	0.4024	
	6.0	0.2754	0.3125	
	8.0	0.2253	0.2564	
10.0	0.1909	0.2177		
10°	0.1	0.967347	0.986104	0.980330
	0.2	0.93835	0.97200	0.96127
	0.4	0.88938	0.94451	0.92584
	0.6	0.84990	0.91904	0.89445
	0.8	0.8176	0.8960	0.8670
	1.0	0.7908	0.8756	0.8432
	2.0	0.7058	0.8035	0.7621
	4.0	0.6348	0.7381	0.6899
	6.0	0.6051	0.7107	0.6589
	8.0	0.5895	0.6970	0.6425
10.0	0.5802	0.6892	0.6328	
20°	0.1	0.978646	0.999546	0.988540
	0.2	0.96027	0.99816	0.97764
	0.4	0.93057	0.99407	0.95804
	0.6	0.90793	0.98941	0.94150
	0.8	0.89034	0.98492	0.92770
	1.0	0.87642	0.98087	0.91625
	2.0	0.8370	0.9682	0.8813
	4.0	0.8108	0.9633	0.8564
	6.0	0.8022	0.9660	0.8480
	8.0	0.7984	0.9699	0.8442
10.0	0.7963	0.9736	0.8421	

$T$	$(L/r_m)^a$	$W$	$f$	$(f^*/r_m^2)^a$
30°	0.1	0.986915	1.008954	0.993868
	0.2	0.976141	1.016307	0.988198
	0.4	0.95973	1.02782	0.97848
	0.6	0.94812	1.03652	0.97079
	0.8	0.9396	1.0434	0.9648
	1.0	0.93338	1.04919	0.96004
	2.0	0.9177	1.0687	0.9473
	4.0	0.9095	1.0908	0.9401
	6.0	0.9073	1.1044	0.9381
	8.0	0.9065	1.1140	0.9373
10.0	0.9060	1.1212	0.9369	
40°	0.1	0.992680	1.014589	0.997083
	0.2	0.987008	1.026941	0.994494
	0.4	0.97902	1.04683	0.99034
	0.6	0.97389	1.06220	0.98732
	0.8	0.97044	1.07444	0.98513
	1.0	0.96806	1.08446	0.98352
	2.0	0.96288	1.11632	0.97974
	4.0	0.9607	1.1462	0.9780
	6.0	0.9603	1.1618	0.9776
	8.0	0.9601	1.1720	0.9775
10.0	0.9599	1.1793	0.9774	
45°	0.1	0.994775	1.016077	0.998104
	0.2	0.990881	1.029628	0.996468
	0.4	0.985662	1.051287	0.993949
	0.6	0.98249	1.06782	0.99221
	0.8	0.98047	1.08086	0.99101
	1.0	0.97912	1.09143	0.99015
	2.0	0.9764	1.1242	0.9883
	4.0	0.9754	1.1536	0.9875
	6.0	0.9752	1.1684	0.9874
	8.0	0.9751	1.1778	0.9873
10.0	0.9750	1.1844	0.9873	
50°	0.1	0.996420	1.016729	0.998831
	0.2	0.993877	1.030684	0.997855
	0.4	0.99066	1.05267	0.99642
	0.6	0.98883	1.06918	0.99549
	0.8	0.98772	1.08202	0.99489
	1.0	0.98701	1.09231	0.99447
	2.0	0.98570	1.12355	0.99363
	4.0	0.9853	1.1504	0.9933
	6.0	0.9852	1.1636	0.9933
	8.0	0.9851	1.1717	0.9932
10.0	0.9851	1.1774	0.9932	

$T$	$(L/r_m)^a$	$W$	$f$	$(f^*/r_m^2)^a$
60°	0.1	0.998591	1.015712	0.999644
	0.2	0.997715	1.028324	0.999374
	0.4	0.996761	1.047307	0.999026
	0.6	0.996304	1.060889	0.998831
	0.8	0.99606	1.07108	0.99873
	1.0	0.99592	1.07904	0.99866
	2.0	0.99571	1.10207	0.99854
	4.0	0.9957	1.1205	0.9985
	6.0	0.9957	1.1289	0.9985
	8.0	0.9956	1.1338	0.9985
10.0	0.9956	1.1372	0.9985	
70°	0.1	0.999631	1.011961	0.999936
	0.2	0.999450	1.020864	0.999895
	0.4	0.999296	1.033229	0.999853
	0.6	0.99924	1.04141	0.99983
	0.8	0.99921	1.04724	0.99982
	1.0	0.99920	1.05160	0.99982
	2.0	0.9992	1.0635	0.9998
	4.0	0.9992	1.0721	0.9998
80°	0.1	0.999966	1.006048	0.999999
	0.2	0.999957	1.009755	0.999997
	0.4	0.999951	1.014072	0.999996
	0.6	0.99995	1.01651	1.00000
	0.8	0.99995	1.01809	1.00000
	1.0	0.99995	1.01919	1.00000
	2.0	1.0000	1.0219	1.0000
	4.0	1.0000	1.0236	1.0000

a.  $r_m$  = radius of smaller end of orifice.  $(f^*/r_m^2)$  is the appropriate recoil force correction for Converging orifices when  $(L/r)$  for the orifice is calculated with  $r_m$  rather than  $r_0$  (see Figure 1 and references 12 and 14).

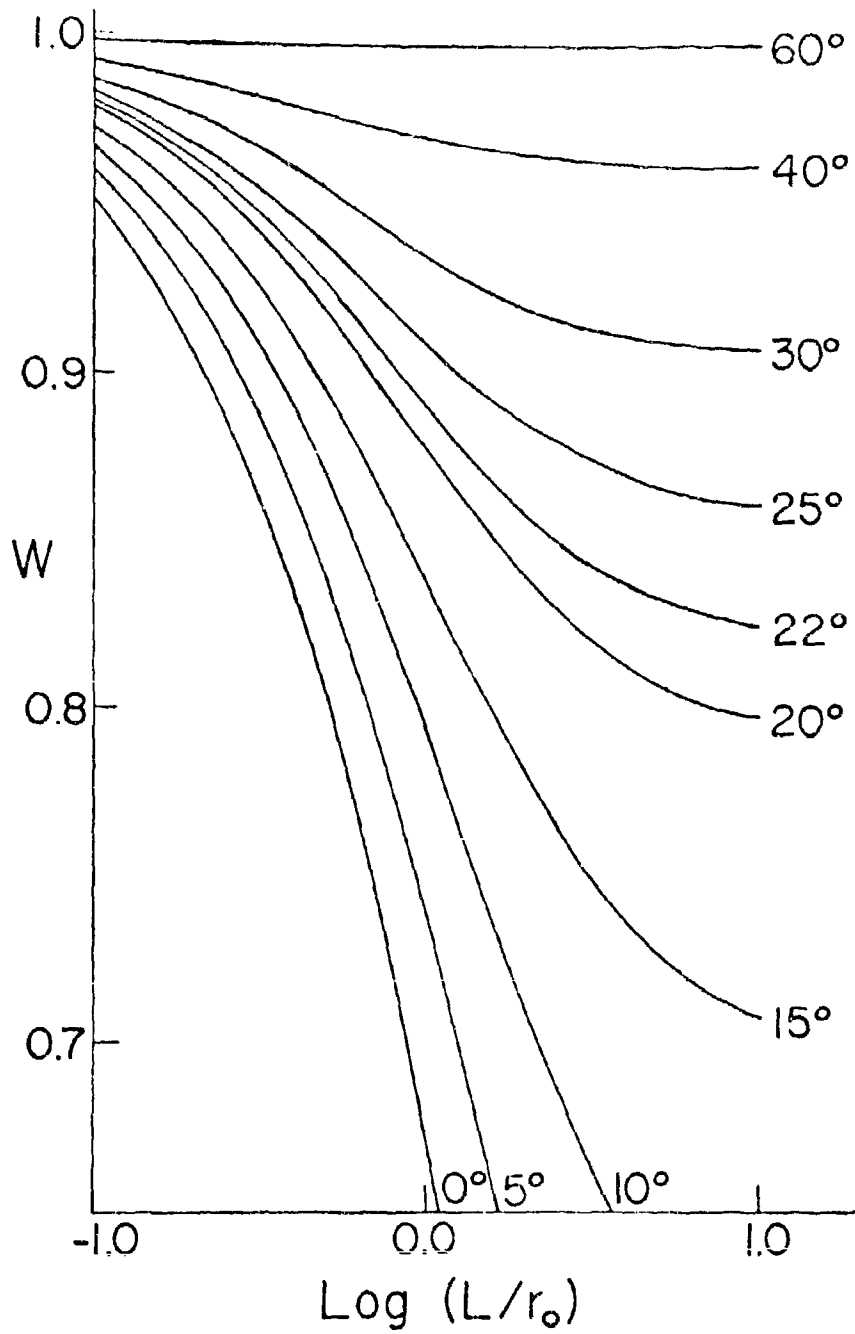


Figure 2. The Transmission Probability  $W$  as a function of  $\log(L/r_0)$  at various values of  $I$ .

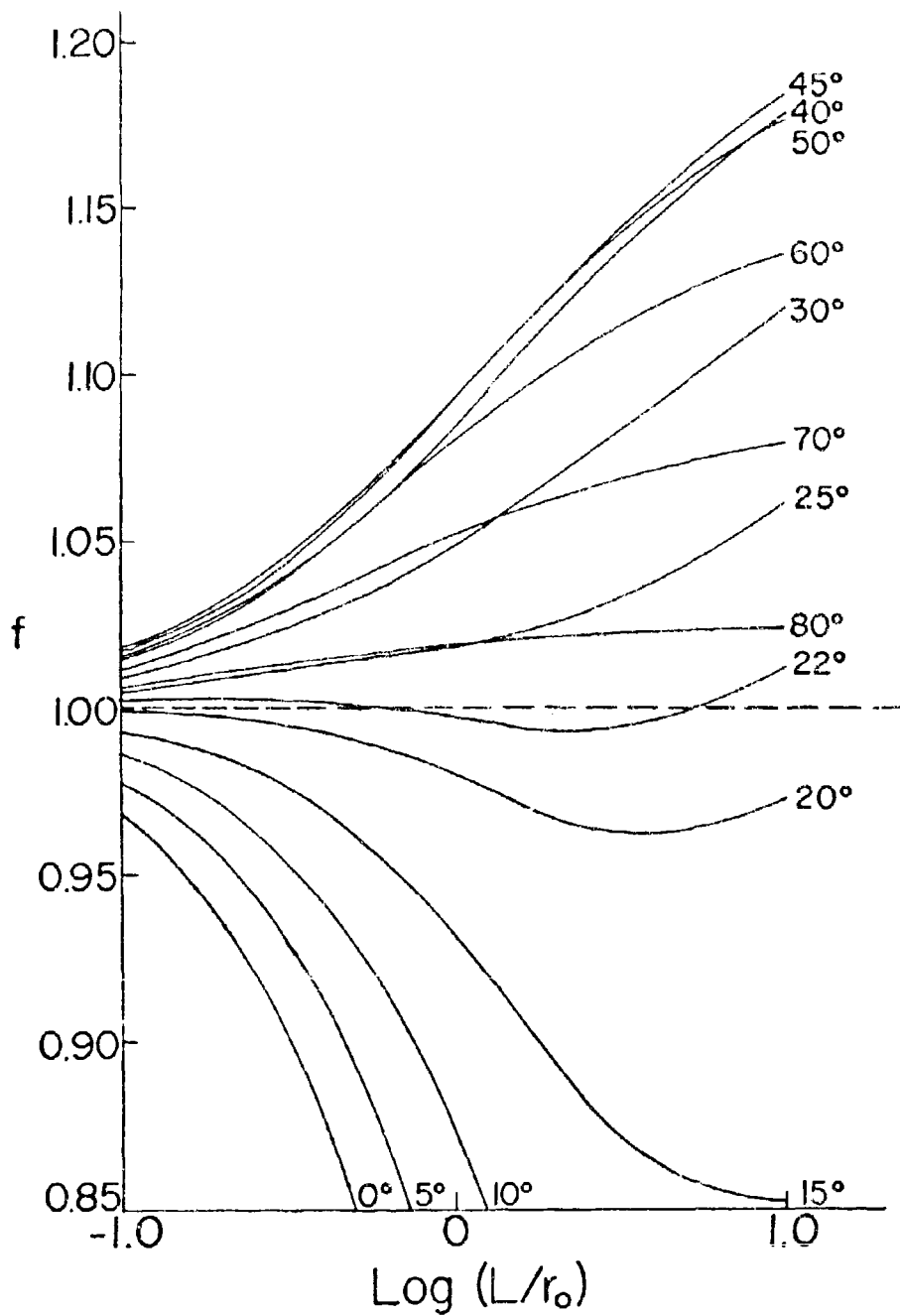


Figure 3. The Recoil Force Correction  $f$  as a function of  $\log(L/r_0)$  at various values of  $T$ .

configuration because, for a given orifice geometry,  $\underline{W}$  is the same for gas flow in either direction<sup>14</sup>. The logarithmic scale on the abscissa of Figures 2 and 3 is used only to simplify presentation of the results.

Table 1 and Figure 2 reveal no unexpected variation of  $\underline{W}$ ; it decreases with increasing  $L/r_0$  and increases as  $|\underline{T}|$  increases, as would be predicted intuitively. However, Figure 3 reveals an unexpected variation of  $\underline{f}$  with  $\underline{T}$ : for  $\underline{T} > 22^\circ$ ,  $\underline{f}$  is greater than unity. Hence, the recoil force generated by molecular effusion from a conical orifice with  $\underline{T} > 22^\circ$  is greater than that from the corresponding<sup>4</sup> ideal orifice. This result arises because (1) the average angle at which molecules effuse from conical orifices is smaller than for the ideal orifice, and (2) as  $\underline{T}$  increases above  $20^\circ$ , the transmission probability rapidly approaches unity; the momental component along the conical orifice axis is therefore greater than that along the ideal orifice axis and the recoil force is greater. This "focusing" effect of conical orifices is a maximum at  $\sim 45^\circ$ , the precise value depending on  $(L/r_0)$ .

Numerical values for various other quantities, e.g., the incident molecular flux on the orifice wall and the angular distribution of effusing molecules, have been calculated but are not presented here; an extensive tabulation of these functions is available elsewhere<sup>14</sup>.

## B. COMPARISON WITH OTHER THEORETICAL RESULTS

It was shown in Part I and in CES that, where comparison was possible, the results presented were in agreement with those of other workers. In particular, our results are in excellent agreement with the transmission probabilities of Iczkowski, et al.<sup>11</sup> for conical orifices, and with the closely-bounded values for the transmission probabilities of cylindrical orifices obtained by DeMarcus and Hopper<sup>12</sup>. In view of the different approaches, the independent verification of derivations, and the considerably different numerical techniques used in solving the integral equations, by four groups<sup>5, 9, 13, 14</sup> there can be little doubt of the validity of the numerical values for the transmission probability for cylindrical and conical orifices; these values apply rigorously only to the assumed model, of course.

We know of no other analysis of angular distribution for conical orifices, and for cylindrical orifices only of Clausing's analysis<sup>10</sup>. Clausing assumed that the normalized incident density (or molecular flux) on the walls of a cylindrical orifice could be expressed as a linear function of the distance, along the orifice axis, from the entrance. The accuracy of this approximation has been discussed by Edwards<sup>16</sup> who has also shown that, with this approximation, Clausing's distribution function<sup>10, 11</sup>  $T(\theta)$  may be derived in detail directly from our more general distribution functions which apply to conical and cylindrical orifices; it has also been possible to integrate in closed form the resulting angular distribution equation for cylindrical orifices.

One further argument may be advanced for the validity of our angular distribution results. In solving the various equations<sup>13</sup> the first quantity obtained is  $\psi(x)$  the normalized incident density on the orifice walls; these values of  $\psi(x)$  are then used to obtain  $\underline{W}$  in a direct way. The same values of  $\psi(x)$  are used in the more involved computation of  $\underline{W}$  by numerical integration of the angular distribution functions. The two values of  $\underline{W}$  are in good agreement with each other<sup>13</sup> and, as already noted, with the values of Iczkowski, et al.<sup>8</sup>, which would seem to indicate that both  $\psi(x)$  and the angular distribution functions are correct.

It is difficult to compare our results with those of Davis, et al.<sup>17</sup>; their paper lacks detail in both derivation and results. Our impression is that their derivation is not rigorous. In any case the results shown in their Figure 7 for the transmission probability of "conical nozzles" appear to be higher than those of Table 1 by several percent for small angles  $\underline{T}$  and lower for large angles  $\underline{T}$ .

Sparrow and Jonsson<sup>13</sup> have also analyzed the mass flow through conical orifices and have used the results to formulate analysis of energy transfer between gas and orifice walls. If, in their equation (12) and the ordinate of their Figure 3,  $\underline{P}_2$  is made zero, the resulting term is equivalent to our transmission probability  $\underline{W}$ . The results in their Figure 3 appear to be in good agreement with values of  $\underline{W}$  in Table 1, and  $\underline{f}(x/L)$  of their figure (2) appear to agree with our  $\psi(x)$ <sup>14</sup>. Sparrow and Jonsson obtain a number of useful but seldom used relations (their equations 6-11), some of which we have also generated<sup>13, 14</sup>.

Richley and colleagues have recently reported a series of analyses of molecular flow through cylindrical tubes<sup>19a,c</sup>, converging and diverging tubes<sup>19b</sup> and slots<sup>19b,d</sup>, and through cylindrical tubes with contribution from surface diffusion<sup>19c,e</sup>. The investigation by Cook and Richley of angular distribution from cylindrical orifices is based on Clausing's analysis<sup>10</sup> which has already been correlated with the present results. In their analysis<sup>19b</sup> of flow through converging and diverging tubes and slots, Richley and Reynolds obtain, by iterative solution of the appropriate Fredholm integral equation, values for the normalized incident density  $\psi(x)$  on the orifice wall (their "flux ratio  $n_2/n_1$ ") and use these values to obtain the flux distribution over the plane of the exit end of the orifice; finally, the exit plane flux distribution is integrated over the exit area of the orifice to obtain the transmission probability  $\underline{W}$  (their  $\underline{P}_T$ ). The minor discrepancies which exist between their results and ours appear to arise from (1) their use of an iterative solution for  $n_2/n_1$  rather than our more direct solution<sup>13,14</sup> for  $\psi(x)$ , and (2) their introduction of an additional numerical integration (i.e., to evaluate the exit plane flux distribution) in the computational sequence leading to  $\underline{W}$ , rather than calculation of  $\underline{W}$  directly from the  $\psi(x)$  in one step<sup>13</sup>.

### C. OPTIMIZATION OF ORIFICE GEOMETRY

An orifice geometry will be considered optimum if, for any given rate of effusion, the quantity being measured is maximized with respect to the orifice parameters  $\underline{T}$  and  $(\underline{L}/\underline{r}_0)$ ; the effusion rate may always be adjusted, if necessary, by varying the orifice area  $\underline{a}_0$  while maintaining a fixed geometry, i.e., fixed values of  $\underline{T}$  and  $(\underline{L}/\underline{r}_0)$ . This criterion for optimization is directly applicable when any one of the following typical conditions exist: (a) a very small amount of sample is available; (b) introduction of new sample into the apparatus requires a comparatively long down-time (as in mass spectrometry); (c) the material under study vaporizes incongruently and vaporization characteristics change with the composition of the condensed phase; and (d) a low evaporation coefficient imposes the need to minimize the total flux from the cell, thereby minimizing the displacement of the actual pressure from the equilibrium value. Under each of

these conditions it is clearly desirable to maximize the measured quantity while simultaneously minimizing the total rate of effusion of sample from the cell.

We shall now determine the orifice geometry which maximizes each of the following: (1) the near-axial flux density of the effusing molecular stream; (2) the recoil force generated on the effusion cell; and (3) the force exerted on a target suspended in the effusing gas stream.

1. Optimization of Molecular Beam Intensity on and near the Orifice Axis. In Part I<sup>12</sup> and CES<sup>13</sup> we obtained expressions for what we shall here call the incremental transmission probability  $dW_\theta$ , i.e., the probability that a molecule which enters one end of the orifice will exit from the opposite end into the incremental solid angle  $d\omega$  located at angle  $\theta$  from the orifice axis. With the solid angle  $d\omega$  expressed in spherical coordinates and the assumption of circular symmetry in the distribution around the orifice axis, the equations may be written as

$$dW_\theta = 2Q_n \sin\theta \cos\theta d\theta; \quad (1)$$

the  $Q_n$  ( $n = 1, 2, 3$ ) are complicated functions of the orifice parameters  $T$ ,  $(L/r_0)$ , and, depending on the range in which  $\theta$  lies, also of  $\theta$ . The integral of  $dW_\theta$  over  $0 \leq \theta \leq \pi/2$  is just the transmission probability  $W$  (designated  $W_\theta$  in Part I and CES to distinguish a calculation from angular distribution considerations).

We now define the quantity  $W_Y$ ,

$$W_Y = \int_0^Y dW_\theta = \sum_{n=1}^3 \int_0^Y 2Q_n \sin\theta \cos\theta d\theta, \quad (2)$$

which may be called the angular transmission probability, i.e., it is the ratio of the number  $N_Y$  of molecules which effuse per second into a cone which is coaxial with the orifice and has semi-apex angle  $Y$ , to the number  $N_0$  of molecules which enter the orifice through  $r_0$  per second.

The quantity to be maximized is the ratio of  $N_Y$  to the total number  $N_L$  of molecules which effuse from the orifice, i.e.,  $N_Y/N_L = (N_Y/N_0)/(N_L/N_0) = W_Y/W$ , and from equation (2),

$$W_Y/W = (2/W) \int_0^Y Q_n \sin\theta \cos\theta d\theta. \quad (3)$$

If we restrict  $Y$  to Range I<sup>13, 14</sup> (i.e., to  $0 \leq Y \leq |T|$ ),  $Q_n$  becomes  $Q_1$

and is independent of  $\theta$ ; equation (3) may be now integrated to obtain

$$W_\gamma/W = (Q_1/W) \sin^2 \gamma; \quad 0 \leq \gamma \leq |\underline{T}|. \quad (4)$$

Quite obviously, the fraction of effusing molecules which flow into the cone defined by the orifice axis and the angle  $\gamma$  can be varied by varying  $\gamma$ ; the pertinent problem is to maximize that fraction for a given  $\gamma$  determined by a particular experimental apparatus. Considering then that  $\gamma$  is fixed, we re-write equation (4) as

$$W_\gamma/(W \sin^2 \gamma) = (Q_1/W), \quad (0 \leq \gamma \leq |\underline{T}|), \quad (5)$$

and note that the quantity  $(Q_1/W)$  now to be maximized is a function solely of orifice geometry.

A plot, prepared from data tabulated elsewhere<sup>14</sup>, of  $(Q_1/W)$  vs.  $\underline{T}$  for various  $(L/r_0)$  is given in Figure 4. It is readily apparent that a maximum exists at  $\underline{T} = 0^\circ$  for each  $(L/r_0)$  and that the maximum becomes sharper as  $(L/r_0)$  increases. We now note that under the restriction  $0 \leq \gamma \leq |\underline{T}|$ , when  $\underline{T} = 0^\circ$ ,  $\gamma$  can have only the value  $0^\circ$ ; hence, the points in Figure 4 for  $\underline{T} = 0^\circ$  apply only to the beam intensity along the orifice axis where  $\gamma = 0^\circ$ .

To determine whether  $W_\gamma/(W \sin^2 \gamma)$  is also a maximum at  $\underline{T} = 0^\circ$  when  $\gamma$  has typical experimental values of  $5^\circ$  and  $10^\circ$ , values of  $W_\gamma$  for cylindrical orifices ( $\underline{T} = 0^\circ$ ) have been calculated, in effect by integration of equation (2), but in fact from a closed-form solution<sup>14, 15</sup>. The results, plotted as  $W_\gamma/(W \sin^2 \gamma)$ , are in Figure 5 in which the curves for  $\underline{T} \leq -10^\circ$  and for  $\underline{T} \geq +10^\circ$  duplicate those of Figure 4 since in these ranges ( $\gamma \leq |\underline{T}|$ ).

It is evident in Figure 5 that for  $\gamma = 5^\circ$ ,  $W_\gamma/(W \sin^2 \gamma)$  is larger for  $\underline{T} = 0^\circ$  than for any  $\underline{T} \geq 5^\circ$ ; similarly, for  $\gamma = 10^\circ$   $(W_\gamma/W \sin^2 \gamma)$  is larger for  $\underline{T} = 0^\circ$  than for any  $\underline{T} > 10^\circ$ . It appears to be true in general (although we have not made extensive computations to confirm this) that for a given  $(L/r_0)$  and a given  $\gamma$ ,  $(W_\gamma/W \sin^2 \gamma)$  is larger for  $\underline{T} = 0^\circ$  than is  $(Q_1/W)$  for any  $\underline{T} \geq \gamma$ .

For a short orifice  $(L/r_0 < 2.0)$  and a given  $\gamma$ , the two quantities  $(Q_1/W)_{\underline{T}=\gamma}$  and  $(W_\gamma/W \sin^2 \gamma)_{\underline{T}=0}$  are the same within 1%; for longer orifices the difference is somewhat greater.

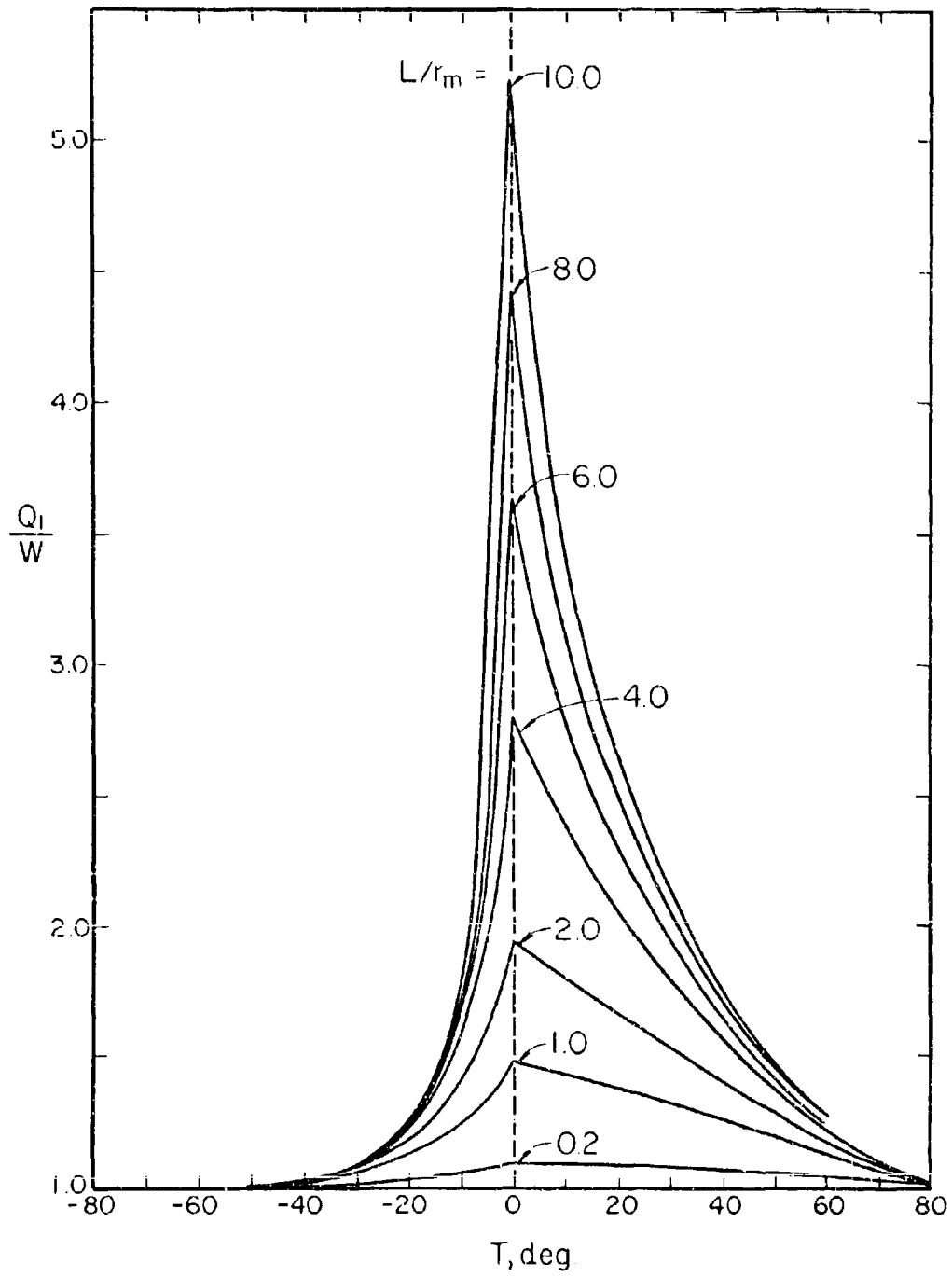


Figure 4. Collimating effect of various orifice geometries on effusing molecules.

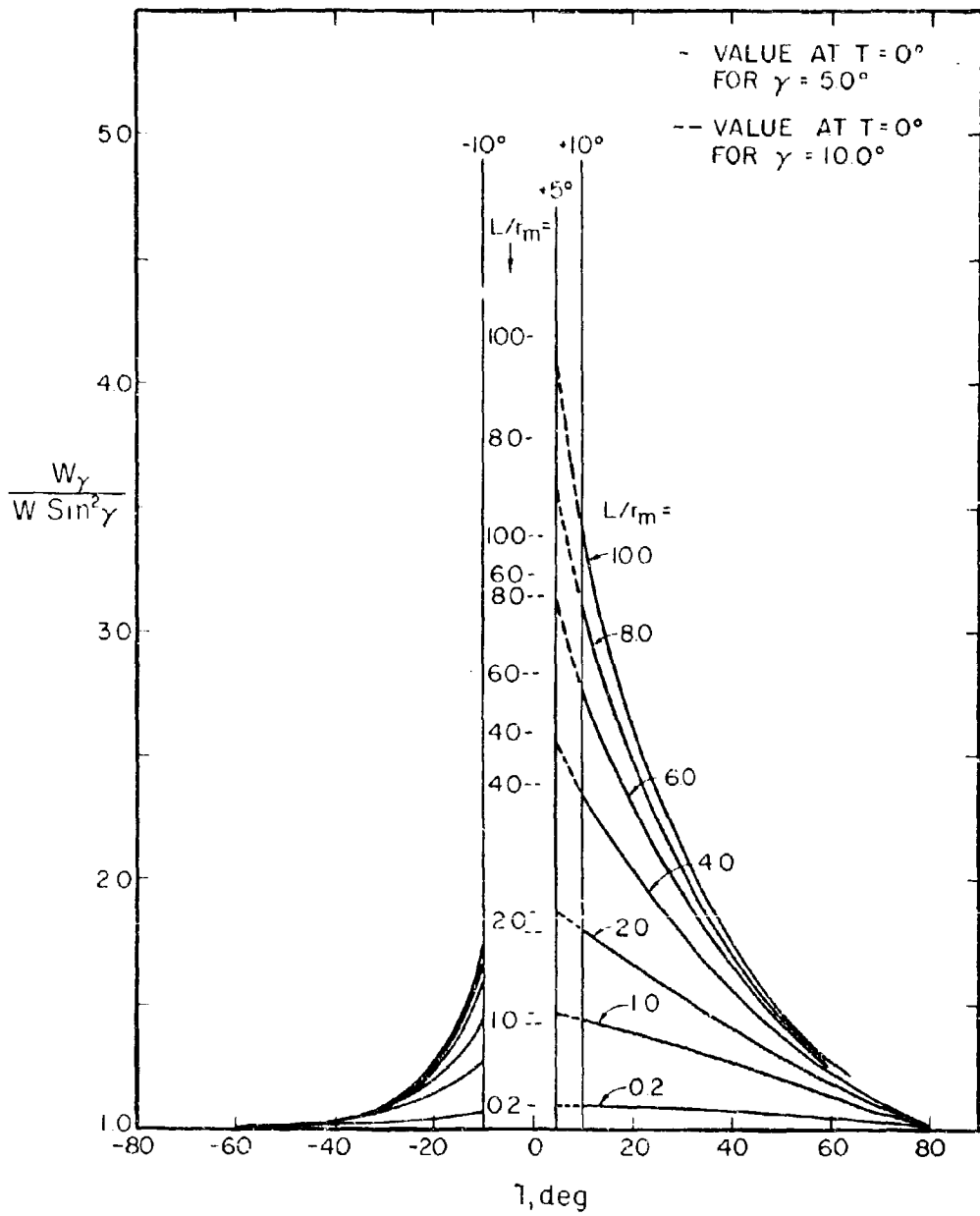


Figure 5. Collimating effect of various orifice geometries or effusing molecules.

There remains the question of the relative value of  $(\underline{W}_v/\underline{W} \sin^2 \gamma)$  for  $\underline{T} = 0^\circ$  and for some  $\underline{T} < \gamma$ , e.g., for  $\underline{T} = 0^\circ$  and  $\underline{T} = 5^\circ$  with  $\gamma = 10^\circ$ . For these cases  $(\underline{W}_v/\underline{W} \sin^2 \gamma)$  is larger for the conical orifice ( $\underline{T} > 0$ ) and increases slowly with increasing  $\underline{T}$ .

## 2. Optimization of the Effusive Recoil Force

In CES<sup>13</sup> (equation 19) it was demonstrated that the "incremental recoil-force correction factor"  $df_\theta$  (designated  $dF_\theta$  in CES), (i.e., the recoil force  $d\phi$  generated on a cell by effusion of molecules into the incremental solid angle  $d\omega$  at angle  $\theta$  from the orifice axis, divided by the total recoil force  $\phi_i$  for the corresponding<sup>4</sup> ideal orifice:  $df_\theta = d\phi/\phi_i$ ) is related to  $dW_\theta$  by

$$df_\theta = (3/2) \cos\theta dW_\theta$$

or, with equation (1),

$$df_\theta = 3Q_n \sin\theta \cos^2 \theta d\theta. \quad (6)$$

The (total) recoil force correction factor<sup>11,3</sup> is then given by

$$f = \int_{\theta=0}^{\theta=\pi/2} df_\theta = \sum_{n=1}^3 \int_{a_n}^{b_n} 3Q_n \sin\theta \cos^2 \theta d\theta; \quad (7)$$

The integration limits ( $a_n, b_n$ ) are discussed in CES and reference 14. The factor  $f$  is, of course, the quantity tabulated in Table 1.

Optimum orifice geometry in this situation requires maximization of recoil force for any given rate of effusion, which is equivalent to maximizing the ratio  $(f/W)$ . In Figure 6 this ratio is plotted vs.  $\underline{T}$  for various  $(L/L_0)$ . It is evident from Figures 2 and 3 that a maximum must occur in a plot of  $(f/W)$  vs.  $\underline{T}$ . However, it is rather surprising that this maximum occurs at, or very near,  $\underline{T} = +30^\circ$  for a very wide range of  $L/L_0$ . It is quite clear from Figure 6 that the optimum orifice for recoil force measurements would have a semi-apex angle  $\underline{T}$  of  $+30^\circ$  (i.e., diverging) and would be as long as practicable (within the range of  $L/L_0$  covered in Figure 6).

## 3. Optimization of the Force Exerted on a Target in an Effusing Molecular Beam: We shall restrict our consideration to cases in which the target is circular and coaxial with the orifice, and in which the molecules striking the target either all condense or all

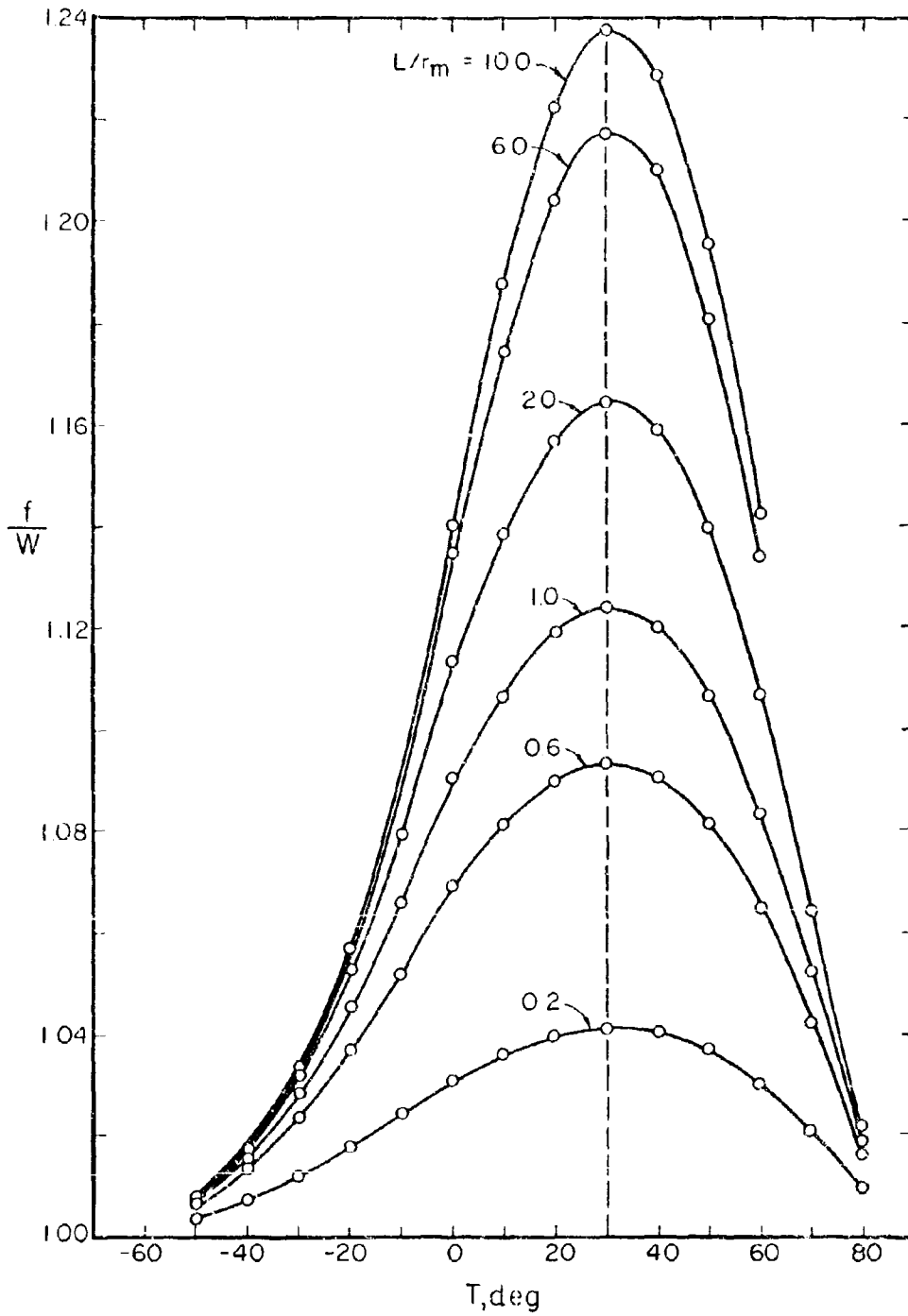


Figure 6. Optimization of orifice geometry for recoil force

revaporize. The angle subtended at the orifice by the target is designated  $2\gamma$ ;  $\gamma$  then has the same meaning as in equation 2.

If all molecules condense on the target, the ratio of the force  $F_\gamma$  exerted on the target to the force  $F_0$  which would be exerted by all molecules effusing from the corresponding<sup>4</sup> ideal orifice, is given by equation (7) with integration over  $0 \leq \theta \leq \gamma$ :

$$f_\gamma = F_\gamma/F_0 = \int_0^\gamma 3Q_n \sin\theta \cos^2\theta \, d\theta. \quad (8)$$

If  $\gamma$  is restricted to  $0 \leq \gamma \leq |\underline{T}|$  so that only  $Q_1$  (= constant) is required in the integration, equation (8) becomes

$$f_\gamma = Q_1(1 - \cos^3\gamma).$$

We wish to maximize this force at a given flow rate and for a given  $\gamma$ ; therefore, we write

$$\frac{f_\gamma}{W(1 - \cos^3\gamma)} = \frac{Q_1}{W}.$$

The quantity to be maximized is  $Q_1/W$ , as in subsection 1 above, and the arguments given there apply.

If the molecules revaporize from the target, there will be exerted on the target an additional force which, with all extra-orifice parameters fixed, will depend on the molecular flux onto the target<sup>3</sup>. Maximization of this flux at a given total flux from the orifice was the subject of subsection 1 above; again,  $Q_1/W$  is the quantity to be maximized.

## SECTION III

### MEASUREMENT OF ANGULAR DISTRIBUTION OF MOLECULAR FLOW THROUGH CONICAL ORIFICES

Of the various quantities which are derived in the theoretical analysis<sup>12, 13, 14</sup> (see Section II) and which are amenable to experimental study, the most critical is the angular distribution of molecules effusing from an orifice, i.e., the variation with  $\theta$  of the number  $\frac{dN_\omega}{d\omega}$  of molecules which pass per second from the orifice into the incremental solid angle  $d\omega$  located at angle  $\theta$  from the orifice axis. The theoretical analysis predicts that  $\frac{dN_\omega}{d\omega}$  is proportional to  $Q_n \cos \theta$ ;  $Q_n$  is the complicated function of orifice parameters which arises from the non-ideality of the orifice (for the ideal orifice,  $Q_n$  is always unity). Measurement of  $\frac{dN_\omega}{d\omega}$  or an equivalent quantity would provide experimental data which could be compared directly with theoretical values for  $Q_n \cos \theta$ .

#### A. EXPERIMENTAL APPARATUS

To accomplish these measurements the apparatus described briefly in this section (and in detail in Part II<sup>21</sup>) has been constructed. It is designed to allow a study of the effusion of a permanent gas (e.g.,  $N_2$ , He,  $CO_2$ ) at any suitable pressure from any orifice with a geometry which can be machined into a small circular plate. Permanent gases are used as effusants so that the apparatus can be operated at room temperature; concern that the reservoir-orifice system may not be isothermal is thereby minimized. For this advantage the ability to study the effusion process as a function of temperature is sacrificed.

The angular distribution of effusing molecules is determined by a molecular beam method<sup>22</sup> incorporating a modulated beam technique<sup>23</sup>. The reservoir from which the molecules effuse can be rotated on an axis which

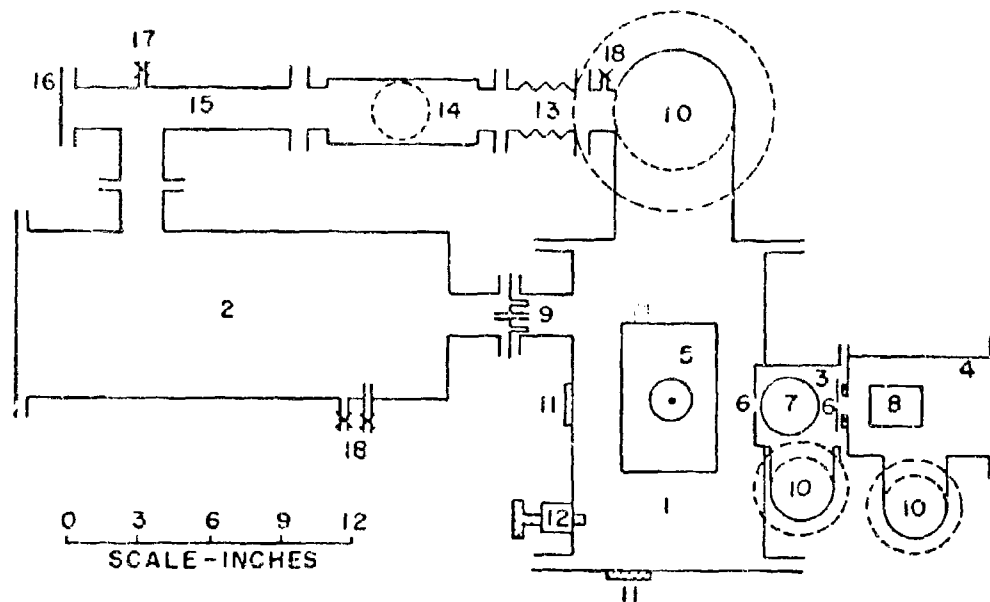
passes through, and is parallel to, the outer face of the orifice under study. Two stationary collimating orifices and the effusion orifice under study define a molecular beam, the beam is modulated by a mechanical chopper, and its intensity is determined by a neutral-beam detector.

The apparatus, a diagrammatic horizontal cross-section of which is shown in Figure 7, consists of five principal components: (1) The Main Vacuum Chamber, which can be maintained at a pressure very low with respect to the pressure in the gas reservoir, and which contains the rotating effusing cell; (2) The Gas Reservoir, a large chamber from which gas flows to the effusion cell and in which the pressure can be kept constant; (3) The Buffer Chamber, a small independently-pumped chamber which is separated from the main chamber by a plate containing the first collimating orifice, and which contains a chopper capable of interrupting the beam about one hundred times per second; (4) The Detector Chamber, an independently-pumped volume which is separated from the buffer chamber by a plate containing the second collimating orifice, and which contains an electron-impact molecular beam detector; (5) The Detector Electronics, which consists of a power supply for the beam ionizer and a system to amplify, measure, and record the ion current from the ion collector.

Each of these components was described in detail in Part II<sup>21</sup>; we shall describe here only significant modifications.

1. Modulation of Molecular Beam: As experimental techniques were refined, it became apparent that the frequency of the mechanical beam chopper (Figure 5, Part II) was not stable; the cause was found to be an overloaded driving motor. When the motor was replaced by one with higher torque, a new motor mounting and chopper housing (items 6 and 12, Figure 5, Part II) was fabricated from stainless steel (rather than brass). The new drive mechanism performed satisfactorily at times, but at others exhibited erratic chopping frequency. This difficulty arose from binding in the bearings which support the chopper shaft; the binding in turn was caused by a slight misalignment of the new motor mount/chopper housing when it was welded into the vacuum system.

At this point an electronically-driven tuning fork chopper



1. The Main Vacuum Chamber
2. The Gas Reservoir
3. The Buffer Chamber
4. The Detector Chamber
5. The Rotating Effusion Cell
6. The Beam Collimating Orifices
7. The Beam Chopper
8. The Beam Ionizer
9. Connectors for Tygon Tubulation Which Carries Gas from the Reservoir to the Rotating Cell
10. Pumping "I"s Which Accommodate Liquid Nitrogen Traps
11. Glass Windows
12. Rotary Vacuum Seal Through Which the Cell is Rotated
13. Brass Bellows
14. Globe Valve
15. Copper Pipe, 1  $\frac{1}{8}$  - in. Diameter
16. Port for Attaching 45-Liter Stainless Steel Tank
17. Valve for Introducing Effusant Gas
18. Connections to the Equibar Pressure Meter

Figure 7. Diagram of the Experimental Apparatus.

(type 40) was obtained. Nominal frequency of the chopper is 170 Hz; the chopping vanes attached to the tines are 10 mm high and have a maximum aperture of 8-10 mm. An electronic signal synchronized with the mechanical oscillations of the tuning fork is an inherent feature of the driving circuit, and is readily available for use as reference signal to the lock-in amplifier.

The new chopper was mounted in the BUFFER CHAMBER (Figure 7), but directly on the flange which is welded onto the MAIN VACUUM CHAMBER and which mates with the BUFFER CHAMBER flange. A new BUFFER CHAMBER equipped with aluminum-foil-sealed flanges<sup>24</sup> was fabricated from stainless steel.

No particular problems have been encountered with the tuning fork chopper; it was used in obtaining essentially all the data reported in Section B.

2. Detector Chamber: The Detector Chamber described in Part II operated satisfactorily, except that the ultimate pressure was relatively high ( $\sim 10^{-6}$  torr). Consequently, the life of the cathode was seriously shortened and the emission current available from the cathode was low. A new chamber was fabricated from stainless steel; aluminum foil flanges<sup>24</sup> were used, and all elastomer O-rings were eliminated; a more efficient liquid nitrogen trap ("Cryosorb") was inserted between the 2" diffusion pump and the chamber.

After a short bake-out at 100-200°C, the new Detector Chamber reaches  $5 \times 10^{-8}$  torr and operates at  $5 \times 10^{-7}$  torr with a beam, from a 0.1 torr source, entering the chamber.

The basic beam detector design and electronics have undergone no significant change. In the improved vacuum system the beam detector has performed quite satisfactorily; cathode life is remarkably lengthened (no quantitative data, as yet) and the emission current is increased by a factor of five.

3. Valve: The sensitivity of the beam detector cathode to oxygen made it desirable to keep the detector chamber evacuated continuously. To achieve isolation of the Detector (and Buffer) Chamber while the Main Chamber was opened, e.g., to change orifices, a sliding, O-ring

sealed valve was installed in the Main Chamber in such a way that closure of the valve sealed the first collimating orifice from the Main Chamber. The design of the valve was adapted from that of Sheffield<sup>25</sup>. It has worked satisfactorily.

4. Alignment of Orifices. The apparatus was designed and constructed to permit direct, visual alignment of the beam defining orifices, if the Faraday ion collector is removed from the beam detector assembly. Alignment of the effusion orifice and the various collimating orifices is rather easily accomplished by viewing with a low-powered telescope along the beam axis. However, with only this check on alignment it is possible for the plane of a given orifice to be tilted appreciably from the desired perpendicularity to the beam axis and the tilt be undetectable through the telescope.

Therefore, to insure parallelism of the planes of all beam-defining orifices while simultaneously establishing all orifices to be coaxial, a second alignment procedure was adopted. A low-powered telescope was fitted with a Gaussian eyepiece and the telescope operated as an autocollimator: A light source on the side of the eyepiece illuminated a cross-hair the image of which was then projected through the telescope onto an optically flat (both sides) front-surfaced mirror attached firmly to the orifice plate being aligned; the orifice plate was adjusted until the reflected image of the cross-hair coincided in the eyepiece with the image of the actual cross-hair; coincidence of the two images requires that the mirror (orifice plate) be perpendicular to the light (molecular) beam.

## B. EXPERIMENTAL RESULTS

Given the apparatus described above and the desired experimental measurement, i.e., the angular distribution of the effusing beam, experimental procedure was rather straightforward. After a given orifice was inserted into the Rotating Effusion Cell and aligned, the entire system was evacuated, e.g., overnight. At the beginning of a run the Gas Reservoir was isolated from the vacuum pumps (by closing valve 14, Figure 7) and filled with gas (helium, nitrogen, nitrous oxide) to the desired pressure as measured by a variable capacitance sensor (Equibar 120). Gases were obtained from high-pressure cylinders; pressure in the reservoir was controlled with a variable-leak valve (Type 9101-M) in the line between the usual cylinder regulator and the reservoir. After steady state flow was established throughout the gas flow system, the pressure in the reservoir remained surprisingly constant ( $\pm 1$  to 2%); a precision pressure regulator originally planned for insertion in the gas line between the cylinder regulator and the variable-leak valve was not required. Purity of the helium and nitrogen used was  $>99.5\%$  and of the  $N_2O$   $>98.0\%$ .

While steady gas flow was being established, the electronic circuitry was energized, adjustment of the lock-in amplifier checked, and, in particular, the filament current of the beam detector was adjusted to provide an electron emission current of 1.0mA. The isolating valve (section III.A.3) was then opened; the molecular beam could then pass to the detector and measurements were begun.

With the gas pressure in the reservoir constant, beam intensities in arbitrary units (i.e., the output from the lock-in amplifier) were recorded with the Effusion Cell rotated to orientations varying by angular increments of  $5^\circ$  between  $0^\circ$  and  $+90^\circ$  and also between  $0^\circ$  and  $-90^\circ$ . Typical concordance between data for  $+\theta$  and for  $-\theta$  is illustrated in Figure 8.

Angular distribution data have been obtained for five orifices with three gases at various pressures; Table 2 gives the details of the various parameters.

In Figures 9-14 the results of various measurements are plotted as  $I_\theta$  vs.  $\theta$ ;  $I_\theta$  is the relative molecular beam intensity normalized to 1.0 at

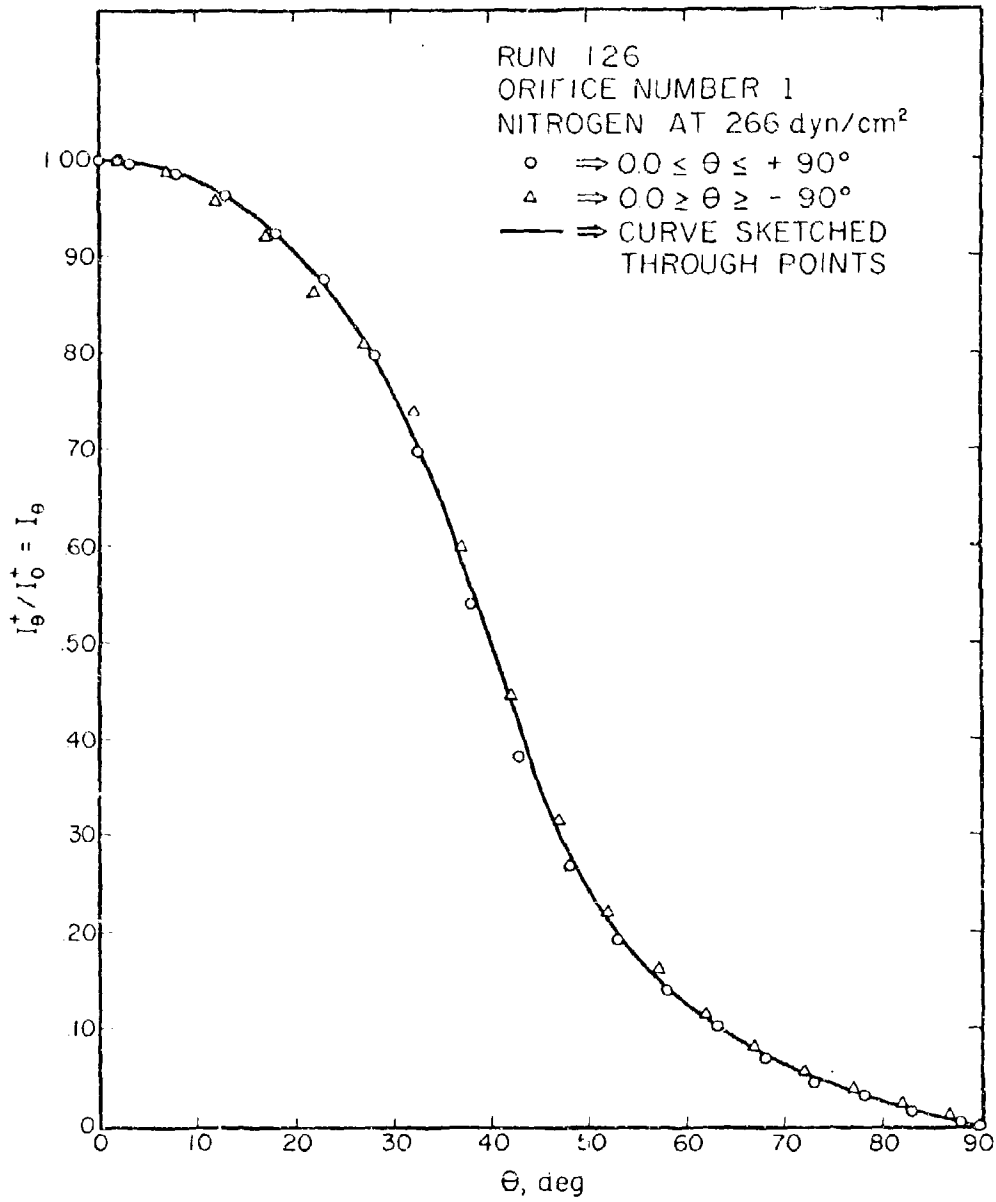


Figure 8. Experimental angular distribution data (Normalized beam intensity) for Nitrogen through orifice 1 ( $T = 25.65^\circ$  and  $(L/r_m) = 4.010$ ).

TABLE 2

ORIFICES, GASES, AND PRESSURES  
USED IN  
ANGULAR DISTRIBUTION STUDIES

Orifice Number	T, deg	L/r <sub>m</sub>	r <sub>m</sub> , cm	PRESSURE, millitorr		
				GAS		
				He	N <sub>2</sub>	N <sub>2</sub> O
1	25.65	4.010	0.0460	190., 70.0, 45.0, 20.2	670., 200., 72.7, 41.0, 27.5, 20.2, 7.0	195., 69.0, 45.0, 22.0, 6.9
2	8.50	10.08	0.0455	190., 71.0, 41.5, 21.0	660., 210., 70.0, 22.0, 7.0	207., 70.0, 41.5, 20.0, 6.2
3	-58.93	11.01	0.0292	230., 74.0, 41.5	700., 180., 66.0, 14.0	690., 200., 69.0, 24.0
4	27.98	1.987	0.0931	--	126., 120., 91.0, 73.0, 40.0, 24.0	--
5	0.0	2.439	0.0782	45.5, 33.0	70.0, 46.0, 23.5, 22.0, 8.9	--

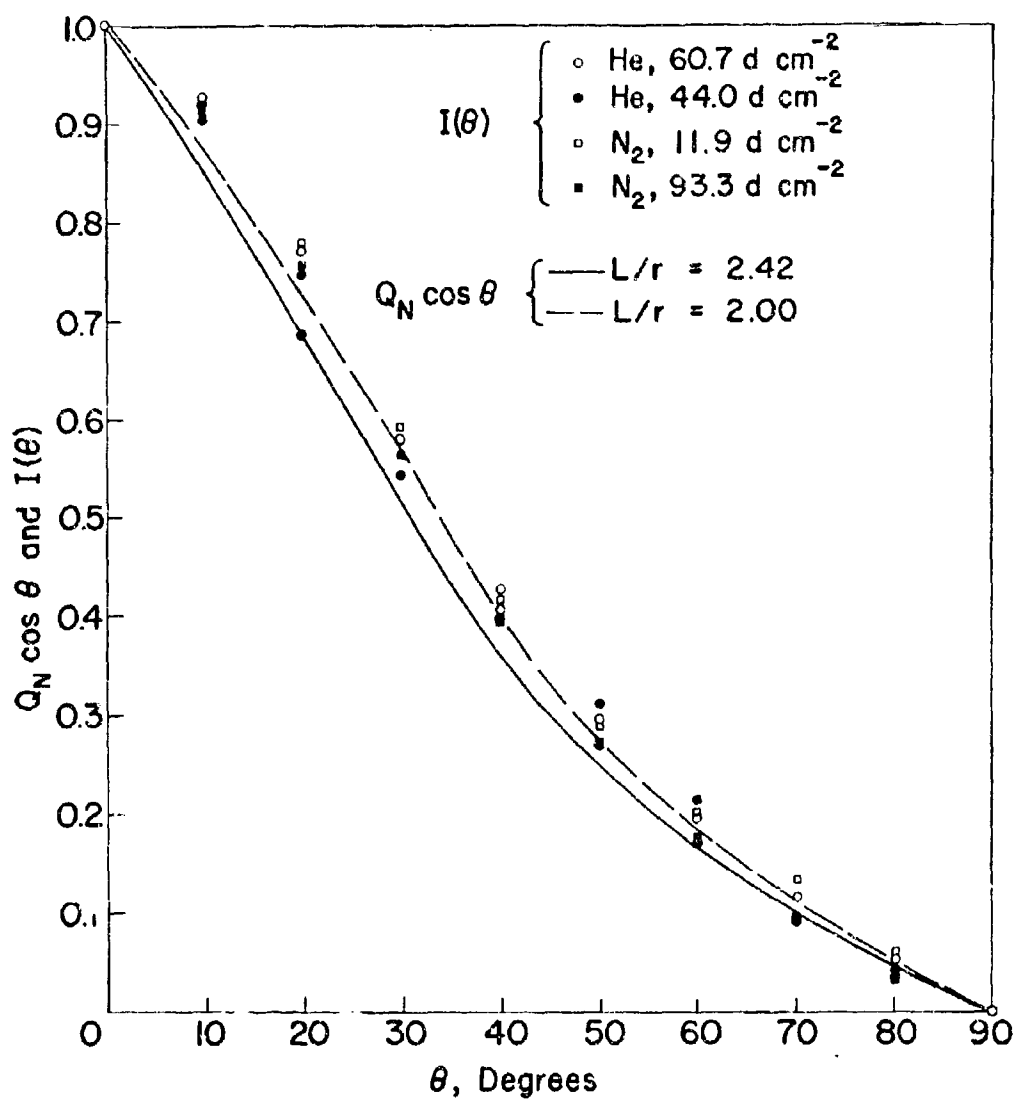


Figure 9. Experimental  $[I(\theta)]$  and Normalized Theoretical  $[Q_N \cos \theta]$  Angular Distribution Data for  $T = 0.0^\circ$ ,  $L/r_m = 2.44$ .

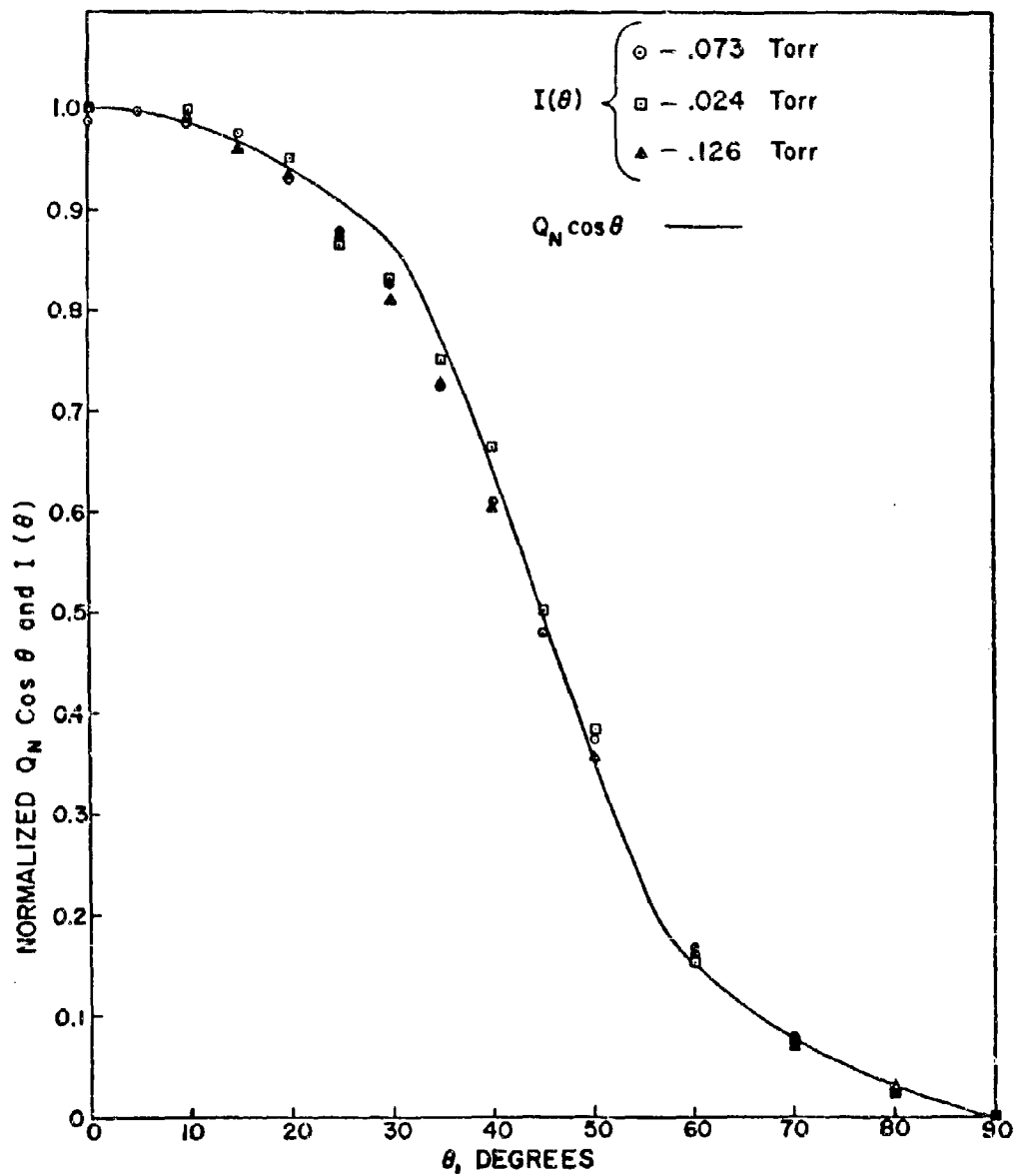


Figure 10. Experimental  $[I(\theta)]$  and Normalized Theoretical  $[Q_N \cos \theta]$  Angular Distribution Data for  $T = 30^\circ$ ,  $L/r_m = 2.0$ , with Nitrogen.

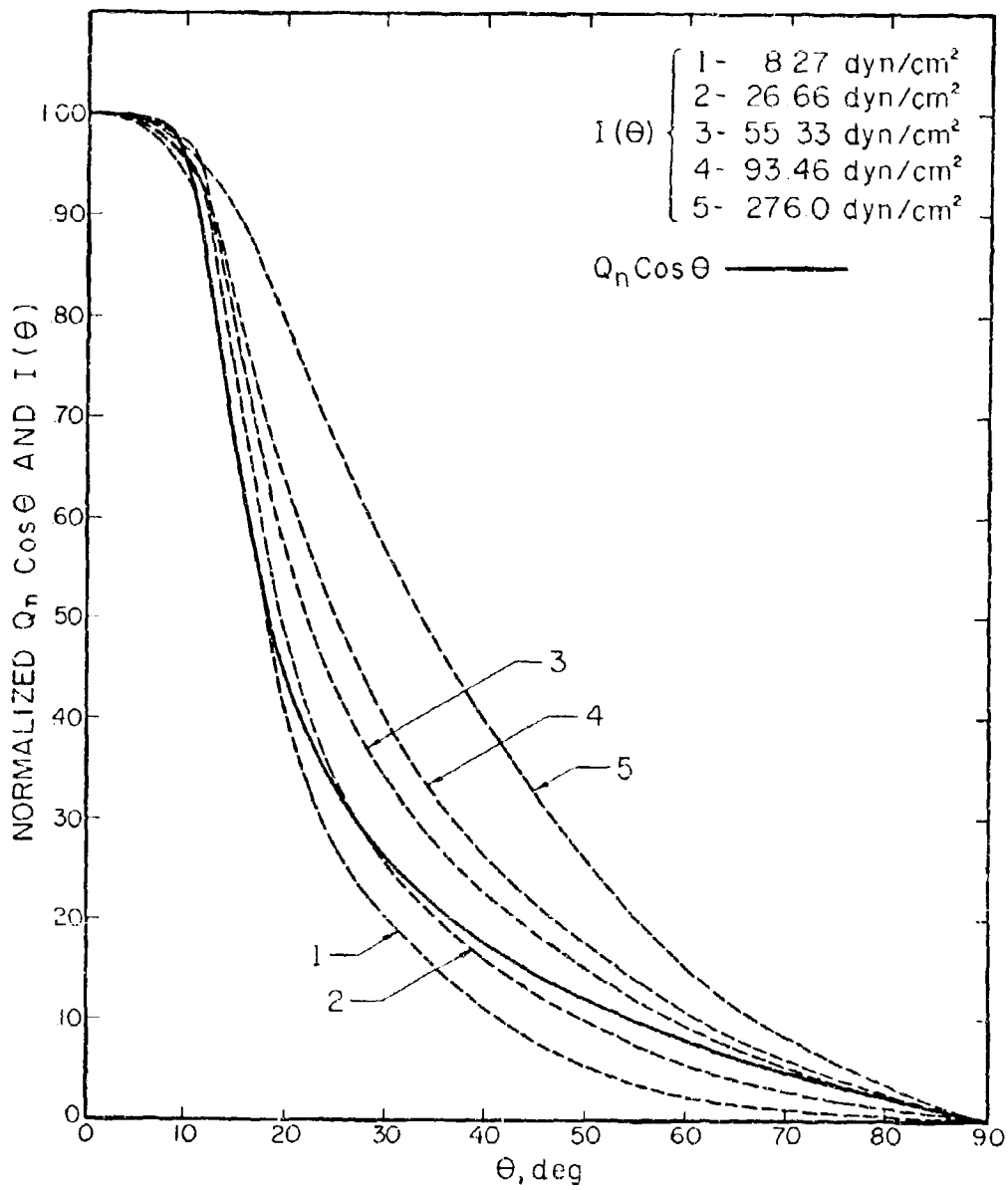


Figure 11. Normalized Experimental  $[I(\theta)]$  and Theoretical  $[Q_n \cos \theta]$  Angular Distribution Data for Nitrous Oxide through Orifice 2 ( $T = 8.500^\circ$ ,  $L/r_m = 10.08$ ).

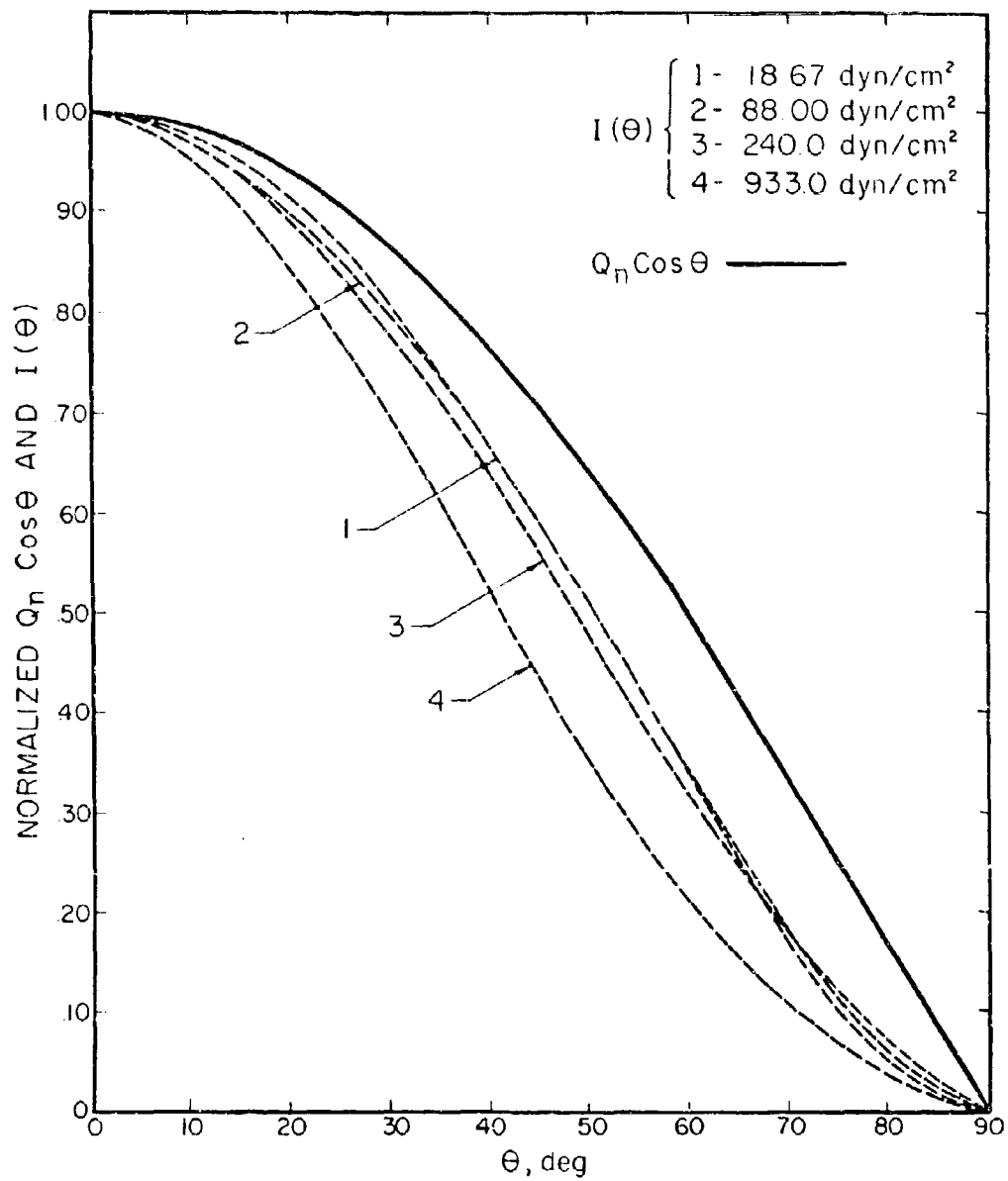


Figure 12. Normalized Experimental  $[I(\theta)]$  and Theoretical  $[Q_n \cos \theta]$  Angular Distribution Data for Nitrogen through Orifice 3 ( $T = -58.93^\circ$ ,  $L/r_m = 11.01$ ).

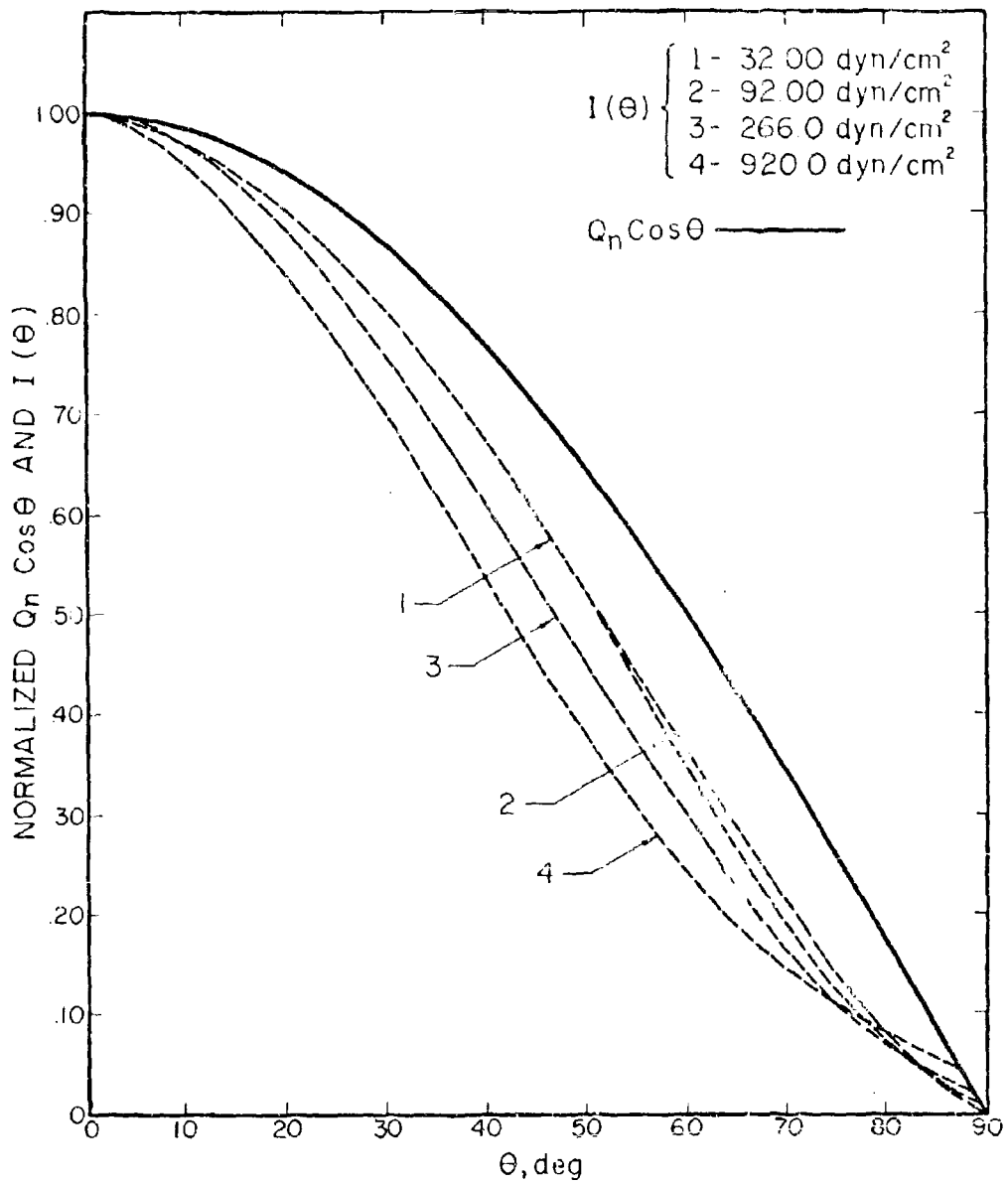


Figure 13. Normalized Experimental  $[I(\theta)]$  and Theoretical  $[Q_n \cos \theta]$  Angular Distribution Data for Nitrous Oxide through Orifice 3 ( $T = -58.93^\circ$ ,  $L/r_m = 11.01$ ).

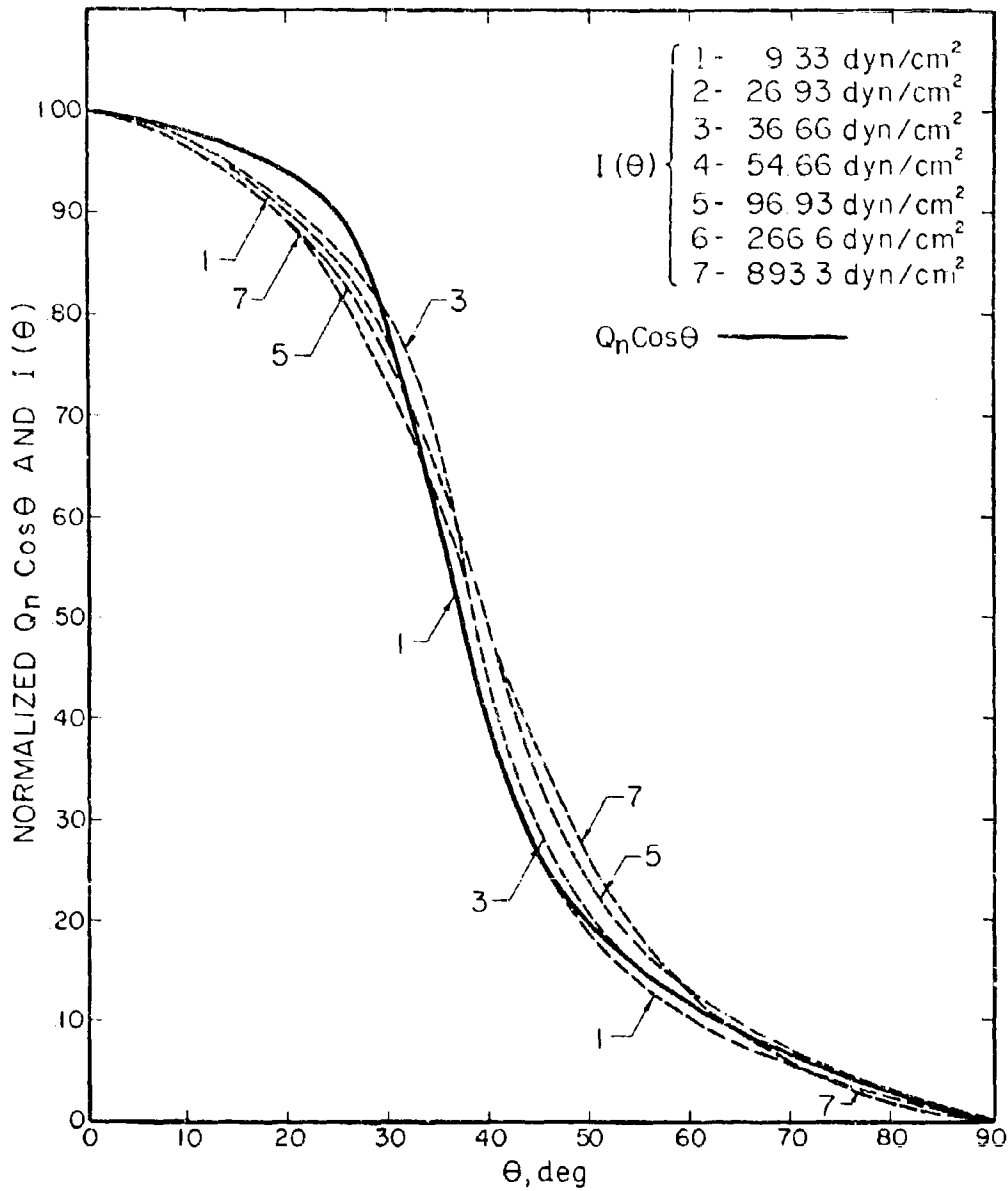


Figure 14. Normalized Experimental  $[I(\theta)]$  and Theoretical  $[Q_n \cos \theta]$  Angular Distribution Data for Nitrogen through Orifice 1 ( $T = 25.65^\circ$ ,  $L/r_m = 4.010$ ).

$\theta=0^\circ$ , i.e.,  $I_\theta = I_\theta^+/I_0^+$ , with  $I_\theta^+$  representing the measured ion current at  $\theta$ .

In Figures 9 and 10 the experimental points are shown, and the lines are drawn through theoretical values. In Figures 11-14, the dashed lines represent smoothed curves drawn through the experimental points for both positive and negative angles; the scatter of points about the smoothed curve in Figure 8 is typical, i.e., not the minimal. The solid line in each figure is drawn through theoretical values which are discussed in the following section.

### C. DISCUSSION

1. Remarks on Theory: Implicitly in Part I<sup>12</sup> and CES<sup>13</sup> and explicitly in Reference 14 the theoretical angular distribution is expressed as

$$dN_\theta(L) = 2\pi\mu_0 Q_n \sin\theta \cos\theta d\theta; \quad (9)$$

$dN_\theta(L)$  is the number of molecules which effuse per second into the solid angle  $2\pi \sin\theta d\theta$ ,  $\mu_0$  is the molecular flux incident on the entrance of the orifice, and  $Q_n$  ( $n = 1, 2, 3$ ) is the complicated function of  $L$ ,  $L/r_0$ , and  $\theta$  which describes deviations from the "ideal" cosine law distribution. We now define

$$Q_\nu = Q_n/\pi \quad (\nu = n = 1, 2, 3), \quad (10)$$

insert  $r_0$  explicitly ( $r_0$  and  $L$  are normalized to  $r_0 = 1$  in the theoretical analysis<sup>12-14</sup>), and write in terms of a generalized incremental solid angle  $d\omega$ :

$$dN_\theta(L) = \mu_0\pi r_0^2 Q_\nu \cos\theta (2\pi \sin\theta d\theta) \quad (11)$$

$$dN_\omega(L) = \mu_0\pi r_0^2 Q_\nu \cos\theta d\omega.$$

The transmission probability  $W$  may be expressed as (number of molecules effusing from orifice)/(number entering orifice), or with equation (11)

$$W = (1/\mu_0\pi r_0^2) \int \mu_0\pi r_0^2 Q_\nu \cos\theta d\omega \quad (a)$$

$$= \int Q_\nu \cos\theta d\omega \quad (b)$$

$$= \int_0^{\pi/2} Q_\nu \cos\theta (2\pi \sin\theta d\theta). \quad (c)$$

Equation (12c) may be compared with equation (1), if equation (10) is noted.

We assume that the aperture of the molecular beam detector subtends at the effusion orifice a solid angle ( $\Omega_d$ ) sufficiently small that  $Q_v \cos\theta$  may be considered constant over  $\Omega_d$ . For two angles  $\theta$  and  $\theta'$  we may now write

$$N_{\Omega}(L)_{\theta'} = \mu_{\text{on}} \pi r_0^2 Q_v' \cos\theta' \Omega_d \quad (a)$$

and (13)

$$N_{\Omega}(L)_{\theta} = \mu_{\text{on}} \pi r_0^2 Q_v \cos\theta \Omega_d. \quad (b)$$

The ratio of equation (13b) to (13a) is, if  $\theta'$  is taken as  $0^\circ$ ,

$$\left[ \frac{N_{\Omega}(L)_{\theta}}{N_{\Omega}(L)_{0}} \right]_{\text{th}} = \frac{Q_v \cos\theta}{(Q_v)_0} \quad (14)$$

Equation (14) gives the theoretical value of the ratio of (number entering detector at  $\theta$ ) to (number entering at  $\theta = 0^\circ$ ).

The basic assumption concerning the operation of the beam detector is that the measured ion current  $I^+$  is proportional to the number of neutral molecules entering the detector, or

$$\left[ \frac{N_{\Omega}(L)_{\theta}}{N_{\Omega}(L)_{0}} \right]_{\text{exp}} = \frac{I_{\theta}^+}{I_0^+} = I_{\theta} \quad (15)$$

We now define the symbol  $\ddagger$  to mean "is (theoretically) predicted to be equal to", and combine equations (14) and (15) to obtain

$$I_{\theta} \ddagger \frac{Q_v \cos\theta}{(Q_v)_0} \quad (16)$$

For any orifice, at  $\theta = 0^\circ$  equation (16) becomes

$$I_{\theta} = \frac{I_0^+}{I_0^{\ddagger}} = 1 + \frac{(Q_v)_0}{(Q_v)_0} \cdot 1 = 1; \quad (17)$$

hence, both the experimental and the theoretical results are self-normalizing to unity at  $\theta = 0^\circ$ . Equation (16) is the basis for the form of the graphs in subsection B.

As indicated in equation (17), the plotting method suggested by equation (16) and used in Figures 8-1, forces agreement between experimental and theoretical results at  $\theta = 0^\circ$ . Furthermore, the nature of the experiment essentially forces agreement at  $\theta = 90^\circ$ . Therefore, whatever the actual nature of the discrepancy between

experimental and theoretical results, in plots of  $I_\theta$  and  $Q_v \cos\theta / (Q_v)_0$  vs.  $\theta$  the apparent discrepancy near  $\theta = 0^\circ$  is small and any real discrepancies are forced to appear in midrange of  $\theta$  and are therefore overemphasized. To circumvent this difficulty Phipps and Adams<sup>23</sup> have introduced, and Wahlbeck and Wang<sup>27</sup> have also used, a probability density function  $P_\theta$  which we now consider.

The experimental probability density function  $P_\theta^x$  is defined<sup>23, 27</sup> by

$$P_\theta^x = I_\theta^+ / \int_0^{\pi/2} I_\theta^+ (2\pi \sin\theta \, d\theta). \quad (18)$$

Obviously, if normalized ion currents (cf. equation 15) are substituted for  $I_\theta^+$ ,  $P_\theta^x$  is unchanged:

$$P_\theta^x = I_\theta / \int_0^{\pi/2} I_\theta (2\pi \sin\theta \, d\theta) \quad (19)$$

We also note that since  $I_{\theta=0} = 1.0$ ,

$$P_0^x = 1 / \int_0^{\pi/2} I_\theta (2\pi \sin\theta \, d\theta) \quad (20)$$

and

$$P_\theta^x = I_\theta P_0^x. \quad (21)$$

It is apparent from equation (21) that a plot of  $P_\theta^x$  vs.  $\theta$  will differ from a plot of  $I_\theta$  vs.  $\theta$  only by the factor  $P_0^x$ . For a given set of  $[I_\theta, \theta]$  data  $P_0^x$  is obviously fixed, but there is no requirement on the constancy of  $P_0^x$  from run to run; hence,  $P_\theta^x$  is not self-normalized and can reflect discrepancies between experimental and theoretical data at  $\theta = 0^\circ$  as well as at other values of  $\theta$ .

The interpretation of  $P_\theta^x$  as a probability density function follows immediately from its definition (equation (18) or (19)):  $P_\theta^x \, d\omega$  is the probability that an effusing molecule will transpire  $d\omega$  at  $\theta$ , or stated differently,  $P_\theta^x$  is the fraction (of effusing molecules) which flow, per steradian, at  $\theta$ . With this interpretation of  $P_\theta^x$  and with equation (11) an expression for the corresponding theoretical quantity  $P_\theta^t$  may be obtained:

$$P_\theta^t = \frac{dN_\theta(L)}{d\omega \cdot N(L)} = \frac{\mu_0 \pi r_0^2 Q_v \cos\theta \, d\omega}{d\omega \cdot \mu_0 \pi r_0^2 W}$$

or,

$$P_\theta^t = (Q_v \cos\theta) / W \quad (22)$$

The quantity  $P_{\theta}^t$  also is not self-normalized, but may be converted to a self-normalized form by multiplying by  $W/(Q_v)_0$ ; the result is then to be compared with equation (16):

$$W P_{\theta}^t / (Q_v)_0 = (Q_v \cos \theta) / (Q_v)_0 \mp I_{\theta}. \quad (23)$$

From equations (23) and (21) one obtains

$$P_{\theta}^x \mp (Q_v)_0 / W. \quad (24)$$

From the above observations we draw the following conclusions:

- (1) A plot of  $P_{\theta}^x$  vs.  $\theta$  reveals no information not already provided by a plot of  $I_{\theta}$  vs.  $\theta$  and by the value of  $P_{\theta}^x$  (cf. equation 21)
- (2) If one attempts to normalize  $P_{\theta}^x$  via equation (23) and compare the results with  $I_{\theta}$  (e.g.,  $\delta_1 = I_{\theta} - P_{\theta}^x W / (Q_v)_0$ ), one obtains nothing new, since

$$\delta_1 = I_{\theta} - P_{\theta}^x W / (Q_v)_0 = I_{\theta} \{1 - P_{\theta}^x W / (Q_v)_0\} \quad (25)$$

and the bracketed portion of the equation is a constant for a given run. If, on the other hand, one attempts to compare  $I_{\theta}$  directly with  $W P_{\theta}^t / (Q_v)_0$  (equation 23) by defining

$$\delta_2 = [I_{\theta} - W P_{\theta}^t / (Q_v)_0] / [W P_{\theta}^t / (Q_v)_0],$$

one finds that

$$\delta_2 = [I_{\theta} (Q_v)_0 / W P_{\theta}^t] - 1, \quad (26)$$

and, by virtue of equations (17) and (22),  $\delta_2$  is inherently normalized to zero at  $\theta = 0^\circ$ . Furthermore, a plot of  $\delta_2$  vs.  $\theta$  is, except for a shift in the zero point of the ordinate caused by non-identity of  $P_{\theta}^x$  and  $(Q_v)_0 / W$  (cf. equation 24), identical to the more useful form now to be described.

- (3) The most informative scheme for comparing experimental and theoretical results is that obtained by defining, and plotting vs.  $\theta$ , the quantities  $\Delta$  and  $f(\Delta)$ :

$$\begin{aligned} \Delta &= P_{\theta}^x - P_{\theta}^t \\ f(\Delta) &= \Delta / P_{\theta}^t = (P_{\theta}^x / P_{\theta}^t) - 1. \end{aligned} \quad (27)$$

A plot of  $f(\Delta)$  vs.  $\theta$  provides a direct, non-normalized indication of the discrepancy between experimental and theoretical results, expressed as a fraction of the theoretical value. The only restriction on the value of  $f(\Delta)$  is that  $P_{\theta 0}^t = 0$  and  $P_{\theta 0}^x$  (i.e.,  $I_{\theta 0}$ ) is adjusted to zero by subtracting background ion current; therefore,  $f(\Delta)_{\theta 0} = 0$ . The one difficulty presented by the use of  $f(\Delta)$  is that at  $\theta > 70^\circ$   $P_{\theta}^x$  and  $P_{\theta}^t$  may be rather small (e.g. 0.02 of the value at  $\theta = 0^\circ$ ); the difference  $\Delta$  may be small compared to experimental error in obtaining  $I_{\theta}$ , but  $f(\Delta)$  can be quite large (e.g., 0.20 - 0.40) because  $P_{\theta}^t$  is small. In other words, the fractional errors are magnified as  $P_{\theta}^t$  approaches zero. For this reason, one might prefer to plot  $\Delta$  vs.  $\theta$ ; both types of plots are illustrated subsequently.

2. Experimental Results: Figures 15-20 present various portions of our results in the form:  $(P_{\theta}^x/P_{\theta}^t) - 1$  vs.  $\theta$ , i.e.  $f(\Delta)$  vs.  $\theta$ , except for Figure 16 which is a replot of Figure 15 in the form  $(P_{\theta}^x - P_{\theta}^t)$  vs.  $\theta$ , i.e.,  $\Delta$  vs.  $\theta$ . Comparison of Figures 15 and 16 illustrate the point made in the preceding section: the large excursions of  $f(\Delta)$  at  $\theta > 70^\circ$  do not realistically reflect the discrepancy between  $P_{\theta}^x$  and  $P_{\theta}^t$ . At  $\theta < 60^\circ$  plots of  $\Delta$  vs.  $\theta$  and of  $f(\Delta)$  vs.  $\theta$  are very similar except for scaling.

Figure 21 is a replot in the form  $[(I_{\theta}(Q_v)_0/WP_{\theta}^t) - 1]$  vs.  $\theta$ , i.e.  $\delta_2$  vs.  $\theta$ , (cf. equation 26) of Run 125 in Figure 15, and is included to illustrate two points: (1) a plot of  $\delta_2$  vs.  $\theta$  is normalized to zero at  $\theta = 0^\circ$ , and (2) except for point (1) and scaling, the shape of the curve is the same as that of  $f(\Delta)$  vs.  $\theta$  in Figure 15.

Before we examine the various curves in detail, it may be useful to note again the geometry of the conical orifice and the two important angles  $\Gamma$  and  $\theta^*$ ; these are illustrated in Figure 22 for the diverging orifice ( $\Gamma > 0$ ). For  $0 \leq \theta \leq \Gamma$ , the detector may receive molecules directly from all of the circular entrance to the orifice and from all elements of the orifice wall; this corresponds<sup>13</sup> to Range 1 and  $n = 1$

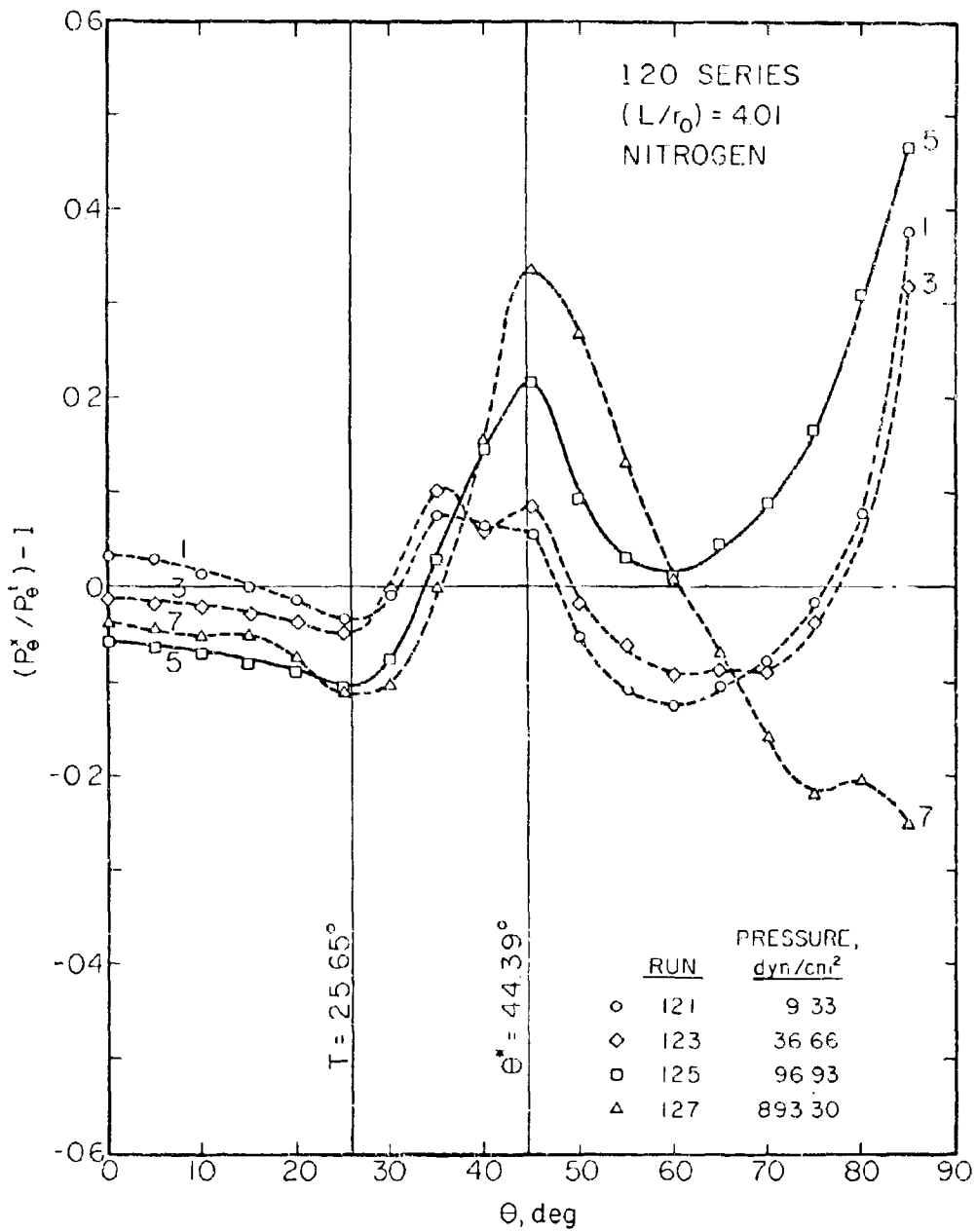


Figure 15.  $f(\Delta)$  plots for 120 series.

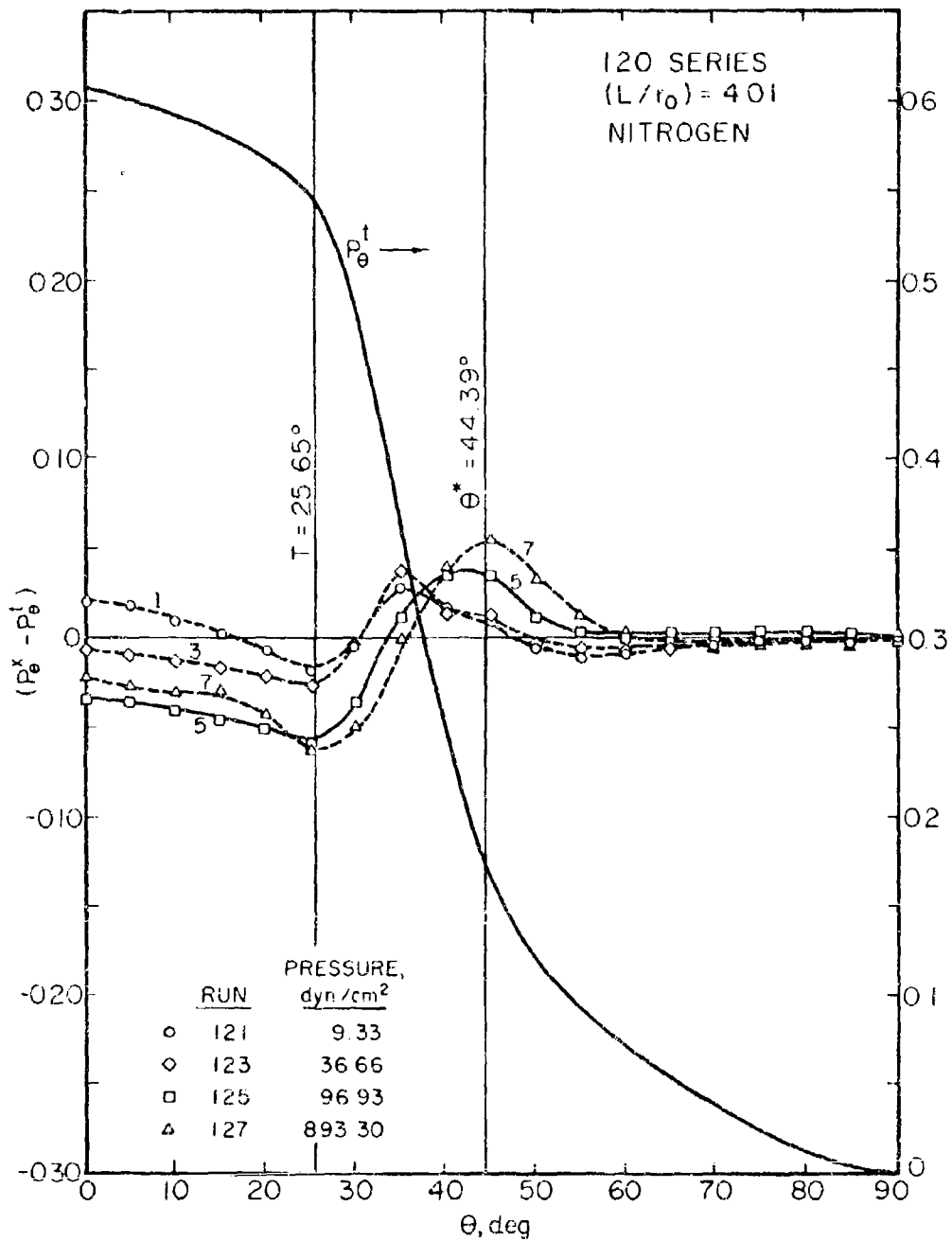


Figure 16.  $\Delta$  plots for 120 series.

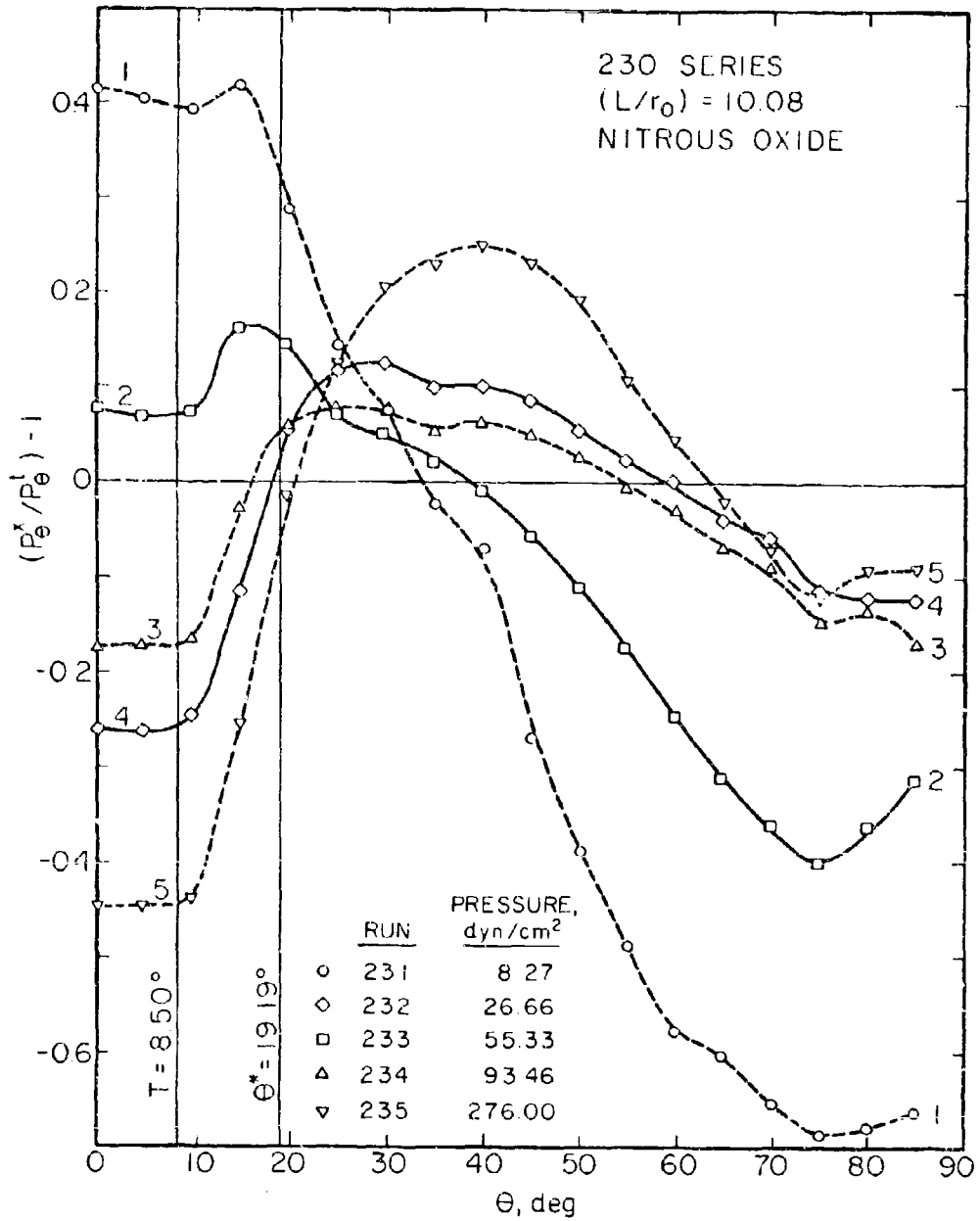


Figure 17.  $f(\Delta)$  plots for 230 series.

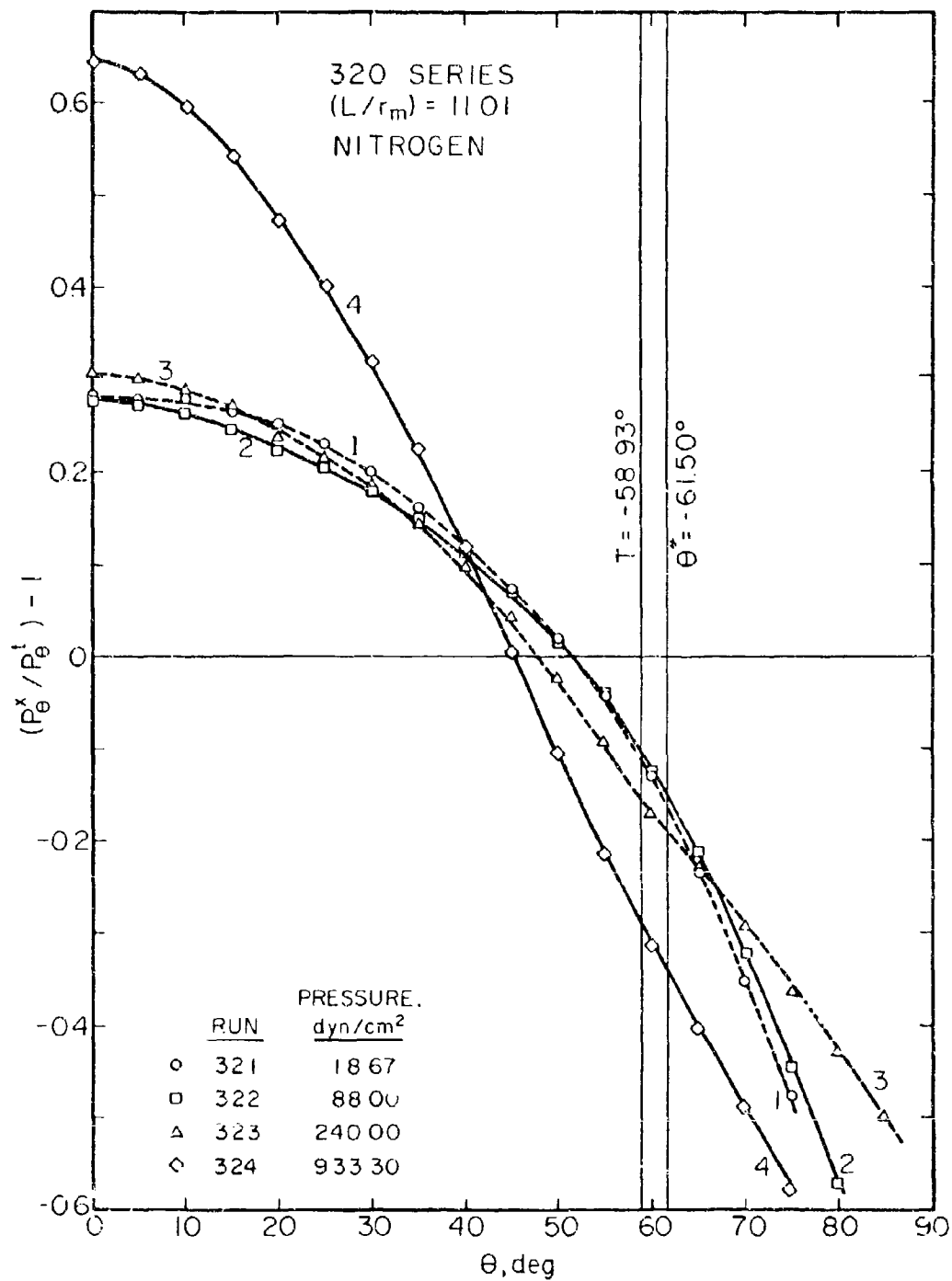


Figure 18.  $f(\Delta)$  plots for 320 series.

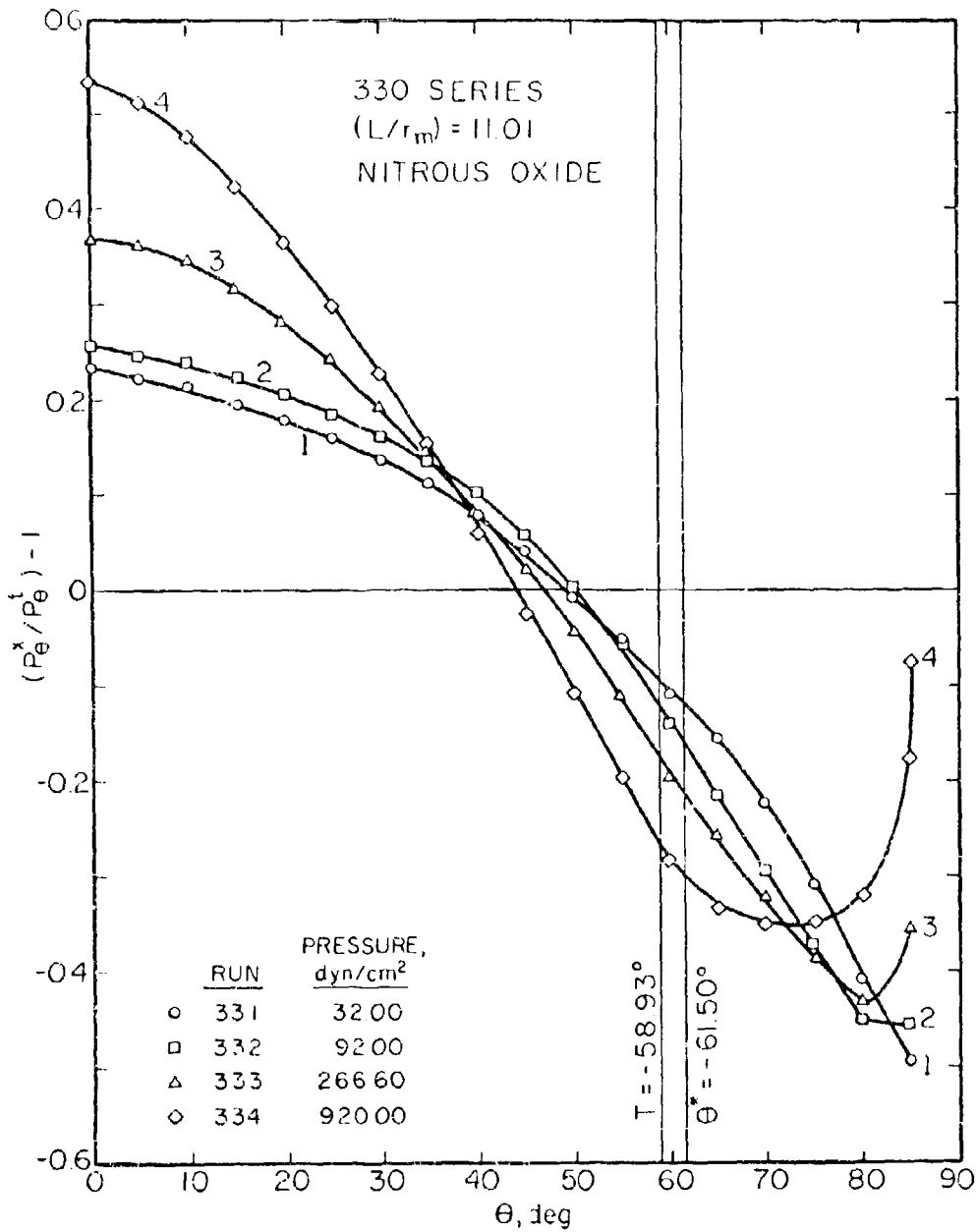


Figure 19.  $f(\Delta)$  plots for 330 series.

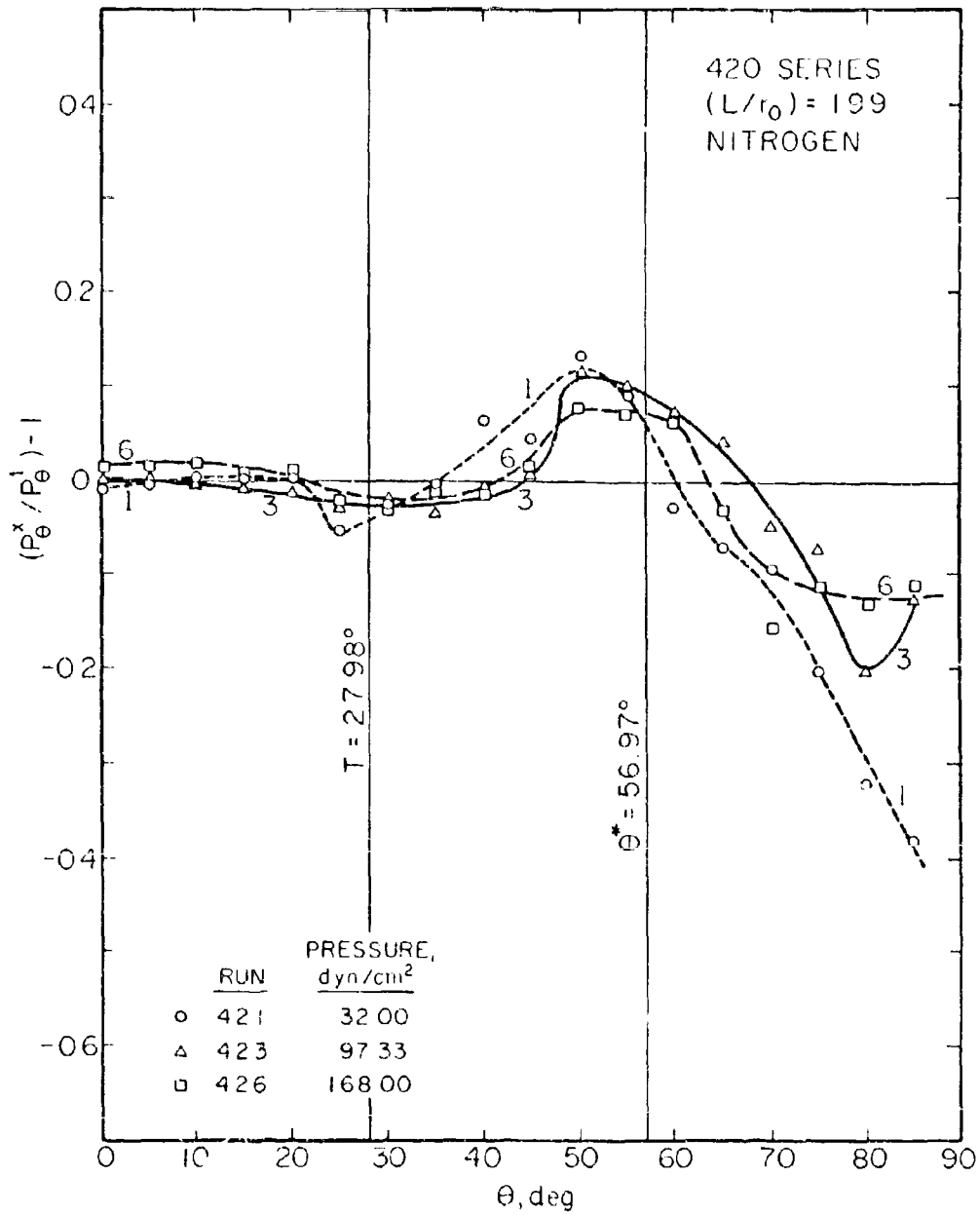


Figure 20.  $f(\Delta)$  plots for 420 series.

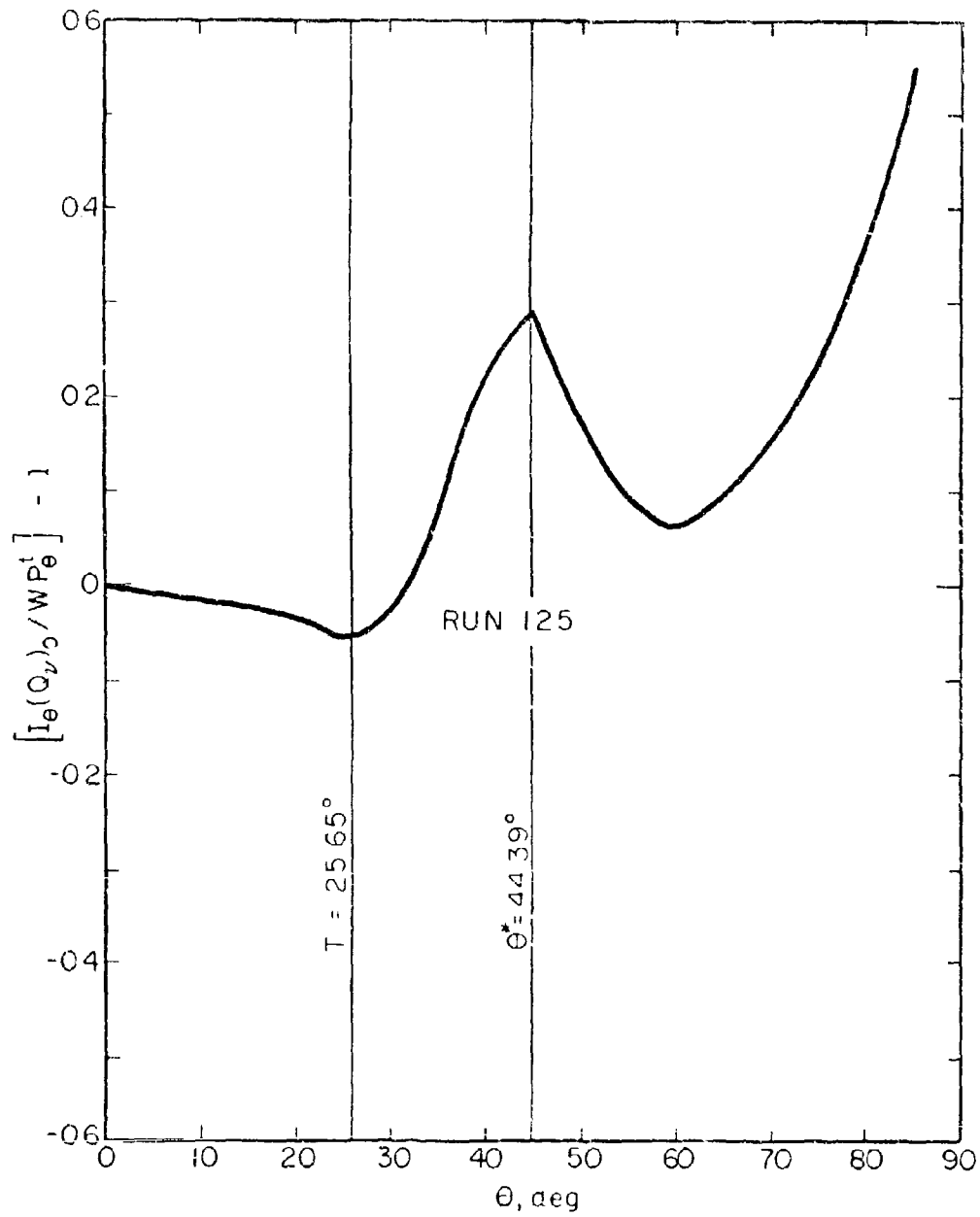


Figure 21.  $\delta_2$  plot (cf. equation 26) for Run 125. Compare with Run 125 in Figure 15.

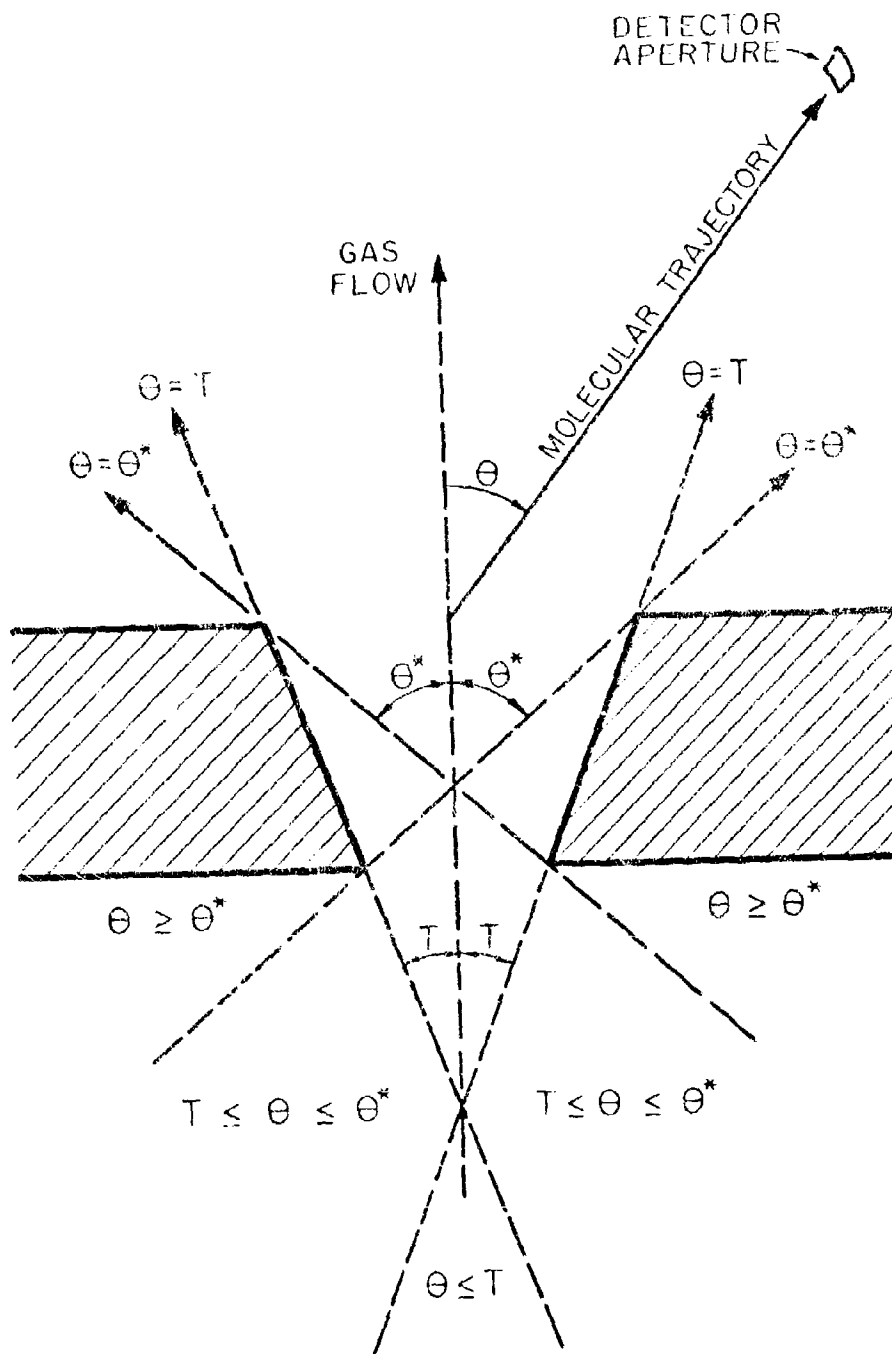


Figure 22. The Critical Angles and the Angular Ranges for a Conical Orifice

(cf. equation 9 and 10). For  $T < \theta < \theta^*$ , the detector may receive molecules directly from elements of the orifice wall over the entire length of the orifice and from part of the entrance to the orifice, but a portion of the wall, and of the entrance, are shielded from the detector by the outer rim of the orifice; this case corresponds to Range II<sup>13</sup> and  $n = 2$ . Finally, for  $\theta^* \leq \theta \leq \pi/2$  the detector receives molecules only from part of the orifice wall; molecules which traverse the orifice entrance cannot proceed directly to the detector; this is Range III<sup>13</sup>, and  $n = 3$ . For the converging orifice ( $T < 0$ ), the above statements are also valid (1) if  $T$  is replaced by  $|T|$ , and (2) if the description of Range I is modified to read: "receive molecules directly only from a portion of the orifice entrance".

The significance of  $T$  and  $\theta^*$  with regard to angular distribution may be summarized: For  $\theta < |T|$ , all elements of the orifice wall ( $T > 0$ ), or no elements ( $T < 0$ ), contribute to the flux at the detector aperture. As  $\theta$  increases in the range  $|T| \leq \theta \leq \theta^*$ , a decreasing portion of both the orifice entrance and the orifice wall contribute to the detected flux. For  $\theta > \theta^*$ , the orifice entrance makes no contribution, all molecules reach the detector from a portion of the orifice walls, and this portion decreases to 0 as  $\theta \rightarrow \pi/2$ .

We shall now examine the features of the curves in Figures 15-20, beginning with Figures 20 and 15. The agreement between experimental and theoretical values for  $P_\theta$  for the 420 series (Figure 20) is very good except in the range  $40^\circ \leq \theta \leq 60^\circ$  where there is a maximum in each curve. Similarly, in the 120 series the discrepancy  $\Delta = P_\theta^x - P_\theta^t$  for the lower pressure runs (121 and 123) is zero within 2 to 4%, i.e., very nearly within experimental error, for  $\theta \leq T$ ; however, there is again a maximum in the curves at  $\theta \approx 40^\circ$ . At higher pressures (Runs 125 and 127)  $f(\Delta)$  is -0.05 to -0.10 at  $\theta < T$ , the maximum in each curve is higher and is shifted to larger  $\theta$ . We now note the correlation, in Figures 15, 16, and 20, of the maxima with the angles  $T$  and  $\theta^*$ , and that the magnitude of both the maxima and the discrepancy  $f(\Delta)$  increases with increasing pressure and with increasing  $(L/r)$ .

Support for this last generalization was sought in Wang's data for the effusion of cesium chloride through cylindrical ( $\tau = 0.0^\circ$ ) copper and nickel orifices; data required for the  $\Delta$  vs.  $\theta$  plots in Figures 23 and 24 have been calculated by us from  $[I_\theta^+/I_0^+; \theta]$  data tabulated by Wang<sup>27</sup>. Maxima in the various curves at 10-15° and minima at 60-70° are immediately obvious (but note that the  $\Delta$  scale is expanded by a factor of five compared with Figures 15-21). The discrepancy  $\Delta$  does indeed appear to decrease with increasing pressure, but this assertion must be qualified: Run 75 in Figure 24 is "out of order" for no apparent reason; in Figure 23 Runs 21 and 26 were made with one experimental configuration, Runs 27, 28, and 35, with another; within each group  $\Delta$  decreases with increasing pressure; the reason for the discrepancy between the groups is not apparent. The shift of the maximum to higher  $\theta$  with increasing pressure is quite evident in Run 91, Figure 24, but is not clearly exhibited in Figure 23, perhaps because data were not taken at sufficiently high pressures.

It might appear that Wang's data, then, provide support for, if not confirmation of, our generalization about the variation of  $\Delta$  with  $(L/r)$  and with pressure. However, we were surprised that for low pressures the maxima in Figures 23 and 24 occur in the same angular range (10-15°) despite the difference in  $(L/r)$  for the two orifices. Upon investigation, we find that in Wang's apparatus<sup>27</sup> the angle from the orifice to the annulus which surrounds the baffle plate in the front oven is in the range 10 to 15°. It is therefore not clear whether the maxima in the curves from Wang's data arise from gas flow-orifice phenomena or from the baffle-annulus acting as a (relatively) concentrated source of molecules.

An obvious question, then, is whether the maxima in Figures 15, 16 and 20 arise from a cell effect rather than an orifice effect. The cylindrical interior of our simulated Knudsen Cell is 1.00" in diameter and 1.10" high; the bottom of the cell is completely open to the flow of gas from the reservoir<sup>14,21</sup>. The interior wall of the cell is macroscopically smooth. Hence, the only discontinuity in the emitting surface "seen" by the detector through the effusion orifice is at the "bottom corner" of the cell; the angle from the orifice to the "bottom corner"

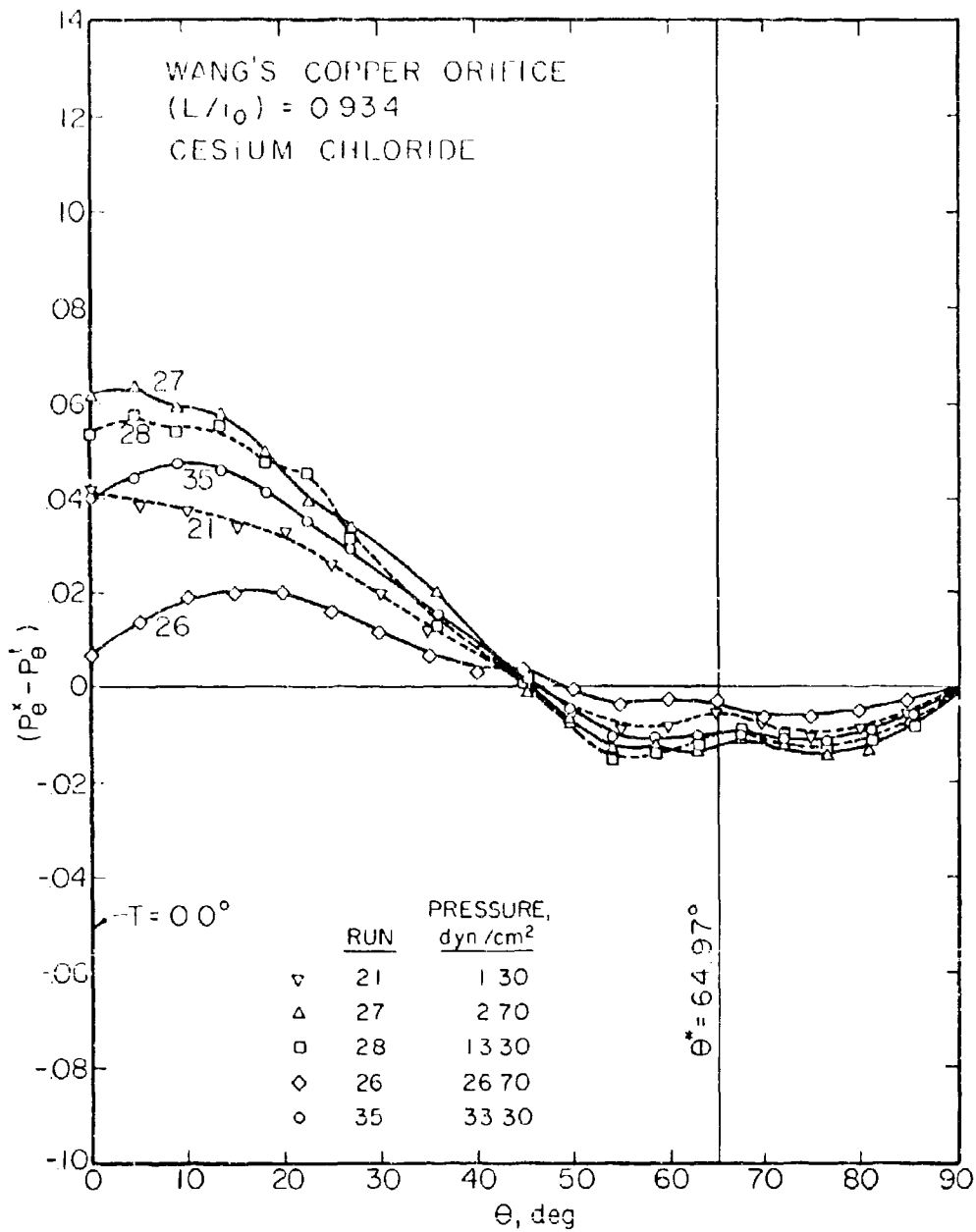


Figure 25.  $\Delta$  plot for K. C. Wang's angular distribution data<sup>27</sup> for orifice with  $T = 0.0^\circ$  and  $L/r_0 = 0.934$ .

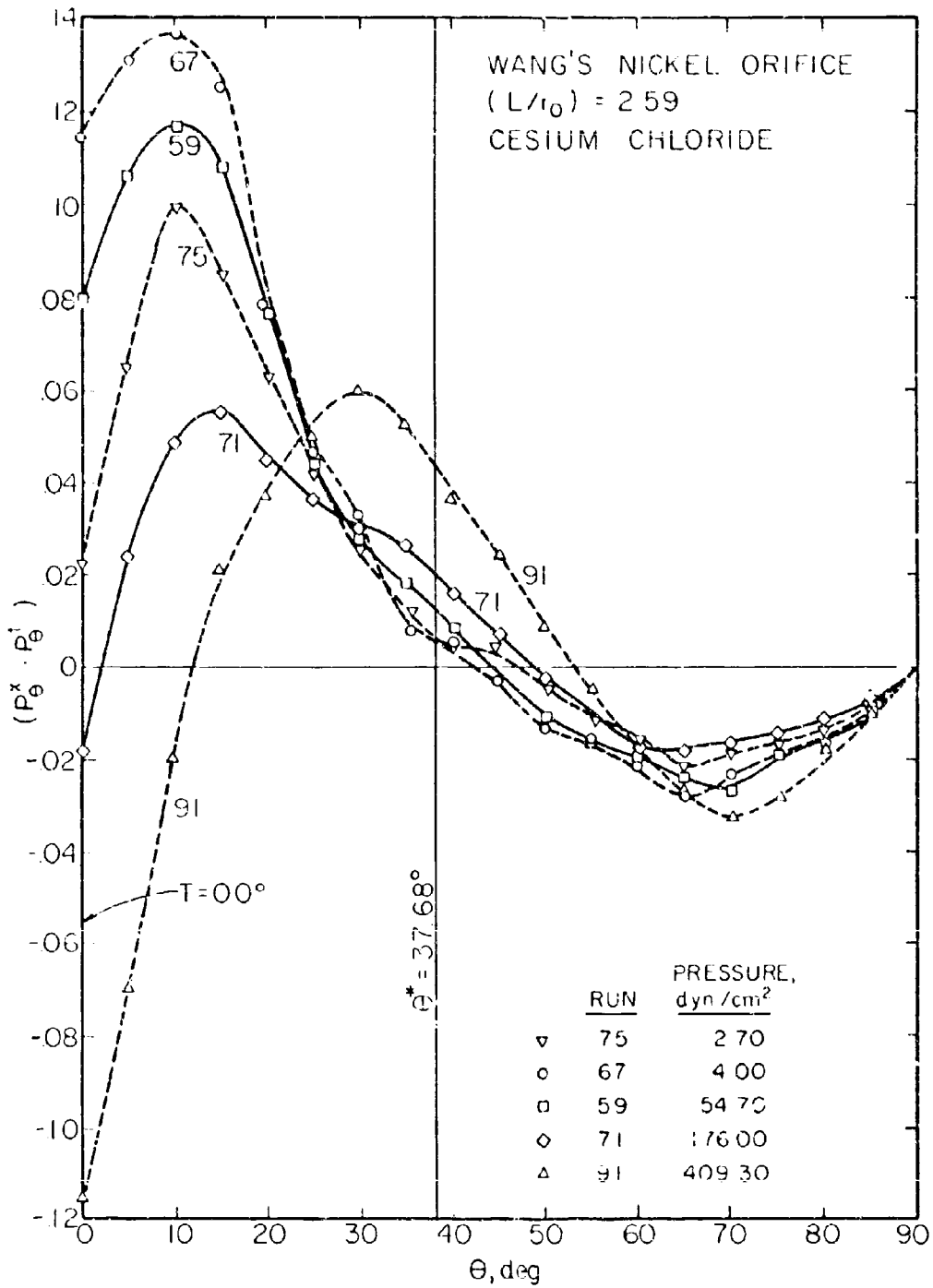


Figure 24.  $\Delta$  plot for K. C. Wang's angular distribution data<sup>7</sup> for orifice with  $T = 0.0^\circ$  and  $L/r_0 = 2.59$ .

is  $\sim 25^\circ$ . For  $\theta$  greater than  $\sim 25^\circ$  molecules can travel directly from the cell wall through the orifice (if  $\theta^* > 25^\circ$ ) to the detector; for  $\theta$  less than  $\sim 25^\circ$ , the detector cannot "see" the cell wall and receives no molecules directly from it. We now examine Figures 19 and 20 for evidence of a cell effect and find that in Figure 16  $\underline{T}$  is so near  $25^\circ$  that one cannot hope to distinguish cell effects from orifice effects; in Figure 20 the situation is similar. However, the data for Figures 18 and 19 were obtained for a converging orifice with  $\underline{T} = -58.9^\circ$ ; in this case the orifice presents no obstruction to molecules traveling along a  $\theta = 25^\circ$  trajectory from the region of the surface discontinuity to the detector. Figures 17 and 18 provide no evidence (i.e., no maxima, no minima, no breaks in the curves) for a cell effect at or near  $\theta = 25^\circ$ , but there is a definite change (more pronounced at higher pressures) in the curvature of the various curves in the narrow range  $|\underline{T}| \leq \theta \leq \theta^*$ . We therefore conclude that the deviations from theoretical behavior, exhibited by the curves in the various figures, are orifice effects.

We return our attention to Figures 16 and 20 and consider the two mechanisms frequently cited as causes of deviation from theoretical behavior: specular reflection from the orifice wall and surface diffusion along the orifice wall<sup>9</sup>. One would expect any enhancement of intensity by specular reflection to occur at angles  $\theta < \underline{T}$ . Enhancement at angles  $\theta > \underline{T}$  requires specular reflection through angles greater than  $2\underline{T}$ , and the maxima of Figures 16 and 20 would require preferential enhancement by specular reflection through angles  $> 50^\circ$  with no concurrent depletion at smaller angles (cf. especially Figure 20). Available experimental data<sup>28</sup> on angular distribution of molecules reflected from surfaces do not support these rather stringent requirements.

If surface diffusion occurs along the orifice wall, the concentration of molecules resident within any incremental area on the wall is expected to be greater than if surface diffusion did not occur; consequently, the flux from the orifice wall to the detector is expected to be greater. Therefore, one might expect any discrepancy between theoretical and experimental data for angular distributions, which results from surface diffusion, to be most prominent in the range(s) of  $\theta$  in which the flux

from the orifice wall area makes the maximum relative contribution to the total flux into the detector.

The area  $\Delta_w$  of the projection of the orifice wall onto a plane perpendicular to the orifice-detector line defined by  $\theta$  may be calculated from the following equations (see Figure 1 for symbols):

$$\begin{aligned} A_L &= \pi r_L^2 \cos \theta \\ A_O &= \pi r_O^2 \cos \theta \\ A_E &= A(D_O; D_L) \cos \theta \end{aligned} \quad (28)$$

[ $A(D_O; D_L)$  is the area of overlap of the circle  $\pi r_O^2$  with the projection at angle  $\theta$  onto the plane of that circle of the circle  $\pi r_L^2$ ; derivation of this quantity has been described in detail<sup>12, 13, 14.</sup>]

$$\begin{aligned} \text{If } \theta > \theta^*, A_w &= A_L \\ \text{If } |\underline{T}| < \theta < \theta^*, A_w &= A_L - A_E \\ \text{If } \theta \leq |\underline{T}| \text{ and } T > 0.0, A_w &= A_L - A_O \\ \text{If } \theta \leq |\underline{T}| \text{ and } T < 0.0, A_w &= 0.0 \end{aligned} \quad (29)$$

The results of these calculations for the orifices for which angular distribution data were obtained are shown in Figures 25-28 wherein, for convenience in plotting, the areas have been normalized to  $\underline{\Delta}_L(\theta=0.0)=1.0$ . In the ranges  $\theta \geq \theta^*$  and  $\theta \leq T$ , the variation of  $\underline{\Delta}_w$  with  $\theta$  is given by  $\cos \theta$ . However, in the range  $|\underline{T}| \leq \theta \leq \theta^*$ ,  $\underline{\Delta}_w$  exhibits a rather different behavior which produces a minimum (or virtual minimum) in  $\underline{\Delta}_w$  at  $\theta = \underline{T}$  and a maximum (or virtual maximum) at  $\theta = \theta^*$ .

As  $\theta$  increases over the range  $|\underline{T}| \leq \theta \leq \theta^*$  for a diverging ( $T > 0.0$ ) orifice, the entrance of the orifice is eclipsed by the outer rim of the exit, and therefore the fractional contribution from the wall to the total flux to the detector increases to unity at  $\theta = \theta^*$ . In the range ( $\theta \geq \theta^*$ ) over which the fractional contribution from the wall is unity, the projected wall area "seen" by the detector is a maximum at  $\theta = \theta^*$ . Therefore, if there were an increase in the flux from the orifice wall above that predicted by our extension of Clausing's Model, one should expect to see maxima in  $\underline{\Delta}$  vs.  $\theta$  plots at or near  $\theta = \theta^*$ .

This is precisely what is observed in Figures 15, 16, 17, and 20, and in lieu of any acceptable alternative, we tentatively conclude that the

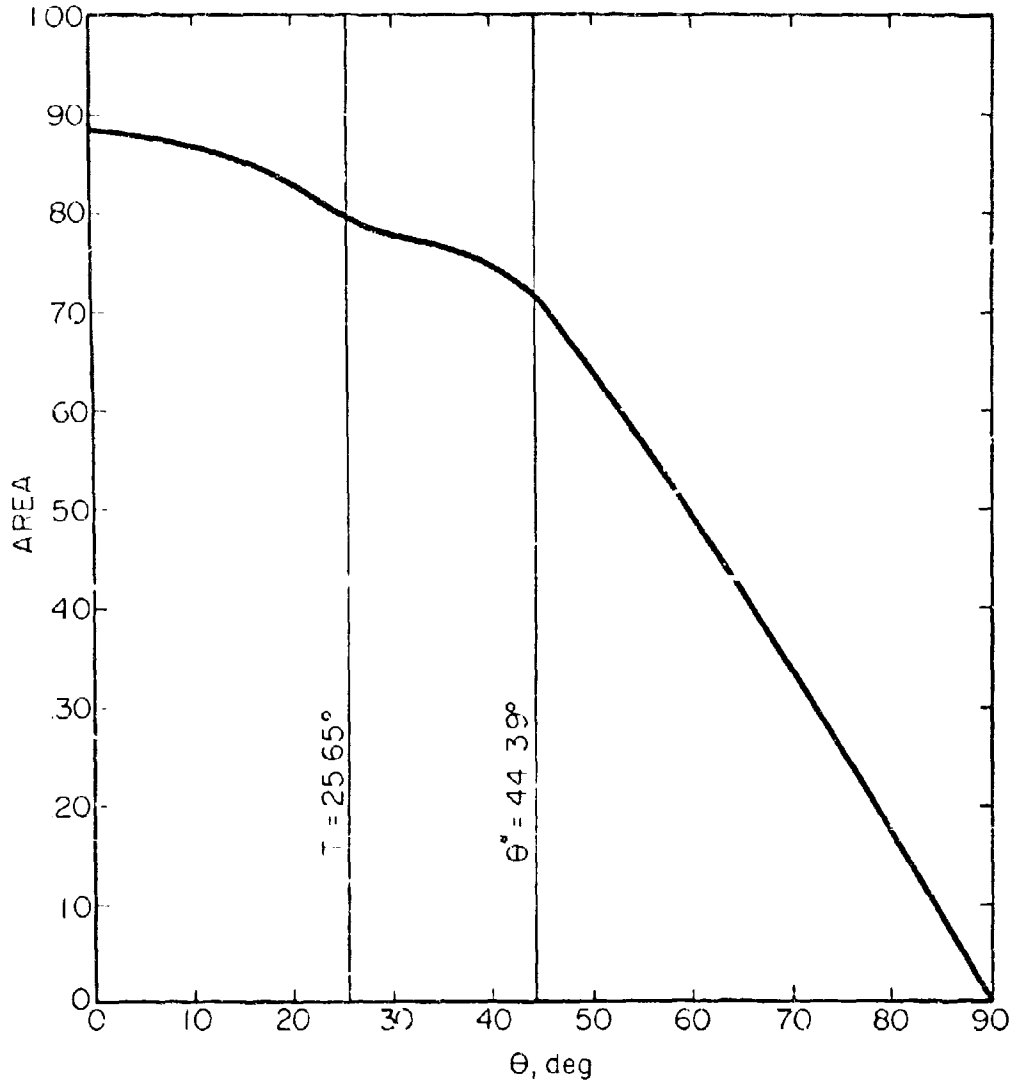


Figure 25. Normalized projected area of inside wall of Orifice 1.

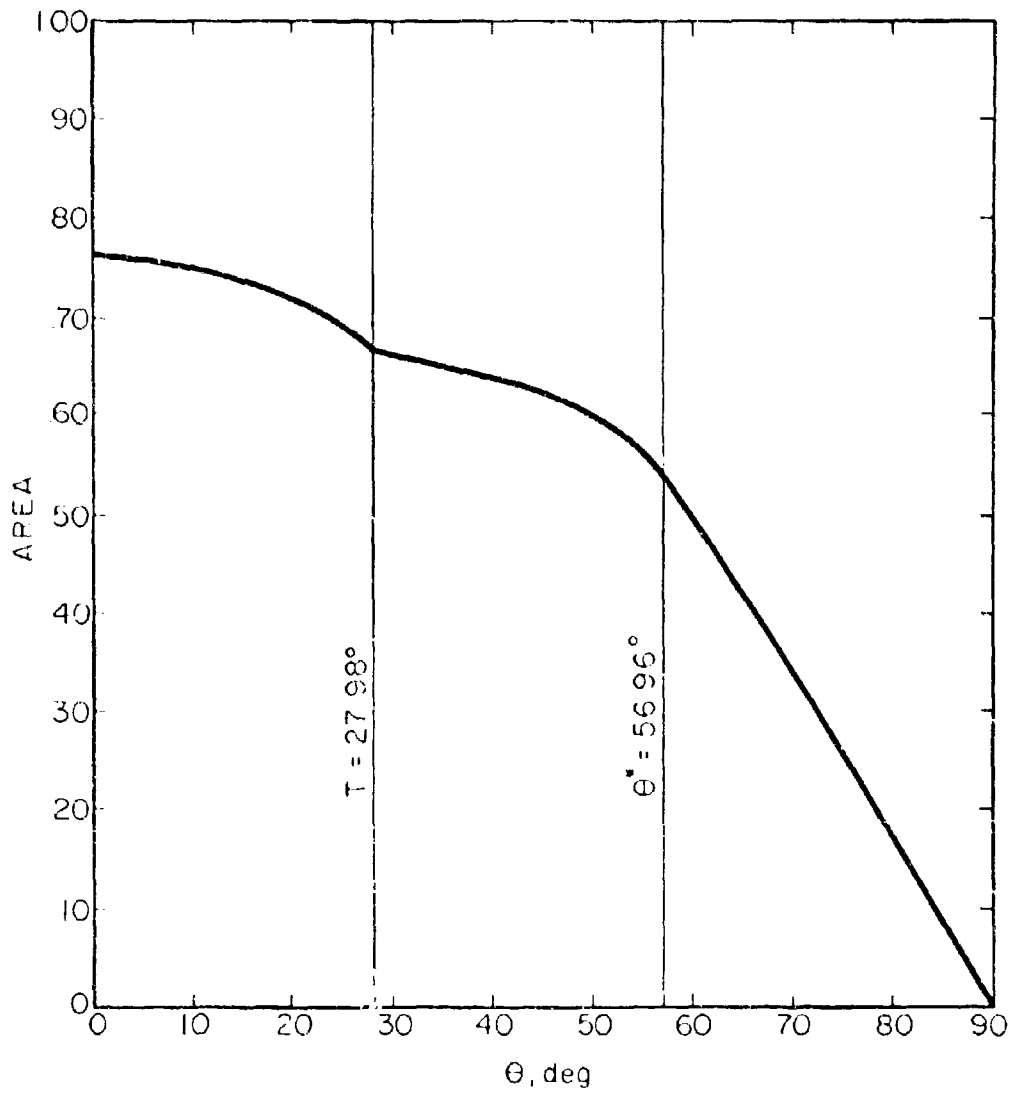


Figure 26. Normalized projected area of inside wall of Orifice 4.

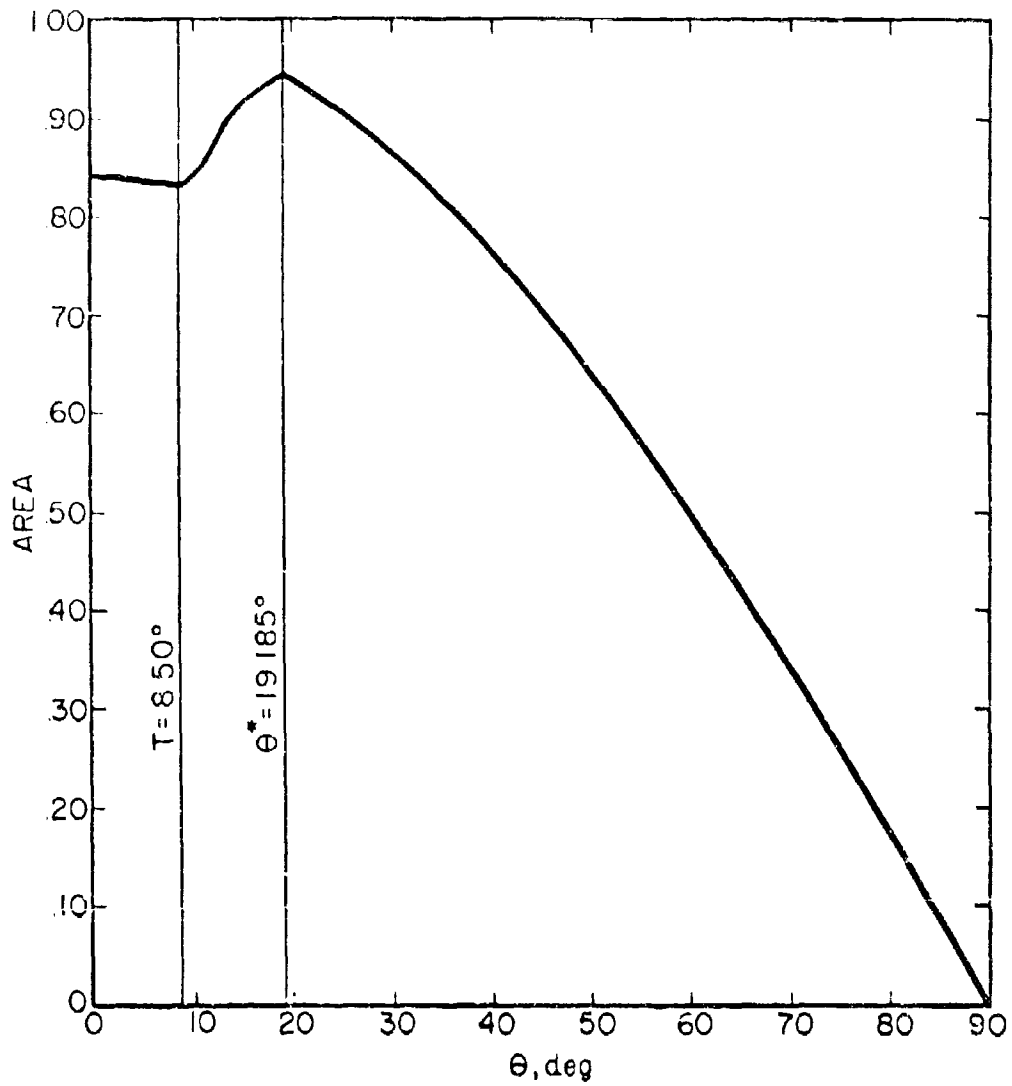


Figure 27. Normalized projected area of inside wall of Orifice 2.

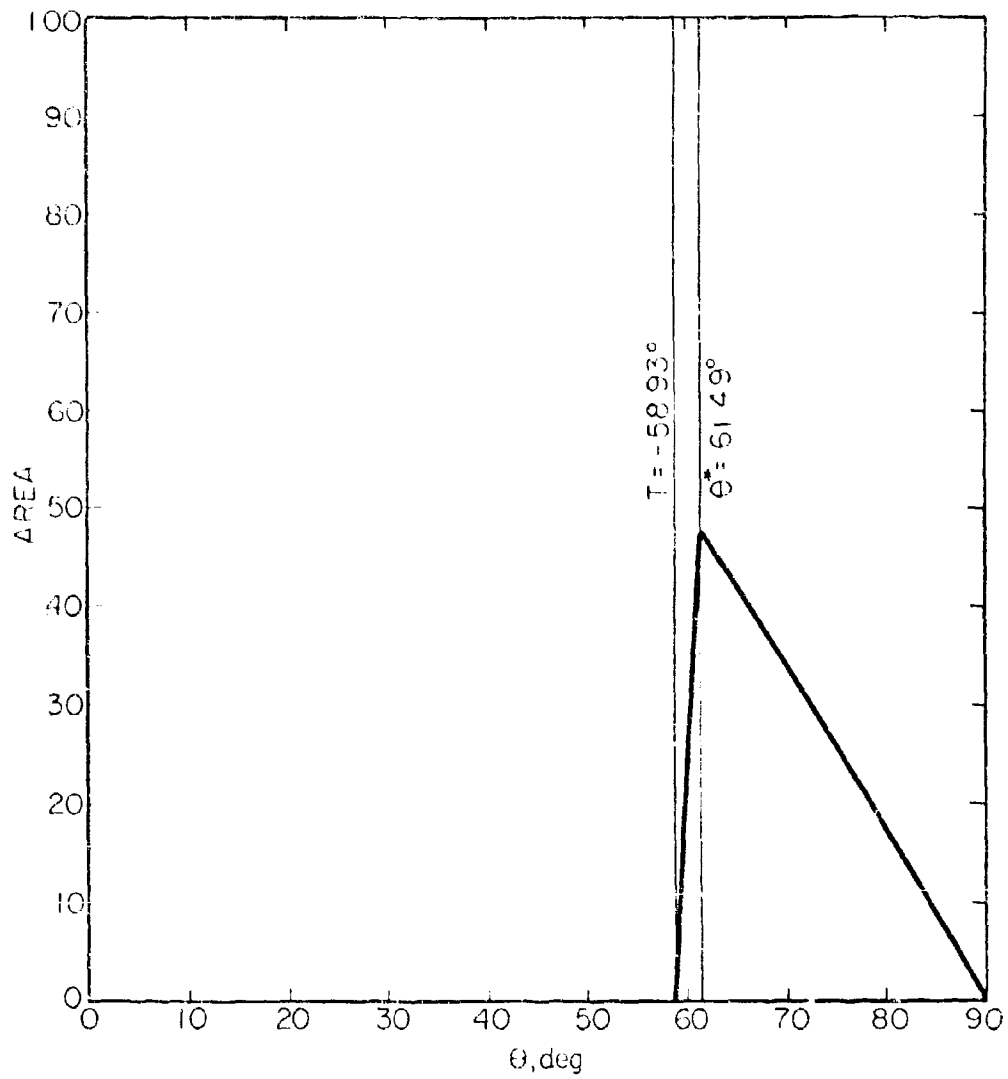


Figure 28. Normalized projected area of inside wall of Orifice 3.

increased flux from the orifice wall results from surface diffusion.

We have not yet made a more detailed analysis of a model including surface diffusion; Ruth and Hirth<sup>28</sup> have reported the corresponding analysis for cylindrical orifices.

Other features of the  $f(\Delta)$  vs.  $\theta$  plots, e.g. variations with pressure and nature of the gas, are being analyzed and will be reported in the open literature.

## SECTION IV

### THE MULTICELL TECHNIQUE FOR EXPERIMENTAL DETERMINATION OF TRANSMISSION PROBABILITIES FOR MOLECULAR FLOW THROUGH CONICAL ORIFICES

The Knudsen effusion technique<sup>1-3</sup> has been widely used to obtain vapor pressure data in the range  $10^{-3}$ - $10^{-9}$  atm. The technique has several variants<sup>3</sup>, but basically the experimentally measured variable is the isothermal rate of flow of vapor through an orifice, e.g., 1 mm in diameter and 0.5 mm long. The equation which relates the pressure of the gas to the flux through the orifice contains a factor which is often called the Clausing factor, or more properly, the transmission probability, of the orifice, i.e., the probability that a molecule which has entered one end of the orifice will exit from the opposite end. Numerical values for the transmission probability are available from theoretical analyses<sup>5-8, 12-14</sup> of molecular flow of gas through orifices with various geometries. Although these theoretical transmission probabilities are widely<sup>2-3</sup> used to correct the observed rate of flow for the effect of finite orifice length, reliable experimental data with which to compare the theoretical transmission probabilities are scarce<sup>3, 31, 33</sup>.

The Multicell technique, which we describe below, provides a simple method for obtaining experimental values for transmission probabilities and also offers a means for critically testing various assumptions which have been made<sup>9, 34-36</sup> concerning molecular flow within a Knudsen cell. Application of the technique to the determination of experimental transmission probabilities is discussed in this section.

#### A. THE MULTICELL APPROACH

In a Multicell effusion experiment a number (e.g., 4 to 10) of effusion cells<sup>2, 3</sup> which are as nearly identical as possible except in the

variable under study are subjected simultaneously to a given environment for a given time. Comparison of results (e.g., weight lost from each cell) for the several cells in a given experiment permits isolation of the effect of the variable of interest since all other variables are constant, or vary simultaneously and identically, for all cells.

In the application of this approach to the determination of experimental transmission probabilities, Knudsen cells are fabricated to be essentially identical except that each orifice is different from the others; each cell is loaded with an equal amount of a given sample (e.g., cadmium or mercury), and then heated simultaneously in vacuum for a given time  $\tau$  and at an appropriate temperature  $\theta$  which are identical for all cells. The weight lost from each cell during the experiment is determined by weighing before and after the heating period. The weight  $dg_i$  lost from the  $i$ th cell in time  $dt$  is given by<sup>37</sup>

$$dg_i = a_i K_i [P(M/2\pi R\theta)^{1/2} dt] \quad (30)$$

in which  $P$  is the pressure in the cell at temperature  $\theta$ ,  $M$  is the molecular weight of the effusing molecules,  $K_i$  is the experimental transmission probability and  $a_i$  the cross-sectional area for the  $i$ th orifice. For the experimental conditions described above,  $P$ ,  $\theta$ , and  $M$  are, at each instant, the same for all  $m$  cells; therefore, the integral of the bracketed portion of equation (30) over the interval 0 to  $\tau$  is the same for each cell. Hence, if  $g_i$  is the total weight lost in time  $\tau$ , we write

$$\int_{t=0}^{t=\tau} dg_i = g_i = a_i K_i I$$

with  $I$  representing the integral which is constant for the several cells in a given run, but which varies from run to run. Since the various  $g_i$  and  $a_i$  are directly measurable quantities, it is convenient to define  $J_i = g_i/a_i$  and then to write

$$J_i = K_i I. \quad (31)$$

Clausing's theory predicts<sup>5-8, 13</sup> that, for conical ( $-\pi/2 < T < \pi/2$ ) and cylindrical ( $T = 0$ ) orifices, the variation in a given run of the values  $J_i$  for the various cells depends only on the ratio of length  $L$  to diameter  $D$  for the orifices and on  $T$  the semi-apex angle of the cone of which the

orifice is a truncated section. Therefore, if the values  $J_1$  are plotted against some suitable function of  $(L/D)$  and  $T$ , designated by  $F(L/D, T)$ , and extrapolated to  $F(0, T)$ , one may write from Equation (31),  $J_0 = K_0 I$ , in which the subscript designates the condition:  $L/D = 0$ . But  $(L/D = 0)$  defines<sup>5-9, 13</sup> the "ideal" orifice for which the transmission probability,  $J_0$  is unity regardless of the value of  $T$  (which in fact is meaningless when  $L/D = 0$ ); therefore,

$$J_0 = I \quad (32)$$

Hence, the intercept at  $F(0, T)$  is just the weight loss per unit area  $J_0$  to be expected, under the conditions of the run, from an ideal orifice. With this experimental value for  $J_0$ , the experimental transmission probability for each of the cells is calculated from Equations (31) and (32):

$$K_1 = J_1/J_0. \quad (33)$$

The most suitable choice for  $F(L/D, T)$  appears to be  $W$ , the theoretical transmission probability<sup>5-9, 13</sup> calculated from the orifice dimensions. This choice results in a conveniently bounded plot with abscissa values ranging from zero to one; more important, if the theoretical transmission probabilities predicted by Clausius's theory<sup>5</sup> and its extensions<sup>6-9, 13</sup> are correct, a plot of  $J_1$  versus  $F(L/D, T)_1 = W_1$  should give a straight line which may be precisely extrapolated to  $W_1 = 1$  (i.e., to  $L/D = 0$ ) to obtain the intercept  $J_0$ . The slope of the straight line resulting from such a plot should also equal  $J_0$ .

## B. EXPERIMENTAL RESULTS AND DISCUSSION

The results reported here were obtained with a typical Multicell configuration: various sets of eight nickel-plated, steel Knudsen cells, machined to be "identical" except for the lengths of the cylindrical orifices and/or the semi-apex angles  $T$  of the conical orifices, were placed into closely-fitting, symmetrically-arranged cavities in an aluminum (or copper) block which, during a run, sat inside a stainless steel vacuum chamber. During the heating period, the entire vacuum chamber and several inches of connecting stainless steel vacuum line were inside a circulating-hot-air, constant-temperature oven. The cells were charged with equal amounts of high-purity cadmium metal.

The dimensions of the orifices and the detailed results of the various runs are available elsewhere<sup>39, 40</sup>; the results of a typical run are presented in Table 3 and in Figure 29 in which the least-squares straight line ( $\underline{J}_1^c = m\underline{W}_1 + b$ ) for the data points is also given.

For each run, the experimental transmission probabilities were calculated in two ways: (1) the ordinate value of each experimental point (i.e., each  $\underline{J}_1$ ) was divided by  $\underline{J}_0$  (cf. equation 33) to obtain the values  $\underline{K}_1^p$ ; (2) the corresponding ordinate value ( $\underline{J}_1^c$ ) on the least-squares line was divided by  $\underline{J}_0$  to obtain the values  $\underline{K}_1^c$ . In Table 3, the transmission probabilities calculated in the two ways from the data of Run 7 are compared with the theoretical transmission probabilities.

For each orifice the transmission probability calculated from the results of several runs will be more reliable than a value obtained from any single, arbitrarily-chosen run. "Average" transmission probabilities  $\bar{K}_1$  for the various sets of orifices, and the transmission probabilities  $\underline{K}_1$  calculated from the individual runs are given in Tables 4-6. Two values are given for each orifice: the upper of each pair of numbers is the transmission probability calculated from the experimental points (cf.  $\underline{K}_1^p$ , Table 3), and the lower number is the value calculated from the least-squares line for the points of a given run (cf.  $\underline{K}_1^c$ , Table 3).

As shown in the last column of Tables 4-6, the discrepancies between the experimental values for transmission probabilities (for cadmium vapor passing through nickel-plated, cylindrical orifices) and the theoretical values lie in the range  $\pm 5\%$  (with two notable exceptions in Table 6, for which we have no explanation), if the experimental points are considered. If the results from the least-squares lines are used, the discrepancies are appreciably smaller. Similar agreement for a very limited number of "short" orifices has been obtained by McKinley and Vance<sup>33</sup> and by Carlson, Gilles and Thorn<sup>37</sup>.

In general, the experimental values  $\bar{K}_1$  are less than the theoretical  $\underline{W}_1$ , and there is a slight trend for the discrepancy to become larger as  $\underline{L}/\underline{D}$  increases. These observations are exactly opposite to what would be expected if surface diffusion<sup>9, 36</sup> through the orifice contributed significantly to the total efflux.

The agreement between theoretical predictions and the experimental results reported here (especially Table 4) is appreciably better than the

TABLE 3

COMPARISON OF EXPERIMENTAL AND THEORETICAL  
TRANSMISSION PROBABILITIES: RUN 7

Orifice, L/D	$W_I$	$g_I, \text{mg}$	$K^P$	$\frac{100(K^P - W)}{W}$	$K^C$	$\frac{100(K^C - W)}{W}$
0.195	0.837	42.36	0.843	+0.7	0.831	-0.8
0.290	0.777	38.16	0.759	-2.3	0.767	-1.3
0.414	0.711	35.62	0.709	-0.3	0.699	-1.8
0.448	0.695	32.94	0.656	-6.0	0.682	-1.8
0.521	0.664	33.83	0.673	+1.4	0.649	-2.2
0.522	0.663	31.91	0.635	-4.4	0.649	-2.2
0.667	0.609	28.85	0.574	-6.1	0.592	-2.9
0.800	0.567	28.55	0.568	+0.2	0.549	-3.4

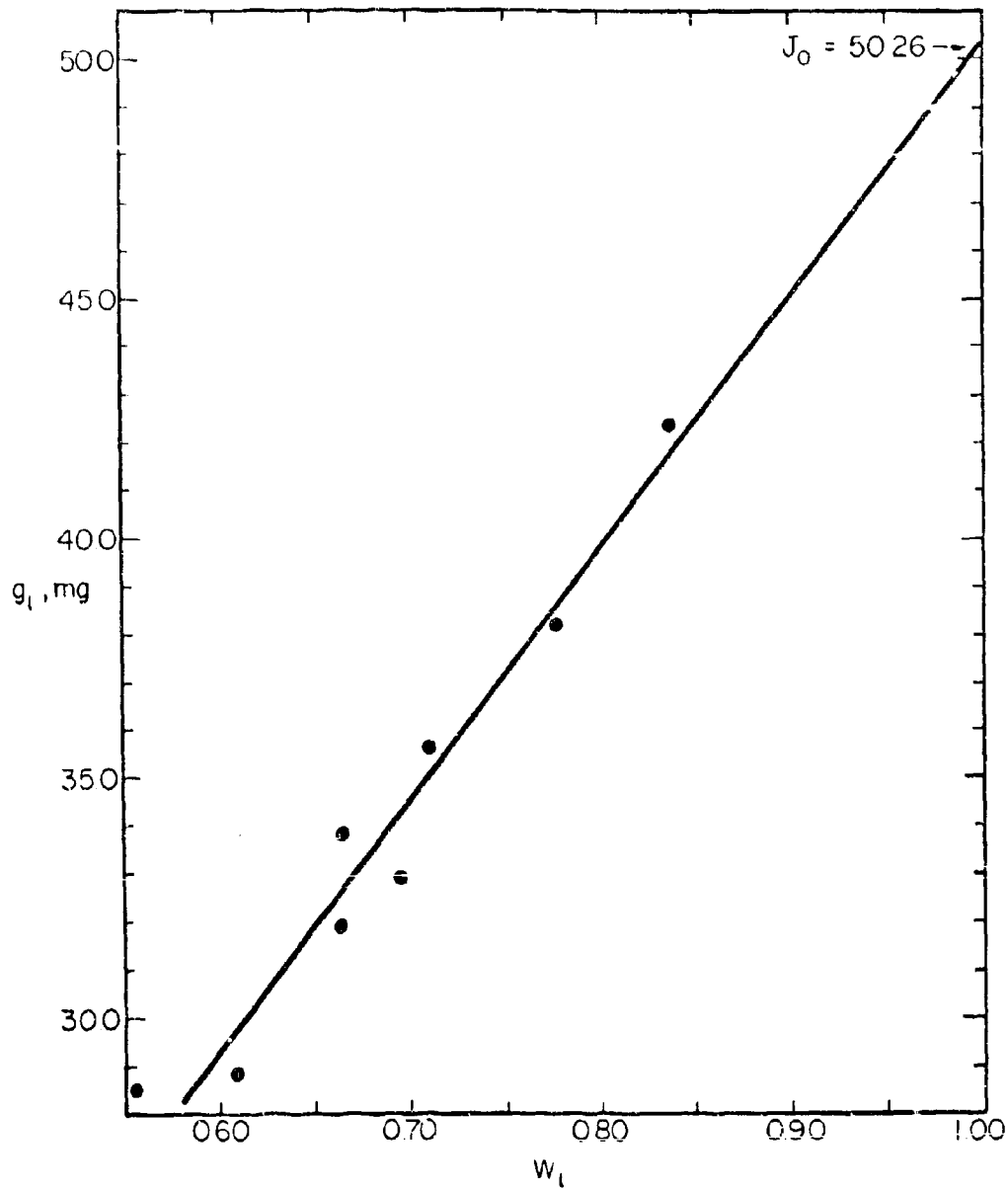


Figure 29. Weight loss through orifices with various (L/D) ratios vs. theoretical transmission probability.

TABLE 4  
 EXPERIMENTAL TRANSMISSION PROBABILITIES  
 FOR EIGHT CYLINDRICAL ORIFICES (SET I)

Orifice, L/D	W	K				$\bar{K}$	$100(\bar{K}-W)$
		Run 4	Run 5	Run 6	Run 7		W
0.195	0.837	0.8354 <sup>a</sup>	0.8512	0.8550	0.8429	0.846	+1.1
		0.8297 <sup>b</sup>	0.8392	0.8378	0.8305	0.834	-0.4
0.290	0.777	---	0.7207	0.7546	0.7593	0.745	-4.1
		---	0.7791	0.7772	0.7672	0.775	-0.3
0.414	0.711	0.6952 <sup>a</sup>	0.7393	0.6888	0.7068	0.708	-0.4
		0.6973 <sup>b</sup>	0.7141	0.7116	0.6986	0.706	-0.7
0.448	0.695	0.6636 <sup>a</sup>	0.6918	0.6991	0.6555	0.678	-2.4
		0.6810 <sup>b</sup>	0.6986	0.6960	0.6824	0.690	-0.7
0.521	0.664	0.6510 <sup>a</sup>	0.7413	0.6905	0.6732	0.689	+3.8
		0.6477 <sup>b</sup>	0.6672	0.6643	0.6492	0.657	-1.1
0.522	0.663	0.6617 <sup>a</sup>	0.6572	0.6828	0.6350	0.659	-0.6
		0.6469 <sup>b</sup>	0.6665	0.6636	0.6485	0.655	-1.1
0.667	0.609	0.5796 <sup>a</sup>	0.6120	0.5893	0.5741	0.589	-3.3
		0.5903 <sup>b</sup>	0.6130	0.6096	0.5921	0.601	-1.3
0.800	0.567	0.5549 <sup>a</sup>	0.5356	0.5701	0.5681	0.557	-1.8
		0.5463 <sup>b</sup>	0.5716	0.5679	0.5485	0.559	-1.4
m = slope		38.15	34.57	30.76	52.39		
b = intercept							
at ( $W_1 = 0$ )		-1.71	+0.38	+0.20	-2.13		
$J_0$ = intercept							
at ( $W_1 = 1$ )		36.44	34.95	30.95	50.25		

- a. The upper number of each pair is the value obtained from the experimental points.  
 b. The lower number of each pair is the value obtained from the least squares line.

TABLE 5  
EXPERIMENTAL TRANSMISSION PROBABILITIES  
FOR EIGHT CYLINDRICAL ORIFICES (SET II)

Orifice, L/R	W	K				$\bar{K}$	$\frac{100(\bar{K}-W)}{W}$
		Run 2	Run 3	Run 4	Run 6		
0.4462	0.819	0.577a	0.854	0.809	0.814	0.838	+2.3
		0.848b	0.811	0.797	0.802	0.815	-0.5
0.6614	0.754	0.735a	0.752	0.754	0.751	0.748	-0.8
		0.761b	0.742	0.724	0.731	0.740	-1.9
1.016	0.669	0.647a	0.649	0.591	0.599	0.622	-7.0
		0.680b	0.652	0.629	0.638	0.650	-2.8
1.291	0.616	0.614a	0.594	0.541	0.577	0.582	-5.5
		0.603b	0.598	0.570	0.595	0.592	-3.9
1.627	0.563	0.590a	0.535	0.497	0.520	0.536	-4.8
		0.575b	0.541	0.510	0.523	0.537	-4.6
1.946	0.521	0.535a	0.484	0.402	0.486	0.497	-4.6
		0.535b	0.497	0.464	0.477	0.493	-5.4
2.263	0.485	0.508a	0.456	0.419	0.404	0.447	-7.6
		0.501b	0.460	0.423	0.437	0.455	-6.2
2.573	0.455	0.464a	0.448	0.414	0.446	0.443	-2.6
		0.469b	0.428	0.390	0.405	0.423	-7.0
m = slope		46.67	66.15	84.28	73.14		
b = intercept							
at ( $W_1 = 0$ )		+1.24	-3.10	-9.07	-6.12		
$J_0$ = intercept							
at ( $W_1 = 1$ )		47.91	63.05	75.21	67.02		

a. The upper number of each pair is the value obtained from the experimental points.

b. The lower number of each pair is the value obtained from the least squares line.

TABLE C  
EXPERIMENTAL TRANSMISSION PROBABILITIES  
FOR EIGHT CONICAL ORIFICES (SET III)

Orifice, L/R	T, deg	n	K		$\bar{K}$	$\frac{100(\bar{K}-W)}{W}$
			Run 8	Run 9		
1.080	22.0	0.8855	0.857a	0.850	0.844	-4.7
			0.887b	0.885		
3.889	26.8	0.8848	0.942a	0.860	0.901	+1.8
			0.886b	0.884		
1.005	18.7	0.8665	0.832a	0.936	0.884	+2.0
			0.867b	0.862		
0.4216	0	0.8252	0.870a	0.857	0.864	+4.7
			0.827b	0.825		
4.051	15.2	0.7375	0.620a	0.581	0.600	-18.7
			0.742b	0.736		
2.183	9.65	0.6898	0.877a	0.829	0.853	+23.6
			0.695b	0.688		
3.857	9.15	0.6187	0.568a	0.595	0.582	-6.0
			0.625b	0.617		
2.072	0	0.5059	0.505a	0.498	0.502	-0.8
			0.515b	0.504		
m = slope			37.97	35.88		
b = intercept at ( $W_1=0$ )			+0.68	-0.17		
$J_0$ = intercept at ( $W_1=1$ )			38.65	35.71		

- a. The upper number of each pair is the value obtained from the experimental points.
- b. The lower number of each pair is the value obtained from the least squares line.

typical agreement between measured vapor pressures reported by two laboratories, both of which use supposedly the same Knudsen effusion technique, and is better than the reproducibility in vapor pressure measurements often obtained within a given laboratory. It would therefore appear that the source of these discrepancies in vapor pressure measurements may lie in phenomena other than flow of gas through an orifice.

Concurrently with our work, Macur, Edwards, and Wahlbeck<sup>41</sup> have attempted to circumvent this problem of poor reproducibility in Knudsen effusion measurements by using a Multicell technique in which the emphasis is on the simultaneous determination of several vapor pressures at the same temperature; the average deviation in the pressures calculated from the several cells in a given run range from 1 to 3% for indium and from 1 to 8% for gallium. The agreement from run to run (i.e., with change in temperature), as reflected in the calculated values of  $\Delta H_{298}^{\circ}$  of vaporization, is equally impressive; the uncertainty quoted is  $\pm 0.10$  Kcal/mole.

## SECTION V

### THE MIKER TECHNIQUE

The Miker technique for determination of vapor pressures and of molecular weights of vapors at high temperatures was described in detail in Part II<sup>21</sup>. In this technique a vacuum microbalance is used to obtain both the rate of effusion from a suspended Knudsen cell and the recoil force which is exerted on the cell as a result of effusion.

The results reported in Part II<sup>21</sup> demonstrated the general validity of the technique, and also demonstrated the need for various refinements if the technique was to provide a significant improvement over typical Torsion-Knudsen effusion-Recoil data. The various refinements will be reported.

#### A. MODIFICATIONS TO APPARATUS

The early results<sup>21</sup> with the Miker apparatus indicated two major deficiencies: (1) When power to the furnace was terminated in the course of measuring the recoil force, the furnace cooled so slowly that an undesirably large correction for effusion during cooling was required. (2) Manual control of the vacuum microbalance was satisfactory for rate of effusion measurements, but not for recoil force measurements; automatic balance control appears to be a requirement for valid recoil force measurements. Most of the modifications to be described were made in the course of overcoming these two deficiencies.

1. Furnace and Power Supply: Rapid cooling by the furnace appeared to be most easily achieved through the use of elements with very low heat-capacity and with high surface area. Tungsten mesh furnace elements were considered but rejected in favor of graphite tape for the following reasons: (1) Graphite tape retains its flexibility

after many cycles to operating temperatures; (2) Required furnace temperatures were not, at least initially, so high that vaporization from the graphite elements posed a problem; (3) Furnace fabrication is simplified and is readily accomplished in our shop; (4) The resistivity of graphite is so high that one may easily fabricate a furnace which operates directly from an SCR-controlled, 100A, 110V, 60Hz line; power at this voltage-current level is much more easily handled and introduced into the vacuum system than is the lower voltage - very high current levels required by metallic heating elements.

The furnace has a cylindrical configuration and consists of six 13-cm lengths of 1.27-cm-wide graphite tape held at top and bottom by machined graphite rings with graphite screws. Electrically, the three lengths of tape which form one hemisphere are in parallel, as are the other three; the two sets of three are then in series, connected electrically by the bottom graphite ring. The resistance of the furnace is  $\sim 1.0$  ohm at  $25^{\circ}\text{C}$ . With no radiation shielding, a current of  $\sim 50\text{A}$  rms produces a temperature of  $1300^{\circ}\text{C}$  in a cell suspended in the center of the furnace. When power to the furnace is terminated, the suspended cell cools initially at a rate of  $\sim 25\text{-}30$  deg C/sec.

As indicated above, power to the furnace is controlled with a single 110A silicon-controlled-rectifier the gate of which is driven by a "Silicontrol" pulse generating unit<sup>42</sup>.

The other units in the control loop are a tungsten-rhenium thermocouple which responds to changes in furnace temperature, a stable, variable reference voltage, an electronic null detector which responds to any error voltage between the thermocouple and the reference voltage, and a Controller which accepts the output of the null detector, provides proportional, derivative, and integral control actions, and supplies an appropriate dc current to drive the Silicontrol unit. The thermocouple is used only for control; temperatures are measured with an automatic photoelectric "Photomatic" pyrometer.

2. Automatic Control of Microbalance: Several changes have been made in the automatic control system, although the basic control loop (Figure 20 in reference 21) remains the same. The magnetic amplifier which supplied current to the compensating coils has been replaced with a well-regulated dc power supply and an emitter-follower circuit which is driven by the output of the Controller. This substitution eliminated a significant ripple voltage from the coils.

The "Photopot" light beam position sensor<sup>21</sup> has been replaced with one of later manufacture, which is more stable and which can be readily operated in high vacuum. The new "Photopot" was mounted inside the balance chamber about 6.3 cm from the mirror affixed to the center of the balance beam. The light beam originates, outside the vacuum system, in a 50W projector lamp, is defined by a 0.010-cm slit, reflected through a lens and window into the balance chamber and onto the balance mirror, and focused onto the "Photopot". The output of the projector lamp is monitored and controlled by a modification of the circuit described by Rosenthal<sup>13</sup>. Power for the "Photopot" bridge circuit is now supplied by mercury batteries.

The weight change which can be compensated by change in current through the balance coils (from 0 to ~100mA) is 28mg. To avoid opening the vacuum system to re-tare the balance after each 25-30mg weight loss, a taring mechanism operable from outside the vacuum system was installed. A bellows-sealed shaft, driven outside the vacuum chamber by a micrometer screw, carries four ~20-mg ring weights formed from Alumel wire 0.020 cm in diameter. As the micrometer screw is rotated, the shaft is translated downward (upward) and the four ring weights are sequentially placed on (removed from) a cross-arm attached to the balance beam.

3. Miscellaneous Modifications: In the Miker technique effusing vapor is directed downward, directly toward the window/prism through which optical pyrometer measurements are made. A shutter protects the window during the interval between pyrometer reading; even so, the window acquires a significant deposit rather rapidly. To avoid opening the entire vacuum system to the atmosphere while the window/

prism is removed, cleaned, and replaced, a very thin, bellows-sealed gate valve was installed in the window mount and between the window/prism itself and the furnace chamber. The valve is a modification of the design reported by Sheffield<sup>35</sup>, and has performed satisfactorily.

The effect of building and equipment vibrations on the micro-balance has been minimized by mounting the vacuum system on a steel-reinforced concrete block (2x2x3 ft. high) which was cast in place on the basement floor; mechanical vacuum pumps in the vicinity have been mounted on vibration-absorbing pads, etc.

For increased pumping capacity, there has been installed in the vacuum system a larger diffusion pump (PMC-720) and a liquid nitrogen trap (Cryo-sorb).

4. Spurious Recoil Forces: In measurements of rate of effusion and of recoil force made immediately after the modifications described above were effected, the measured recoil force was much larger (e.g., by a factor of 1.5-2.0) than expected from the rate of effusion measurements. A major source of the spurious portion of the recoil force has been identified as an interaction between the fields surrounding the furnace power leads and the magnet attached to the balance beam. This interaction has been minimized, and all but eliminated, by arranging the furnace power leads and the furnace elements themselves in a configuration symmetrical with respect to generation of spurious magnetic fields in the balance chamber.

A second major source of spurious recoil force was inadequate shielding of the "Photopot" from stray light in general, and specifically from light from the furnace. Stray light from the furnace caused a shift in the null point of the "Photopot"; when the furnace power was terminated to measure the recoil force, the stray light from the furnace was also terminated. The null point of the "Photopot" shifted back to the "furnace cold" position, but since this shift coincided with a recoil force measurement, the shift was incorporated into the apparent recoil force. Shielding of the "Photopot" was relatively simple, once the difficulty had been identified.

The residual spurious forces which remain appear to arise from pressure-dependent phenomena, e.g., thermomolecular flow forces<sup>44</sup>. However, these residual spurious forces now constitute only ~1% of a typical expected recoil force, compared with ~50 to 100% before the various corrective actions were taken.

## B. EXPERIMENTAL RESULTS

We have only recently eliminated (or minimized) the spurious recoil forces discussed above. The experimental data we report were obtained with the modified furnace and automatic control system, but before the spurious forces were identified and eliminated, and are presented to indicate the precision which has been obtained in recoil force measurements with the microbalance.

The data in Table 7 for the vaporization of tin were obtained with a graphite Miker cell<sup>21</sup> the conical orifice of which is described by  $T = 28.8^\circ$ ,  $(L/r_0) = 4.98$ ,  $W = 0.908$ , and  $f = 1.088$ .

The results of Table 7 are typical illustrations of the reproducibility obtainable with the Miker system. It should be noted in particular that the reproducibility in measurements of recoil force is at least as good as the reproducibility in measurements of rate of effusion.

We expect to observe similar reproducibility and good agreement between effusion and recoil measurements in subsequent vapor pressure determinations.

TABLE 7  
 MIXER DATA FOR VAPORIZATION  
 OF TIN

Temp, °K	Rate of effusion, μg/sec	Recoil Current, mA	Recoil Mass <sup>‡</sup> , μg	Pressure <sup>†</sup> , dyn/cm <sup>2</sup>	
				P <sub>E</sub>	P <sub>R</sub>
1466	1.061	0.306	100.4	11.2	21.7
1470	1.078	0.310	101.7	11.4	22.0
1473	1.138	0.298	97.7	12.1	21.1
1473	1.067	0.302	99.1	11.4	21.4
1486	1.156	0.328	107.6	12.3	23.2
1489	1.070	0.327	107.3	11.4	23.2

‡ Recoil mass is that mass which, under the acceleration of gravity, counterbalances the recoil force; balance calibration = 0.328 mg/mA.

† P<sub>E</sub> is calculated from rate of effusion; P<sub>R</sub> from recoil mass<sup>‡</sup>.  
 The "accepted" value<sup>45</sup> is 7.8 dyn/cm<sup>2</sup> at 1480°K.

## SECTION VI

### CALORIMETRIC STUDIES OF VAPORIZATION PROCESSES

Determination of equilibrium vapor pressures and/or decomposition pressures, with subsequent calculation of enthalpy of vaporization and/or decomposition and of enthalpy of formation of the gaseous species evolved, occupies a key role - one is tempted to say the keystone role - in high temperature chemistry (HTC). From the various measurements of (supposedly) equilibrium pressures in various laboratories have arisen numerous discrepancies: between Knudsen effusion data and mass spectrometric data; between Knudsen effusion data and Langmuir vaporization data; and even between two sets of Knudsen effusion data, both of which were obtained by reputable workers using, supposedly, the same technique. Attempts to resolve these discrepancies have resulted in, among other things, the formation at the 1966 Gordon Research Conference on HTC, of a committee to study establishment of vapor pressure standards above 500°K and below  $10^{-3}$  atmosphere.

In addition to refinement and standardization of effusion techniques, an endeavor to which the previous sections of this report is devoted, new approaches are needed. A more or less obvious one, except for experimental difficulties encountered at high temperatures, is direct calorimetric measurement of enthalpy of vaporization and/or decomposition. Sunner and Morawetz<sup>48</sup> (at the University of Lund, Sweden) have studied intensively the problem of calorimetric measurement of heats of vaporization of various hydrocarbons and other organic compounds at 25°C. They have successfully measured heats of vaporization with a precision and accuracy better than 0.1 kcal/mole for materials with vapor pressures as low as  $10^{-4}$  torr at 25°C. They have also measured differences in heat of vaporization as a function of the effusion orifice geometry.

In conjunction with work supported by another contract we became interested two to three years ago in the possibility of direct calorimetric measurement of enthalpies of decomposition, e.g.  $A(s) \rightarrow B(s) + C(g)$ . Our initial approach to the direct measurement of enthalpy changes was essentially to copy the furnace and calorimeter configuration of Speros and Woodhouse's "quantitative differential thermal analysis" (QDTA) system<sup>47</sup> and to make various changes in the electronic control circuitry and the output signal. In evaluating our QDTA system<sup>48</sup>, we measured enthalpies of fusion of several metals with a precision of 0.5-1.5% and an accuracy of 1-3% in the range 150-450°C. Subsequently we investigated the decomposition of  $PbCO_3$ ,  $ZnCO_3$ , and  $NH_4Cl$ ; with QDTA we were able to determine with reasonable precision and accuracy the enthalpy change for these decompositions, including the change for each of three steps in the decomposition of  $PbCO_3$ .

Our experience with the QDTA concept has led us to make several significant modifications in the furnace-calorimeter configuration and in the control-output circuitry; we refer to the new system as "Differential Scanning Calorimetry" (DSC)<sup>49</sup>. These modifications are presently (Summer, 1967) being debugged and tested. We expect that with this new DSC we shall be able to measure in the range 30-1000°C, endothermic enthalpy changes resulting from fusion, vaporization, decomposition and phase transition, and perhaps even exothermic enthalpies of reaction.

It is our further opinion that it is feasible, within the present state-of-the-art, to design and build a DSC system which would provide direct measurement of enthalpy changes in the range 1000-2000°K, and perhaps to 2500°K. Such a system would make available to "higher" temperature chemists the capabilities presently available in commercial equipment<sup>49</sup> up to 500°C and expected in our DSC system up to 1000°C.

Another virtue of the DSC technique is this: with the one assumption that the rate of energy input to the calorimeter is proportional to the rate of the (endothermic) process occurring in the calorimeter, the data one obtains are directly interpretable as the rate of the process as a function of temperature and of time. It is then rather straight forward<sup>47, 50</sup> to obtain rate constants over a range of temperatures, and hence the activation energy, from a single 1-to-3-hour run. With the older QDTA system we have obtained<sup>48</sup> energies of activation for the various

steps in the decomposition of  $PbCO_3$ , and for the homogeneous decomposition (in solution) of a complex organic azo compound.

In summary, we are convinced that direct calorimetric measurement of enthalpies of decomposition, vaporization, etc., are presently achievable to  $1000^\circ C$ , and with a relatively modest development effort could be achieved at  $2000^\circ C$ . While these techniques are not likely to replace effusion techniques in the near future, they can provide for high temperature processes data obtained by other-than-equilibrium techniques; such supplementary and complementary data are sorely needed in many high temperature chemical systems.

TABLE 8

## IDENTIFICATION OF MAJOR COMMERCIAL COMPONENTS OF APPARATUS

<u>Item</u>	<u>Supplier</u>
Amplifier, Lock-in PAR JB-5	Princeton Applied Research Corp. Princeton Junction, N.J.
Controller, C.A.T. Type 10877	Leeds and Northrup Company 4901 Stenton Avenue Philadelphia 44, Penna.
Lamp, Projector 8V, 50W, Type 13113C-04 Philips (Holland)	Local Photographic Supply Shop
Null detector, d.c. Type 9834-2	Leeds and Northrup Company 4901 Stenton Avenue Philadelphia 44, Penna.
Photopot	Giannini Controls Corporation 55 N. Vernon Avenue Pasadena, California
Power Supply, 30V d.c., QB28-1	Sorensen Products Raytheon Co. S. Norwalk, Conn.
Pressure Meter, Equibar Type 120	Trans-Sonics, Incorporated P.O. Box 328 Lexington 73, Massachusetts
Pump, diffusion, oil, 4 in., PMC-720	Consolidated Vacuum Corporation 1775 Mt. Read Blvd. Rochester 3, New York
Pyrometer, optical Photoelectric, "Photomatic"	Pyrometer Instrument Co. Bergenfield, N.J.
Valve, vacuum, variable leak Cat. No. 9101-M	Granville-Phillips Company 5675 E. Arapahoe Avenue Boulder, Colorado 80301
Silicontrol Pulse Unit Type VS6332AF	VecTrol Engineering Div. Sprague Electric Co. P.O. Box 1089 Stanford, Conn.
Trap, liquid nitrogen "Cryo-sorb"	Granville-Phillips Co. 5673 E. Arapahoe Ave. Boulder, Colorado 80301
Tuning Fork Type 40	American Time Products 61-20 Woodside Ave. Woodside, N.Y. 11377

REFERENCES

1. M. Knudsen, Ann. Phys. 28, 75, 999 (1909); "Kinetic Theory of Gases," Methuen, London (1934).
2. J. L. Margrave, In "Physico-Chemical Measurements at High Temperatures" (J. O'M. Bockris, J. L. White, and J. D. Mackenzie, eds.). Butterworths Scientific Publications, London (1959).
3. Various chapters in "Characterization of High Temperature Vapors" (J. L. Margrave, ed.). John Wiley and Sons, Inc., New York (1967).
4. By definition, an ideal orifice has zero length; if its radius is the same as the radius of (the smaller end of) an actual (conical) orifice, the orifices are said to correspond.
5. P. Clausing, Physica 9, 65 (1929); Ann. Physik 12, 961 (1932).
6. W. C. DeMarcus, Technical Report K-1502, parts 1-6, Oak Ridge Gaseous Diffusion Plant, Oak Ridge, Tennessee (1957); and W. C. DeMarcus and E. H. Hopper, J. Chem. Phys. 23, 1344 (1955).
7. E. W. Balson, J. Phys. Chem. 65, 1151 (1961).
8. R. P. Ozkowsky, J. L. Margrave, and S. M. Robinson, J. Phys. Chem. 67, 229 (1963).
9. W. L. Winterbottom and J. P. Hirth, J. Chem. Phys. 37, 784 (1962).
10. P. Clausing, Z. Physik 66, 471 (1930).
11. R. D. Freeman and A. W. Searcy, J. Chem. Phys. 22, 762, 113' (1954).
12. R. D. Freeman, "Molecular Flow and the Effusion Process in the Measurement of Vapor Pressures", Technical Report ASD-TDR-754, Part I, 1963 (AD423140).
13. R. D. Freeman and J. G. Edwards, in "Condensation and Evaporation of Solids" (E. Rutner, P. Goldfinger, and J. Hirth, eds.); Proc. Intl. Symposium, Dayton, Ohio, September, 1962. Gordon and Breach, New York (1964). p. 127.
14. J. G. Edwards, Ph.D. Thesis, Oklahoma State University, Stillwater, 1964 (AD469505).
15. J. G. Edwards and R. D. Freeman, to be published.
16. Appendix E of reference 14.
17. D. H. Davis, L. L. Levenson, and N. Milleron in Rarefied Gas Dynamics, (L. Talbot, Ed.) Academic Press, New York (1961). p. 99.
18. E. M. Sparrow and V. K. Jonsson, AIAA Journal 1, 1081 (1963).

19. NASA Technical Notes, Lewis Research Center, Cleveland, Ohio
  - a. E. A. Richley and C. D. Bogart, NASA TN D-2115 (February, 1964).
  - b. E. A. Richley and T. W. Reynolds, NASA TN D-2330 (June, 1964).
  - c. H. Cook and E. A. Richley, NASA TN D-2480 (September, 1964).
  - d. T. W. Reynolds and E. A. Richley, NASA TN D-1864 (October, 1964).
  - e. T. W. Reynolds and E. A. Richley, NASA TN D-3225 (January, 1966).
20. J. W. Ward, "Use of the Knudsen Effusion Method, A Literature Survey" Report LA-3006, Los Alamos Scientific Laboratory of the University of California. (Available from the Office of Technical Services) May, 1964.
21. R. D. Freeman, "Molecular Flow and the Effusion Process in the Measurement of Vapor Pressures," Technical Report ASD-TDR-63-754, Part II (AD612953).
22. N. F. Ramsey, "Molecular Beams", Oxford University Press (1956).
23. W. L. Fite and R. T. Brackman, Physical Review 112, 1141 (1958).
24. T. H. Batzer and R. H. McFarland, Rev. Sci. Instr. 36, 328 (1965);  
T. H. Batzer, private communication.
25. J. C. Sheffield, Rev. Sci. Instr. 36, 1269 (1965).
26. J. Q. Adams, Ph.D. Thesis, University of Illinois, Urbana (1961).
27. K. C. Wang, Ph.D. Thesis, Illinois Institute of Technology, Chicago (1966).
28. F. C. Hurlbut, Report No. AS-66-10, College of Engineering, University of California, Berkeley, August, 1966; paper presented at Rarefied Gas Dynamics Fifth International Symposium, Oxford, England, July, 1966.
29. V. Ruth and J. P. Hirth, (same as 13). p. 99.
30. J. W. Ward, "A Study of Some of the Parameters Affecting Knudsen Effusion", Report LA-3509, Los Alamos Scientific Laboratory of the University of California (Available from CFSTI). Also, Ph.D. Thesis, University of New Mexico, Albuquerque (1966).
31. P. W. Gilles, Ann. Rev. Phys. Chem. 12, 355 (1961).
32. K. D. Carlson, Ph. D. Thesis, University of Kansas, Lawrence (1960);  
Argonne National Laboratory Report ANL-6156 (1960).
33. J. D. McKinley, Jr. and J. E. Vance, J. Chem. Phys. 22, 1120 (1954).
34. K. Motzfeldt, J. Phys. Chem. 59, 139 (1955).
35. C. I. Whitman, J. Chem. Phys. 20, 161 (1952).
36. A. J. Boyer and T. R. Meadowcroft, Trans. Met. Soc. AIME 233, 388 (1965).

37. K. D. Carlson, P. W. Gilles, and R. J. Thorn, J. Chem. Phys. 38, 2725 (1963).
38. C. Hall, Rev. Sci. Instr. 33, 131 (1962).
39. A. L. Ball, Jr., MS Thesis, Oklahoma State University, Stillwater (1963).
40. R. D. Freeman and R. E. Gebelt, unpublished results.
41. G. J. Macur, R. K. Edwards and P. G. Wahlbeck, J. Phys. Chem. 70, 2956 (1966).
42. N. G. Muskovac, Technical Paper TP-63-11, Sprague Electric Co., North Adams, Mass. Figure 8.
43. L. A. Rosenthal, Rev. Sci. Instr. 36, 1329 (1965).
44. First three papers in "Vacuum Microbalance Technique", vol. 5, (K. H. Behrndt, ed.) Plenum Press, New York (1966).
45. R. Hultgren, R. L. Orr, P. D. Anderson, and K. K. Kelley, "Selected Values of Thermodynamic Properties of Metals and Alloys". J. Wiley and Sons, Inc., New York (1963).
46. S. Sunner and E. Morawetz, Acta Chem. Scand. 17, 13 (1963); private communication, June, 1967.
47. D. M. Speros and R. L. Woodhouse, J. Phys. Chem. 67, 2164 (1963).
48. P. D. Gwinup, Ph.D. thesis, Oklahoma State University, Stillwater (1967).
49. Perkin-Elmer Corp., Norwalk, Connecticut, Differential Scanning Calorimeter DSC-113.  
L. S. Watson, et al., Anal. Chem. 36, 1233 (1964).  
M. J. O'Neill, Anal. Chem. 36, 1238 (1964).
50. H. J. Borchardt and F. Daniels, J. Am. Chem. Soc., 79, 41 (1957).

UNCLASSIFIED

Security Classification

DOCUMENT CONTROL DATA - R&D		
<i>(Security classification of title, body of abstract and indexing annotation must be entered when the overall report is classified)</i>		
1 ORIGINATING ACTIVITY (Corporate author) Oklahoma State University Dept. of Chemistry Stillwater, Oklahoma 74074		2a REPORT SECURITY CLASSIFICATION UNCLASSIFIED
		2b GROUP
3 REPORT TITLE "Molecular Flow and the Effusion Process in the Measurement of Vapor Pressures"		
4 DESCRIPTIVE NOTES (Type of report and inclusive dates) Final Report, 1 September 1964 to 31 May 1967		
5 AUTHOR(S) (Last name, first name, initial) Freeman, Robert D.		
6 REPORT DATE November, 1967	7a TOTAL NO. OF PAGES 79	7b NO. OF PAGES 50
8a CONTRACT OR GRANT NO. AF 33(657)-8767	8a ORIGINATOR'S REPORT NUMBER(S) ASD-TDR-53-754, Pt. III	
b. PROJECT NO 7360 Task: 736004	8b OTHER REPORT NO(S) (Any other numbers that may be assigned this report)	
c		
d		
10 AVAILABILITY/LIMITATION NOTICES This document has been approved for public release and sales; its distribution is unlimited.		
11 SUPPLEMENTARY NOTES	12 SPONSORING MILITARY ACTIVITY AF Materials Laboratory (MAYT) Wright-Patterson AFB, Ohio	
13 ABSTRACT Our extensions to conical orifices of Clausius's analysis of angular distribution of molecules effusing from cylindrical orifices has resulted in numerical values for transmission probabilities and recoil-force correction factors which are tabulated. With these results, it is demonstrated that the optimum orifice geometry for (1) recoil force measurements is a diverging conical orifice with semi-apex angle of $30^\circ$ , (2) delivery of maximum fraction of effusing molecules onto (or into) a target (aperture) is a long cylindrical orifice. Modifications to the angular distribution apparatus are described and experimental results given for four orifices and two gases over the pressure range 5 to $900 \text{ dyn/cm}^2$ . The most interesting aspect of the results, one apparently not previously noticed in angular distribution results, is the presence of maxima and minima in plots of $\Delta$ vs. $\theta$ , where $\Delta$ is the (experimental value - theoretical value) of $P_\theta$ , the fraction of effusing molecules which flow per steradian at angle $\theta$ from the orifice axis. These maxima and minima have been correlated with the relative contribution from the orifice wall to the total flux at angle $\theta$ . Additional results for experimental transmission probabilities of orifices determined by the Multicell technique are generally in agreement with theoretical values within 2 to 5%. The Miker technique for simultaneous determination of vapor pressure by rate of effusion and by recoil force measurements has been refined to the point that recoil force data are as reproducible as rate of effusion measurements. Several sources of spurious recoil force have been identified and eliminated. A new furnace and a modified automatic control system for the microbalance are described.		

DD FORM 1473  
1 JAN 65UNCLASSIFIED  
Security Classification

UNCLASSIFIED

Security Classification

14 KEY WORDS	LINK A		LINK B		LINK C	
	ROLE	WT	ROLE	WT	ROLE	WT
Molecular Effusion Vapor Pressure Molecular Flow Transmission Probability for Orifices Microbalance Molecular Beams						

INSTRUCTIONS

1. **ORIGINATING ACTIVITY:** Enter the name and address of the contractor, subcontractor, grantee, Department of Defense activity or other organization (*corporate author*) issuing the report.
- 2a. **REPORT SECURITY CLASSIFICATION:** Enter the overall security classification of the report. Indicate whether "Restricted Data" is included. Marking is to be in accordance with appropriate security regulations.
- 2b. **GROUP:** Automatic downgrading is specified in DoD Directive 5200.10 and Armed Forces Industrial Manual. Enter the group number. Also, when applicable, show that optional markings have been used for Group 3 and Group 4 as authorized.
3. **REPORT TITLE:** Enter the complete report title in all capital letters. Titles in all cases should be unclassified. If a meaningful title cannot be selected without classification, show title classification in all capitals in parenthesis immediately following the title.
4. **DESCRIPTIVE NOTES:** If appropriate, enter the type of report, e.g., interim, progress, summary, annual, or final. Give the inclusive dates when a specific reporting period is covered.
5. **AUTHOR(S):** Enter the name(s) of author(s) as shown on or in the report. Enter last name, first name, middle initial. If military, show rank and branch of service. The name of the principal author is an absolute minimum requirement.
6. **REPORT DATE:** Enter the date of the report as day, month, year, or month, year. If more than one date appears on the report, use date of publication.
- 7a. **TOTAL NUMBER OF PAGES:** The total page count should follow normal pagination procedures, i.e., enter the number of pages containing information.
- 7b. **NUMBER OF REFERENCES:** Enter the total number of references cited in the report.
- 8a. **CONTRACT OR GRANT NUMBER:** If appropriate, enter the applicable number of the contract or grant under which the report was written.
- 8b, 8c, & 8d. **PROJECT NUMBER:** Enter the appropriate military department identification, such as project number, subproject number, system numbers, task number, etc.
- 9a. **ORIGINATOR'S REPORT NUMBER(S):** Enter the official report number by which the document will be identified and controlled by the originating activity. This number must be unique to this report.
- 9b. **OTHER REPORT NUMBER(S):** If the report has been assigned any other report numbers (*either by the originator or by the sponsor*), also enter this number(s).
10. **AVAILABILITY/LIMITATION NOTICES:** Enter any limitations on further dissemination of the report, other than those

imposed by security classification, using standard statements such as:

- (1) "Qualified requesters may obtain copies of this report from DDC."
- (2) "Foreign announcement and dissemination of this report by DDC is not authorized."
- (3) "U. S. Government agencies may obtain copies of this report directly from DDC. Other qualified DDC users shall request through \_\_\_\_\_."
- (4) "U. S. military agencies may obtain copies of this report directly from DDC. Other qualified users shall request through: \_\_\_\_\_."
- (5) "All distribution of this report is controlled. Qualified DDC users shall request through \_\_\_\_\_."

If the report has been furnished to the Office of Technical Services, Department of Commerce, for sale to the public, indicate this fact and enter the price, if known.

11. **SUPPLEMENTARY NOTES:** Use for additional explanatory notes.
12. **SPONSORING MILITARY ACTIVITY:** Enter the name of the departmental project office or laboratory sponsoring (*paying for*) the research and development. Include address.
13. **ABSTRACT:** Enter an abstract giving a brief and factual summary of the document indicative of the report, even though it may also appear elsewhere in the body of the technical report. If additional space is required, a continuation sheet shall be attached.

It is highly desirable that the abstract of classified reports be unclassified. Each paragraph of the abstract shall end with an indication of the military security classification of the information in the paragraph, represented as (TS), (S), (C), or (U).

There is no limitation on the length of the abstract. However, the suggested length is from 150 to 225 words.

14. **KEY WORDS:** Key words are technically meaningful terms or short phrases that characterize a report and may be used as index entries for cataloging the report. Key words must be selected so that no security classification is required. Identifiers, such as equipment model designation, trade name, military project code name, geographic location, may be used as key words but will be followed by an indication of technical context. The assignment of links, rules, and weights is optional.

UNCLASSIFIED

Security Classification